DYNAMIC ANALYSIS OF BEARINGLESS ROTOR BLADE WITH SWEPT TIPS

By

M.UMA MAHESWARAIAH

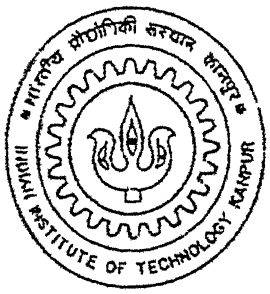

to the

DEPARTMENT OF AEROSPACE ENGINEERING

INDIAN INSTITUTE OF TECHNOLOGY, KANPUR

May 2000

DYNAMIC ANALYSIS OF BEARINGLESS ROTOR BLADE WITH SWEPT TIPS

A Thesis Submitted

in Partial Fulfilment of the Requirements

For the Degree of

MASTER OF TECHNOLOGY

By

M.UMA MAHESWARAIAH

to the

DEPARTMENT OF AEROSPACE ENGINEERING

INDIAN INSTITUTE OF TECHNOLOGY, KANPUR

May 2000

CERTIFICATE

It is certified that the work contained in the thesis entitled "**DYNAMIC ANALYSIS OF BEARINGLESS ROTOR BLADE WITH SWEPT TIPS**", by **M.UMA MAHESWARAIAH** has been carried out under my supervision and that this work has not been submitted elsewhere for a degree

Dr C VENKATESAN

Professor

Dept of Aerospace Engineering

I I T Kanpur

May, 2000

ABSTRACT

This thesis presents the formulation of structural dynamic equations of motion of a general bearingless rotor blade configuration with swept tip The equations of motion have been derived using Hamilton's principle and Rayleigh-Ritz finite element discretisation of the beam First the formulation is validated by comparing the results of the present analysis for a straight bearingless rotor blade with those available in literature

Then a systematic structural dynamic analysis has been performed to identify the effect of control system, location of elastomer and flexbeam-blade-torque tube junction from root The effect of tip sweep angles on the natural frequencies and mode shapes of the bearingless rotor blade, has also been analysed

Quantitative measures of lag-torsion and flap-torsion couplings have been defined based on the contribution of torsional deformation in the in-plane bending and out-of-plane bending modes respectively The effect of tip sweep angles on these couplings have been identified.

ACKNOWLEDGEMENTS

I take this opportunity to express my sincere gratitude to my thesis supervisor Dr C Venkatesan for his constant support and guidance throughout this work His valuable suggestions and innovative ideas helped me a lot in completing this work I am extremely thankful to him for giving me the freedom of work

I am also thankful to Dr. C S Upadhyay for his assignments in the course Introduction to FEM, by which it made me easy to write this code

I am thankful to my friend B Prasad whose support made my stay comfortable at IIT-Kanpur I am thankful to all of my friends especially, my batchmates Mohite, Voolla, Hridya, Body(Phani) and Lalmoni for making my stay at IIT-Kanpur a memorable experience

Words are not enough to explain my feelings towords my Parents, Sister Padma Jyothi and Brothers Babu Rajendra Prasad and Rudra Prasad They have always been the constant source of inspiration for me

M Uma Maheswaraiah

Contents

List of Figures

List of Tables

NOMENCLATURE

a	Torque offset
a_c	Control spring offset
d_c	Control spring deformation
e_1, e_2	Root offset
$\hat{e}_x, \hat{e}_y, \hat{e}_z$	Unit vectors along X,Y and Z axes
E_0	Reference modulus
$Im_{\eta\eta}, Im_{\zeta\zeta}, Im_{\eta\zeta}$	Mass moments of inertia of the beam per unit length
$[K^{cf}]$	Centrifugal stiffening matrix
$[K^E]$	Linear stiffness matrix
K_c	Control spring stiffness(non-dimensionalised with $m\Omega^2 l$)
K_F	Elastomer flap spring stiffness(non-dimensionalised with $m\Omega^2 l$)
K_L	Elastomer lag spring stiffness(non-dimensionalised with $m\Omega^2 l$)
K_ϕ	Elastomer torsonal spring stiffness(non-dimensionalised with $m\Omega$
l	Length of the blade
l_e	Length of each finite element
L_c	Distance of the control spring from root
L_{el}	Distance of the elastomer from root
m	Mass per unit length of the blade
$m\eta_m, m\zeta_m$	First moments of mass of the beam per unit length
$[M]$	Mass matrix
$[M^1], [M^2],$ $[M^3], [M^4]$	Matrices defined in the variation of kinetic energy
$[M^c]$	Coriolis damping matrix
N_b	Number of blades in the rotor system
N	Number of finite elements
O_H	Hub centre
q	Vector of finite element nodal displacements
$\vec{r}_p$	Position vector of a point 'p' on the deformed k^{th} blade

R_x, R_y, R_z	Components of permutational hub motion
t	Time
T	Kinetic energy
$[T_{ij}]$	Transformation matrix between orthogonal co-ordinate systems i and j
u_k, v_k, w_k	k^{th}blade deformation in axial, lead-lag and flap directions
U	Strain energy
V_H	Hub velocity
$\vec{V}$	Velocity of a point 'p' on k_{th} blade
V_x, V_y, V_z	Components of $\vec{V}$ in X,Y and Z directions
$\{V^L\}, \{V^{NL}\}, \{V^I\}$	Vectors defined in the expression of kinetic energy variation
$\{V\}, \{W\}, \{U\}$	Vectors of element nodal degrees of freedom
v'_k	Spatial derivative $(= \frac{d(v_k/l)}{d(x/l)})$
w'_k	Spatial derivative $(= \frac{d(w_k/l)}{d(x/l)})$
W_e	External work due to nonconservative forces
x_k	Coordinate along k^{th} blade axis in n-th element
x, y, z	Coordinate of a point in the $\hat{e}_x - \hat{e}_y - \hat{e}_z$ system
x, η, ζ	Coordinate of a point in the $\hat{e}_x - \hat{e}_\eta - \hat{e}_\zeta$ system
$\overline{x}$	$= x/l$
$Z_u, Z_v, Z_w,$	
$Z'_\phi, Z'_v, Z'_w,$	Notation used for writing the beam kinetic energy in concise form
$\overline{z}_u, \overline{z}_v, \overline{z}_w,$	
$\overline{z}_\phi, \overline{z}'_v, \overline{z}'_w$	
α	Warping amplitude
$\alpha_{xx}, \alpha_{x\eta}, \alpha_{x\zeta}$	Stress components
β_d	Blade predroop angle
β_p	Blade precone angle
β_s	Blade presweep angle
β_k	Local slope in flap bending of k^{th} blade
ζ_k	Local slope in lag bending of k^{th} blade
ϵ	Non dimensional parameter representing the order of

	magnitude of typical elastic blade bending slope
$\epsilon_{xx}, \gamma_{x\eta}, \gamma_{x\zeta}$	Strain components
τ_0	Initial twist rate of the blade
θ_G, θ_g	Geometric pitch in k^{th} blade
ϕ_k	Elastic twist
θ_I	Control pitch input
$\theta_x, \theta_y, \theta_z$	Rigid body perturbational rotation in roll-pitch-yaw
Λ_a	Tip anhedral angle (positive upwards)
Λ_s	Tip sweep angle (aft-sweep positive)
ξ_1	Distance of flexbeam-blade-torque tube junction from the root
ξ_2	Distance of free end of torque tube from the root
ρ	Density
$\{\Phi_c\}, \{\Phi_q\}$	Arrays of Hermite cubic and quardratic interpolation polynomials respectively
$\{\Phi_c'\}, \{\Phi_q'\}$	First derivative of $\{\Phi_c'\}$ and $\{\Phi_q'\}$ with respect to x
ψ_k	Azimutal angle of k^{th} blade
ψ	Non dimensional time ($\psi = \Omega t$)
Ψ	Cross-sectional warping function
$\vec{\omega}_k$	Angular velocity of k^{th} blade
Ω	Speed of rotation of rotor
$\omega_x, \omega_y, \omega_z$	Components of $\vec{\omega}_k$ in x,y and z direction
$(\ )'$	Differentiation of ( ) with respect to x
$d(\ )$	Differential of ( )
$(\ )_\eta, (\ )_\zeta$	Differentiation with respect to η and ζ
$(\ )_x, (\ )_{xx}$	Differentiation with respect to x of variables u,v,w and ϕ
$\delta(\ )$	Variation of ( )
$\{\ \}$	Vector
$[\ ]$	Matrix
$1, 2, 3, 4, c, 5, 6$	Quantities refer to the corresponding coordinate system

Chapter 1

INTRODUCTION

The dynamic characteristics of rotor blades play significant role in the design of helicopter The main rotor system has to provide lift, thrust and control forces Therefore, any analytical study pertaining to the dynamics of helicopters requires the development of suitable mathematical models for

Rotor blade

Fuselage

and Rotor-fuselage interface

Rotor blade model essentially consists of the development of structural, inertial and aerodynamic operators associated with its motion The fuselage model is represented by an idealised structural model of a 3D structure The rotor-fuselage interface model must represent both the geometry of the interface as well as the aerodynamic interaction in an appropriate manner The fundamental tool, necessary for the analysis and design of helicopters, is the rotor blade dynamic model

During operation, the blades experience large bending and centrifugal loads In order to relieve the rotor bending moments experienced by the blades, early rotor blades were provided with flap (out-of-plane bending) and lag (in-plane bending) hinges at the root of the blade In addition, a pitch control bearing was provided to control rotors Such rotor systems are usually referred to as articulated rotors

A schematic diagram of an articulated rotor system is shown in Fig 1 1 The large number of moving parts leads to a mechanically complex rotor hub system accompanied by the associated wear out problem requiring frequent maintenance and replacement of parts With advancement in technology, increasing emphasis has been placed on the development of hingeless rotor systems The construction of these rotors are relatively simple, because of the absence of flap and lag hinges, but a pitch bearing is still provided for blade pitch control A schematic diagram of hingeless rotor system is shown in Fig 1 2

The development of a bearingless rotor system aims to eliminate both the pitch bearing as well as the external damper by incorporating a highly specialised elastomer In this rotor system, the blade is attached to the hub through a flexible structural element called flexbeam The flexbeam is designed to provide the required stiffness in flap and lag deformations of the blade, but it is highly flexible in torsion Surrounding the flexbeam, there is a stiff cuff denoted as torque tube which is attached to the blade-flexbeam junction at the outboard end and to a pitch link at the inboard end as shown in Fig 1 3 The pitch control of the blade is achieved by rotating the torque tube through up/down movement of the point P which in turn twists the flexbeam An elastomer is placed between the torque tube and flexbeam to provide adequate lag damping It also serves the purpose of a spacer between the torque tube and the flexbeam Though a bearingless rotor is mechanically simple, its dynamic analysis becomes very complicated due to presence of elastomer, multiple load path and existence of a kinematic constraint at the pitch link

Eversince the first successful flight of a helicopter in 1942, there has been a continued research effort to develop mechanically simple main rotors with acceptable performance and stability characteristics The development of bearingless rotors aims to achieve this goal Recently bearingless main rotors have been developed by Boeing-Sikorsky company in US and by Eurocopter in Germany These vehicles are currently undergoing flight tests The details of the development of rotor blades can be found in Ref [1]

In order to develop an indigenous rotor blade dynamic model, in Ref [2], Punit Kumar Gupta formulated a finite element model of a hingeless rotor blade undergoing flap, lag, torsion and axial deformations The rotor blade was treated as a straight uniform beam Subsequently, in Ref [3], Venu Gopal extended the model by including non-uniform properties of the blade and swept tip These rotor models included all the complex geometric parameters such as torque offset, blade root offset, pre-cone angle, pre-droop angle, pre-sweep angle, pretwist, tip sweep angle and tip anhedral angle

Recently, an idealised and highly simplified bearingless rotor model was developed by Pohit [1], wherein the elastomer was represented as a combination of nonlinear spring and damper In a preliminary analysis, the elastomer was treated as a linear spring Then, using Power series expansion and Rayleigh-Ritz method the uncoupled natural frequencies and mode shapes of a rotating blade in isolated lag and flap modes were evaluated

1.1 STRUCTURAL MODELLING

Since the rotor blades are long, slender beams, they will undergo moderate deformation A non-linear strain-displacement model is used to describe the coupling effects between axial, bending and torsion deformations Generally, the strains are assumed to be small in comparison to unity Such an assumption is consistent with the design requirement based on fatigue life consideration which states the rotor blades must be designed to have an operating strain level well below the elastic limit of the blade material

During the derivation of equations of motion of the rotor blade with swept-tip, the inertia and structural operators generate a large number of higher order nonlinear terms So one has to use a consistent ordering scheme to avoid complexity in formulation by assigning orders of magnitude to all the non-dimensional parameters of the problem, interms of blade bending slope (which is assumed to be of the order

of ϵ) A third order approximation is used in the formulation i e , the terms of order ϵ^3 are neglected in comparison to terms of order 1, i e ,

$$1 + O(\epsilon^3) \approx 1$$

1.2 OBJECTIVES

Objectives of present study are

(1) to develop a most general beam type finite element model for bearingless rotor blade, including all complex geometric parameters, such as torque offset, blade root offset, pre-cone angle, pre-droop angle, pre-sweep angle, pretwist, tip sweep angle, tip anhedral angle, elastomer, torque tube and control spring,

(2) to validate the model by comparing the results of the study with those available in literature,

(3) conduct detailed studies on the dynamic behavior of bearingless rotor blade with straight and swept tips to determine the effects of bending-torsion coupling due to tip sweep, anhedral angle and control spring

A schematic diagram of a bearingless rotor blade with tip sweep is shown in Fig 1 4 The present study on the dynamic analysis of bearingless rotor blade, is an extension of the work performed by Venu Gopal on hingeless rotor blade [3] In this study, the nonlinear elastomer is idealised as a combination of three linear springs, one each for flap, lag and torsional modes respectively

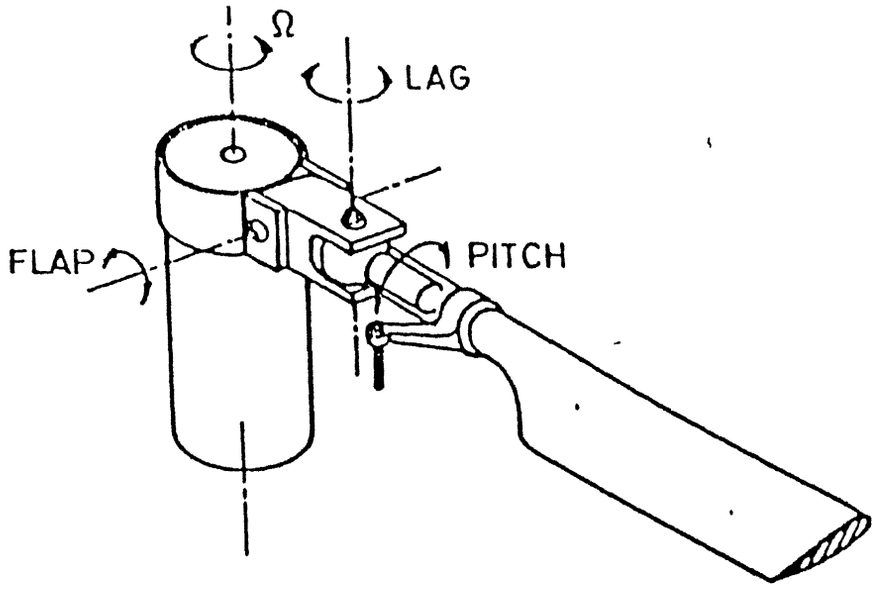

(a) Schematic diagram

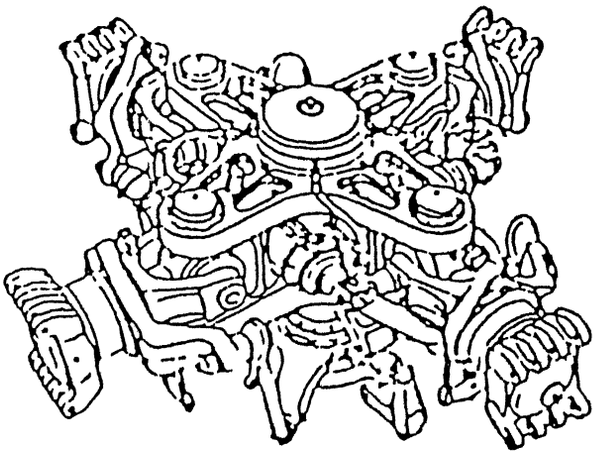

(b) Actual rotor hub (from Ref [1])

Figure 1.1: Schematic diagram of Articulated Rotor

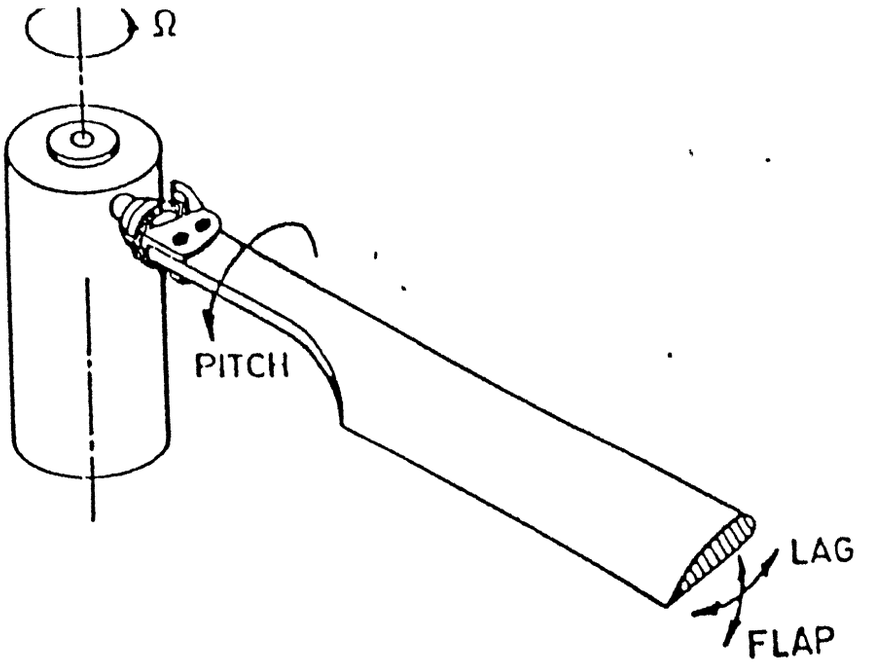

(a) Schematic diagram.

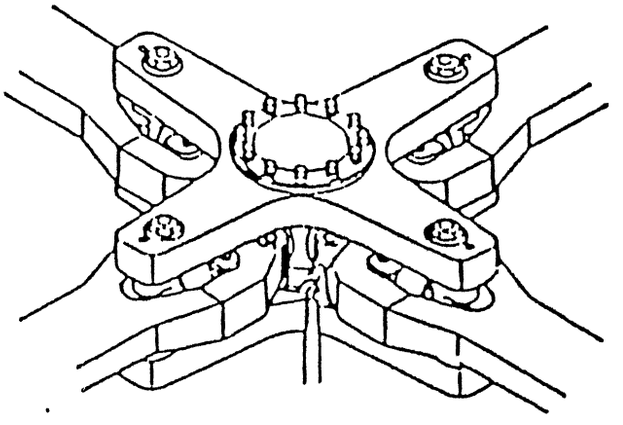

(b) Actual rotor hub (from Ref. [1]).

Figure 1.2: Schematic diagram of Hingeless Rotor

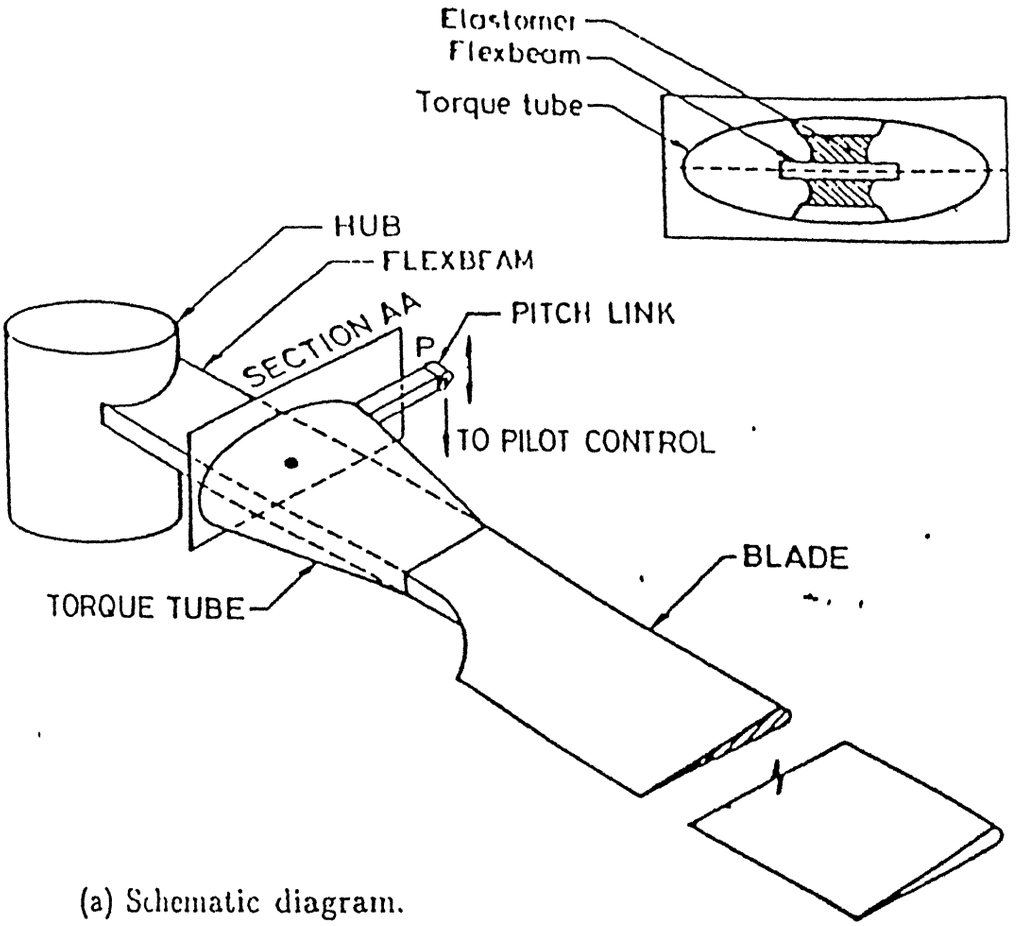

(a) Schematic diagram.

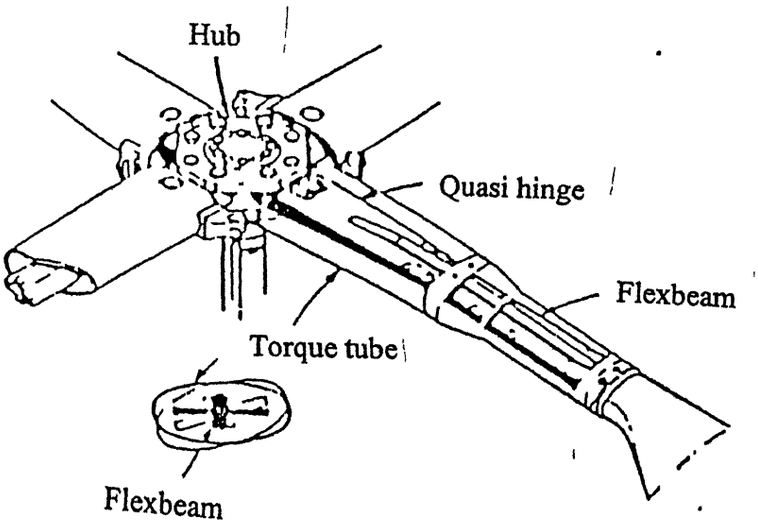

(b) Actual rotor hub (from Ref. [1]).

Figure 1.3: Schematic diagram of Bearingless Rotor without swept tips

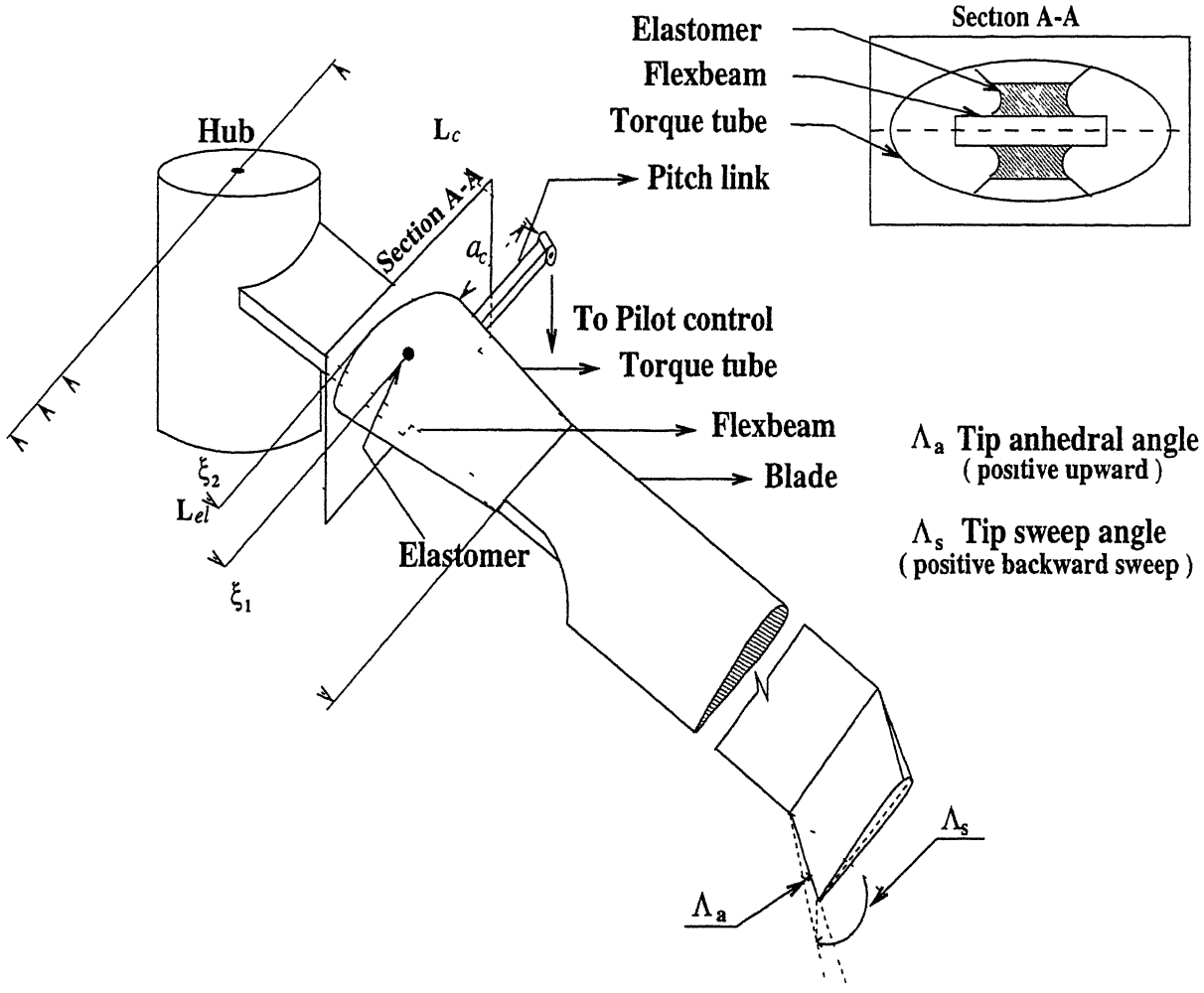

Figure 1 4 Schematic diagram of Bearingless Rotor with swept tips

Chapter 2

ROTOR BLADE MODEL AND ASSUMPTIONS

2.1 ROTOR BLADE MODEL

Dynamics of a bearingless rotor blade is a complex phenomenon In the case of articulated and hingeless rotor systems, the air/ground resonance is usually avoided by providing external mechanical dampers in the lead-lag mode of rotor system Whereas in case of bearingless rotors, a specialised elastomer is used as damper

The geometric parameters describing the configuration of the bearingless rotor system is shown in Fig 2 1 The parameter a represents the torque offset which is the distance from the center of rotation (hub center) to the reference axis of the blade e_1 and e_2 refer to the blade root offset distance from hub β_p represents precone angle defining the orientation of the blade pitch control axis with respect to the hub plane β_s and β_d represent the presweep and predroop angles respectively, representing the inclination of the blade reference axis with respect to the pitch control axis The bearingless rotor can be divided into three parts, namely, (1) flexbeam, (2) blade and (3) torque tube The flexbeam-blade-torque tube junction is at a distance ξ_1 from root and the free end of the torque tube is at a distance ξ_2

from the root An elastomer is placed in between flexbeam and torque tube at a distance of L_{el} from the root The blade consists of a straight portion and a swept tip whose orientation relative to the straight portion is described by sweep angle Λ_s (aft-sweep is positive) and anhedral angle Λ_a (positive upwards) A control spring (K_c) is attached to the torque tube at a distance L_c from root through a pitch link with an offset a_c

2.2 BASIC ASSUMPTIONS

In the formulation of the dynamic model of the rotor blade with swept tip, several assumptions have been made which are given below

1 The blade is treated as an elastic beam

2 The blade is modeled by beam type finite elements along the elastic axis of the beam

3 The speed of rotation (Ω) of rotor is constant

4 The rotor shaft is rigid

5 The blade undergoes moderate deformation in flap, lag, torsion and axial modes

6 The blade cross-section can have general shape with distinct shear center, aerodynamic center and center of mass

7 The blade is assumed to be made of isotropic material but can have nonuniform properties along the span

8 The elastomer is assumed as a combination of three linear springs, one each for flap, lag and torsion modes respectively

9 The effect of control system is represented by a linear spring(K_c) attached at pitch link as shown in Fig 2 1

2.3 ORDERING SCHEME

In the formulation of the equations of motion of a rotor blade with swept tip undergoing moderate deformation, a large number of higher order terms are generated In order to identify and eliminate higher order terms in a consistent manner, an ordering scheme is employed This ordering scheme is based on the assumption that the bending slopes of the deformed elastic blade are moderate and of order ϵ In the derivation of governing equations, it is assumed that terms of order ϵ^3 are neglected with respect to terms of order 1, i,e ,

$$1 + O(\epsilon^3) \approx O(1)$$

The order of magnitude of various non-dimensional parameters governing this problem are given below

ORDER 1

$\cos\phi_k, \sin\phi_k, \Lambda_a, \Lambda_s = O(1)$

$\frac{x_k}{l} = O(1)$

$\frac{1}{\Omega}\frac{d}{dt}() = \frac{d}{d\phi}() = O(1)$

$l\frac{d}{dx_k}() = \frac{d}{dx_k}() = O(1)$

$\xi_1, \xi_2, a_c = O(1)$

ORDER $\epsilon^{\frac{1}{2}}$

$\theta_{GK} = O(\epsilon^{\frac{1}{2}})$

ORDER ϵ

$\frac{a}{l}, \frac{e_1}{l}, \frac{e_2}{l}, \frac{\eta}{\zeta}, \frac{v_k}{l}, \frac{w_k}{l} = O(\epsilon)$

$v_k', w_k', \phi, \beta_p, \beta_d, \beta_s = O(\epsilon)$

ORDER $\epsilon^{\frac{3}{2}}$

$Im_{\eta\eta}, Im_{\zeta\zeta} = O(\epsilon^{\frac{3}{2}})$

$\frac{R_x}{l}, \frac{R_y}{l}, \frac{R_z}{l}, \theta_x, \theta_y, \theta_z = O(\epsilon^{\frac{3}{2}})$

$\underline{ORDER}\ \epsilon^2$

$\frac{u_k}{l}, u_k', m\eta_m, m\zeta_m = O(\epsilon^2)$

It is important to note that ordering scheme is based on physical understanding of the behaviour of actual blade configurations Hence care must be exercised in deleting higher order terms, based on this ordering scheme

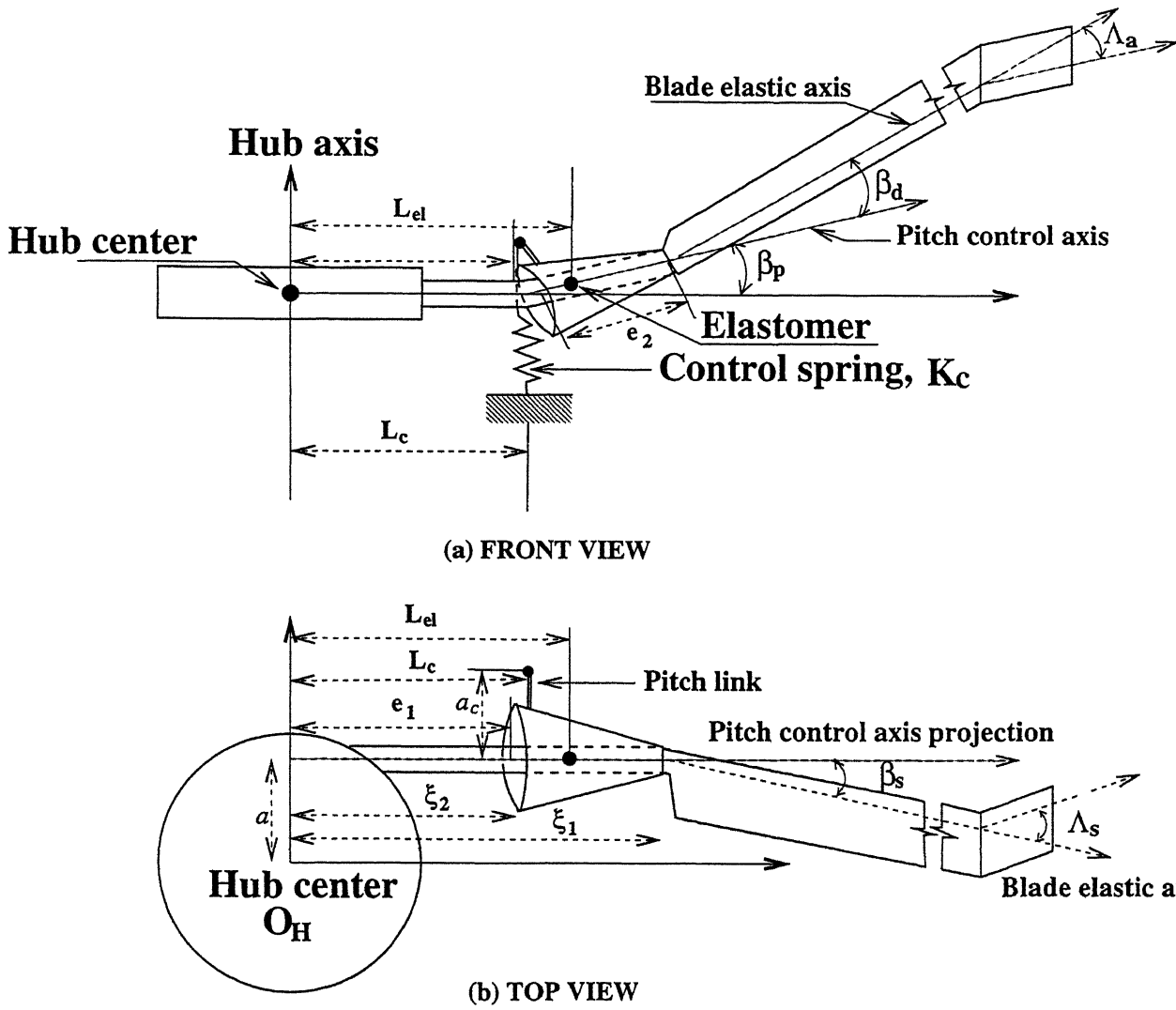

Figure 2 1 Rotor blade with tip sweep and anhedral

Chapter 3

COORDINATE SYSTEMS

The description of the complex deformation of a rotor blade requires several coordinate systems The transformation relation between quantities referred in various inertial, non-inertial coordinate systems is to be established before deriving the equations of motion of the rotor blade These coordinate systems are directly taken from Ref [3] The relation between two orthogonal systems X_i, Y_i, Z_i and X_j, Y_j, Z_j with $\hat{e}_{xi}, \hat{e}_{yi}, \hat{e}_{zi}$ and $\hat{e}_{xj}, \hat{e}_{yj}, \hat{e}_{zj}$ as unit vectors along the respective axes can be written as

$$\begin{Bmatrix} \hat{e}_{xi} \\ \hat{e}_{yi} \\ \hat{e}_{zi} \end{Bmatrix} = [T_{ij}] \begin{Bmatrix} \hat{e}_{xj} \\ \hat{e}_{yj} \\ \hat{e}_{zj} \end{Bmatrix} \tag{3 1}$$

where the transformation matrix $[T_{ij}]$ can be obtained using the Euler angles required to rotate the j-system so as to make it parallel to i-system The coordinate systems used in deriving the equation for the rotor model are described below

3.1 HUB FIXED INERTIAL SYSTEM-R

The coordinate system R shown in Fig 3 1, has its origin at center O_H of the unperturbed hub The x_R axis is pointing towards the helicopter tail and Z_R is pointing upwards The unit vectors along the three axes are $\hat{e}_{xR}, \hat{e}_{yR}, \hat{e}_{zR}$

3.2 HUB FIXED MOVING SYSTEM-H

The coordinate system H shown in Fig 3 2, is a body fixed system with its origin fixed at the centre of rotor hub O_H Prior to perturbational motion of the hub, H-system coincides with R-system If θ_z, θ_y and θ_x represent the sequential yaw-pitch-roll rotations, then the transformation matrix $[T_{HR}]$ can be written as

$$[T_{HR}] = \begin{bmatrix} 1 & 0 & 0 \\ 0 & \cos\theta_x & \sin\theta_x \\ 0 & -\sin\theta_x & \cos\theta_x \end{bmatrix} \begin{bmatrix} \cos\theta_y & 0 & -\sin\theta_y \\ 0 & 1 & 0 \\ \sin\theta_y & 0 & \cos\theta_y \end{bmatrix} \begin{bmatrix} \cos\theta_z & \sin\theta_z & 0 \\ -\sin\theta_z & \sin\theta_z & 0 \\ 0 & 0 & 1 \end{bmatrix} \quad (3\ 2)$$

Since θ_x, θ_y and θ_z are assumed to be of order $\epsilon^{3/2}$, sine and cosine functions can be approximated as

$$\sin\theta \approx \theta, \ \cos\theta \approx 1$$

Substituting the approximation, $[T_{HR}]$ can be simplified as

$$[T_{HR}] = \begin{bmatrix} 1 & \theta_z & -\theta_y \\ \theta_y\theta_z - \theta_z & 1 & \theta_x \\ \theta_x\theta_z + \theta_y & \theta_y\theta_z - \theta_x & 1 \end{bmatrix} \quad (3\ 3)$$

3.3 HUB FIXED ROTATING SYSTEM-1

The coordinate system shown in Fig 3 3, rotates about z_{1H} axis with constant angular speed Ω of the rotor Its origin is fixed at hub centre O_H This system can be obtained by rotating H system by an azimuthal angle ψ_k of the k^{th} blade about z_{1H} axis The transformation matrix is given as-

$$[T_{1H}] = \begin{bmatrix} \cos\psi_k & \sin\psi_k & 0 \\ -\sin\psi_k & \sin\psi_k & 0 \\ 0 & 0 & 1 \end{bmatrix} \tag{3 4}$$

where, ψ_k is azimuth angle of k^{th} blade

$$\psi_k = \psi + (k-1)\frac{2\pi}{N_b} \quad and \quad \psi = \Omega t$$

3.4 ROTATING SYSTEM-2K

The coordinate system 2K shown in Fig 3 4 is a blade fixed coordinate system which rotates with k^{th} blade The origin of the 2K system is at the location of the blade root A (Fig 3 4), which is at a distance $a\hat{e}_{y1} + e_1\hat{e}_{x1}$ from the hub centre 1-system and 2K-system are parallel

3.5 PRECONED, ROTATING SYSTEM-3K

The system 3K shown in Fig 3 5a and 3 5b also rotates with blade This system is obtained by rotating 2K-system by an angle -β_p(precone angle) about y_{2k} axis The transformation matrix between 2K and 3K is given as-

$$[T_{32}] = \begin{bmatrix} 1 & 0 & \beta_p \\ 0 & 1 & 0 \\ -\beta_p & 0 & 1 \end{bmatrix} \quad (3\,5)$$

3.6 PREDROOPED, PRESWEPT, PITCHED, BLADE-FIXED ROTATING SYSTEM-4K

The 4K system shown in Fig 3 5a and 3 5b, is blade fixed system with its origin at pitch bearing B(or flexbeam-blade-torque tube junction) of the blade It may be noted that the pitch axis of the blade is along $\hat{e}_{x3k}$ direction and the blade reference elastic axis is along the $\hat{e}_{x4k}$ direction While changing the control pitch input of the blade, the elastic axis will move on the surface of a cone whose vertex angle is described by the angles β_s and β_d as shown in Fig 3 5c

The 4K-system is obtained by the following steps-

Step-1 Translating the origin of 3K system by a distance 'e_2' along $\hat{e}_{x3k}$

Step-2 Then rotating the system by an angle -β_s(presweep angle) about z_{3k} axis

Step-3 Then rotating the system by an angle -β_d(predroop angle) about y_{3k}

Step-4 Then rotating the system by an angle θ_I about x_{3k}

The transformation matrix is given as-

$$[T_{43}] = \begin{bmatrix} 1 & -(\beta_s \cos\theta_I + \beta_d \sin\theta_I) & (\beta_d \cos\theta_I - \beta_s \sin\theta_I) \\ (\beta_s \cos\theta_I + \beta_d \sin\theta_I) & \cos\theta_I & \sin\theta_I \\ (-\beta_d \cos\theta_I + \beta_s \sin\theta_I) & -\sin\theta_I & \cos\theta_I \end{bmatrix} \quad (3\,6)$$

3.7 UNDEFORMED ELEMENT COORDINATE SYSTEM-e

The e system, shown in Fig 3 6, has its origin at the inboard node of i-th finite element The vector $\hat{e}_{xe}$, is aligned along the elastic axis of the beam element, while the vectors $\hat{e}_{ye}$ and $\hat{e}_{ze}$ are cross-sectional axes For the straight portion of the blade, the $(\hat{e}_{xe}, \hat{e}_{ye}, \hat{e}_{ze})$ system has the same orientation as $(\hat{e}_{x4k}, \hat{e}_{y4k}, \hat{e}_{z4k})$ system For the swept-tip element, the e system is oriented by rotating the $4k$ system about $\hat{e}_{z4k}$ by sweep angle Λ_s, and then about $\hat{e}_{y4k}$ by the anhedral angle Λ_a

The transformation matrix between $4k$ and e system is given as-

$$\begin{Bmatrix} \hat{e}_{xe} \\ \hat{e}_{ye} \\ \hat{e}_{ze} \end{Bmatrix} = [T_{e4}] \begin{Bmatrix} \hat{e}_{x4k} \\ \hat{e}_{y4k} \\ \hat{e}_{z4k} \end{Bmatrix} \tag{3 7}$$

For the element in the straight portion of the blade

$$[T_{e4}] = \begin{bmatrix} 1 & 0 & 0 \\ 0 & 1 & 0 \\ 0 & 0 & 1 \end{bmatrix} \tag{3 8}$$

For the swept-tip element

$$[T_{e4}] = \begin{bmatrix} \cos\Lambda_s \cos\Lambda_a & -\sin\Lambda_s & \cos\Lambda_s \sin\Lambda_a \\ \sin\Lambda_s \cos\Lambda_a & \cos\Lambda_s & \sin\Lambda_s \sin\Lambda_a \\ \sin\Lambda_a & 0 & \cos\Lambda_a \end{bmatrix} \tag{3 9}$$

where Λ_s is the blade tip sweep angle(positive for backward sweep), and Λ_a is the blade tip anhedral angle(positive upwards)

3.8 ROTATING, BLADE-FIXED SYSTEM-5K

The 5k system, shown in Fig 3 7 is a cross-sectional coordinate system of the k^{th} blade In the undeformed state of the blade, both e and 4k system are parallel But the origin of the 5k system is at a distance x_k from the origin of the e system During elastic deformation of the blade, the 5k system translates and rotates with the cross-section After deformation, the origin of the 5k system, from the origin of 4K system, is at the location given by

$$(\sum_{i=1}^{n-1}(l_e)_i)\hat{e}_{x4k} + (x_k + u_k)\hat{e}_{xe} + v_k\hat{e}_{ye} + w_k\hat{e}_{ze} \tag{3 10}$$

The transformation matrix between e and 5k system is obtained following a flap-lag sequence of rotation The Euler angles are respectively $-\beta_k$ and ζ_k corresponding to the local slope of the deformed blade in flap and lag directions The transformation matrix is given by

$$[T_{5e}] = \begin{bmatrix} \cos\zeta_k & \sin\zeta_k & 0 \\ -\sin\zeta_k & \cos\zeta_k & 0 \\ 0 & 0 & 1 \end{bmatrix} \begin{bmatrix} \cos\beta_k & 0 & \sin\beta_k \\ 0 & 1 & 0 \\ -\sin\beta_k & 0 & \cos\beta_k \end{bmatrix} \tag{3 11}$$

Since the angle ζ_k and β_k are of the order $O(\epsilon)$, the transformation matrix can be simplified by noting that-

$$\sin\theta \approx \theta,\ \cos\theta \approx 1$$

The Euler angles can be expressed in the terms of the local slope of elastic deformation of the blade as

$$\beta_k = w_k^{'} \approx \frac{dw_k}{dx}$$

$$\zeta_k = v_k^{'} \approx \frac{dv_k}{dx}$$

$$Note \quad x = \sum_{i=1}^{n-1} (l_e)_i + x_k$$

Substituting the above relations in the transformation matrix $[T_{5e}]$ yields

$$[T_{5e}] = \begin{bmatrix} 1 & v_k' & w_k' \\ -v_k' & 1 & -v_k' w_k' \\ -w_k' & 0 & 1 \end{bmatrix} \tag{3 12}$$

3.9 COORDINATE SYSTEM-6K

The 6K system shown in Fig 3 8 represents the cross-sectional coordinate system in the deformed configuration of the blade $\hat{e}_\eta - \hat{e}_\zeta$ represents the directions of the cross-sectional principal axes 6K-system is obtained by rotating 5K system about $\hat{e}_{x5k}$ through the angle $(\phi_k + \theta_G)$, where θ_G represents the geometric twist angle of the cross-section and ϕ_k represents the elastic twist

The transformation matrix relation is given as-

$$\begin{Bmatrix} \hat{e}_x \\ \hat{e}_y \\ \hat{e}_z \end{Bmatrix}_{5k} = \begin{bmatrix} 1 & 0 & 0 \\ 0 & \cos(\theta_G + \phi_k) & -\sin(\theta_G + \phi_k) \\ 0 & \sin(\theta_G + \phi_k) & \cos(\theta_G + \phi_k) \end{bmatrix} \begin{Bmatrix} \hat{e}_x \\ \hat{e}_\eta \\ \hat{e}_\zeta \end{Bmatrix}_{6k} \tag{3 13}$$

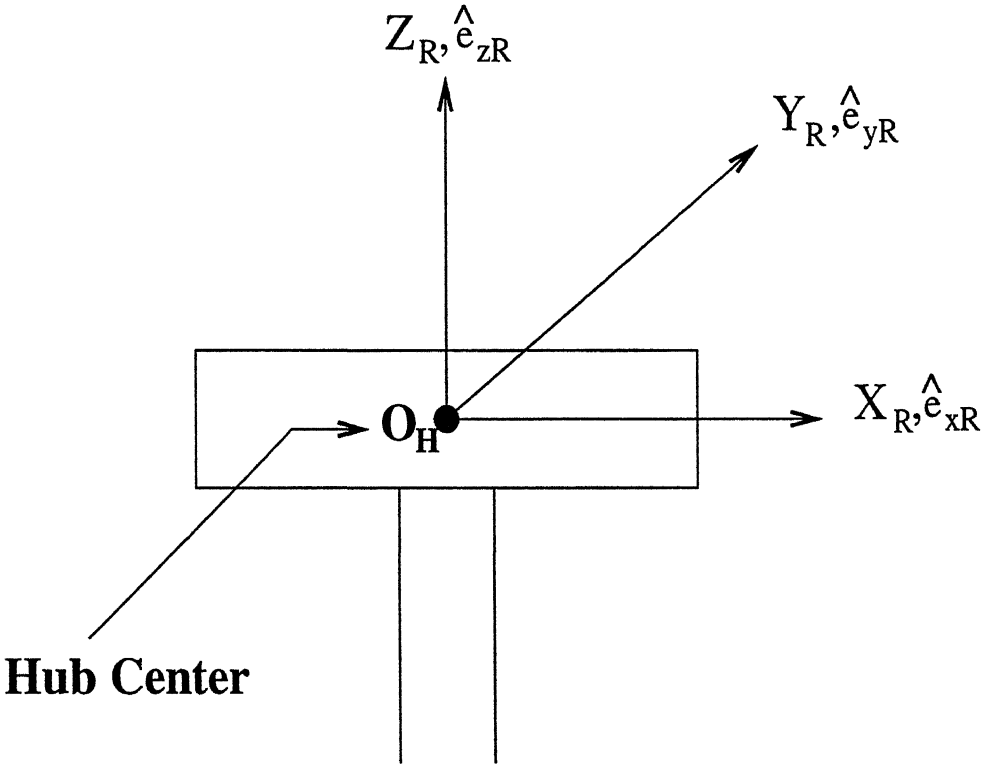

Figure 3 1 Inertial system-R

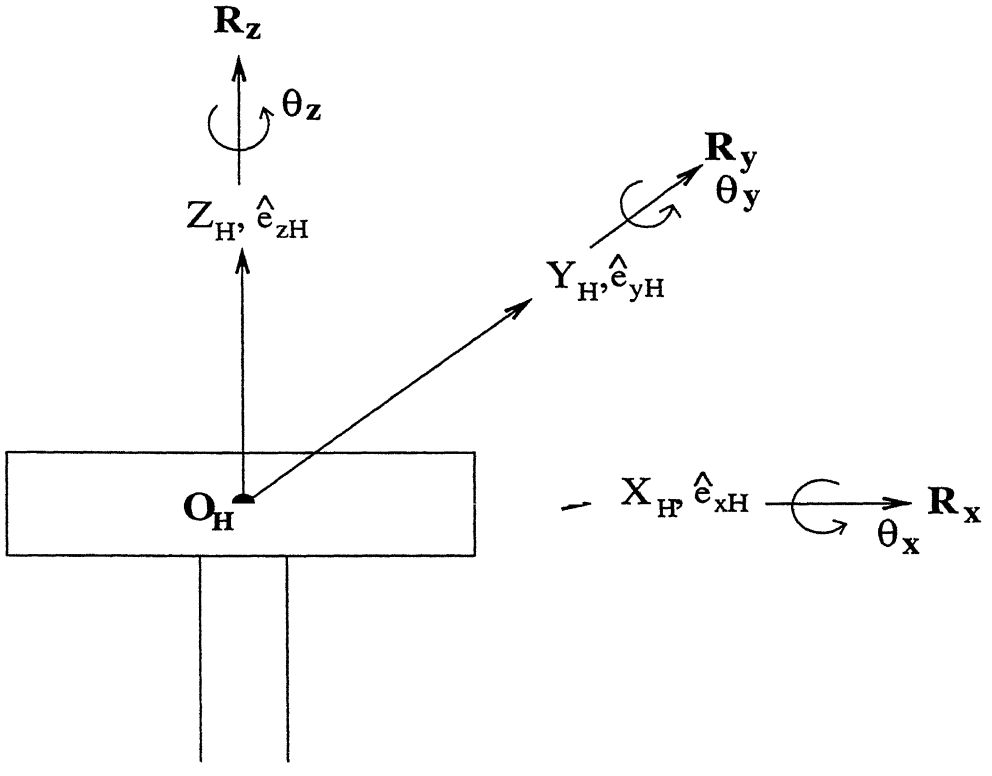

Figure 3 2 Hub fixed coordinate system-H

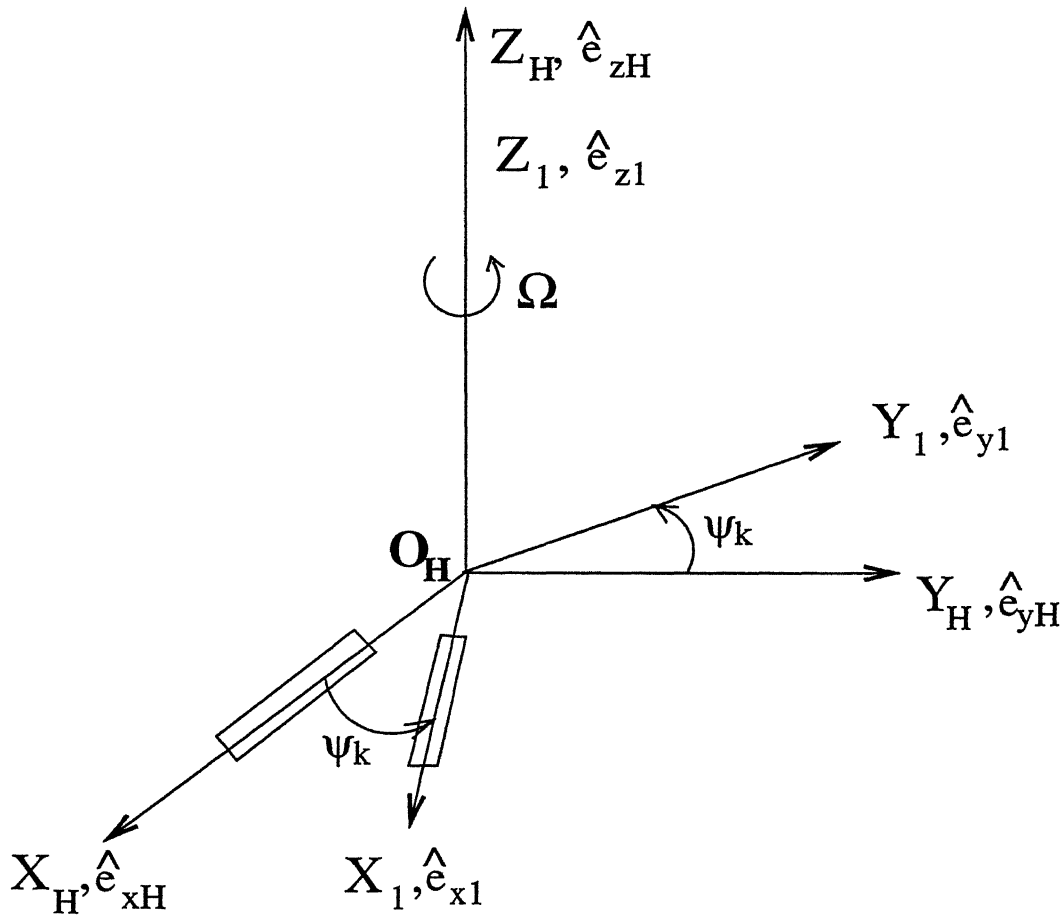

Figure 3 3 Rotating hub system-1

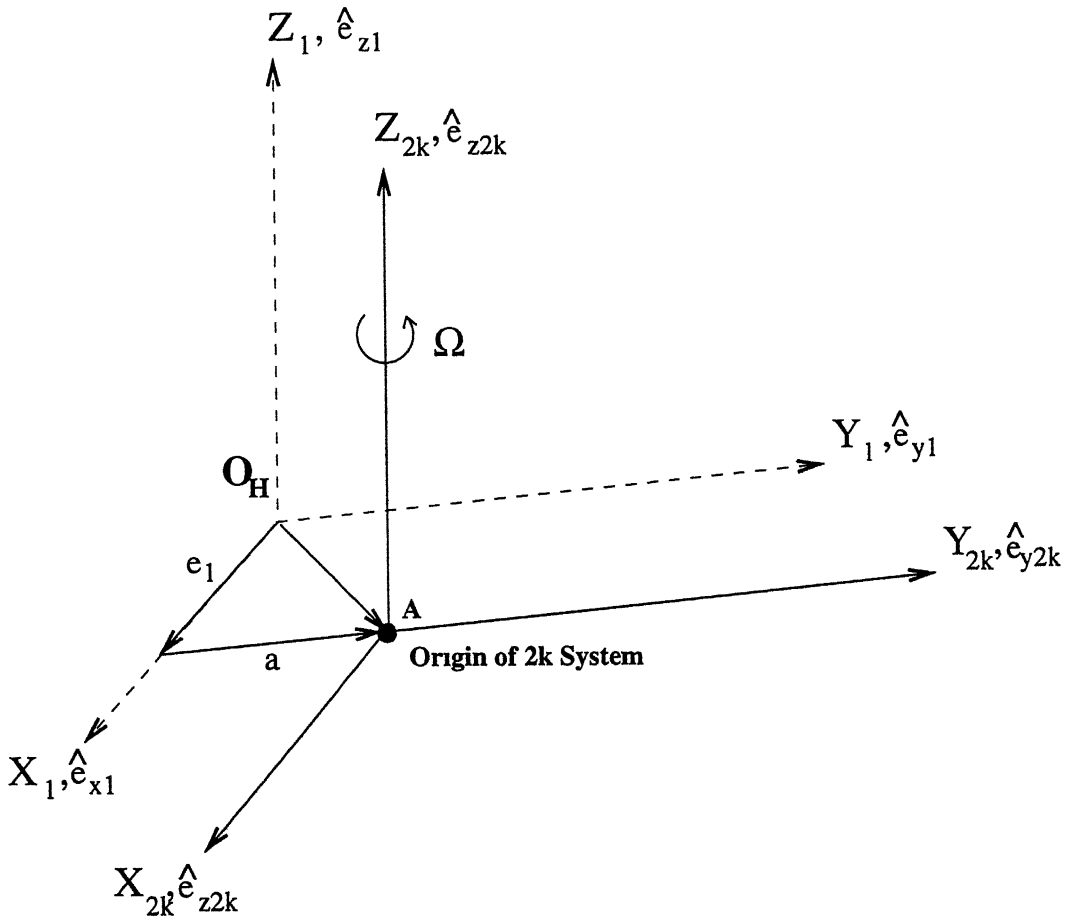

Figure 3 4 Rotating hub system-2

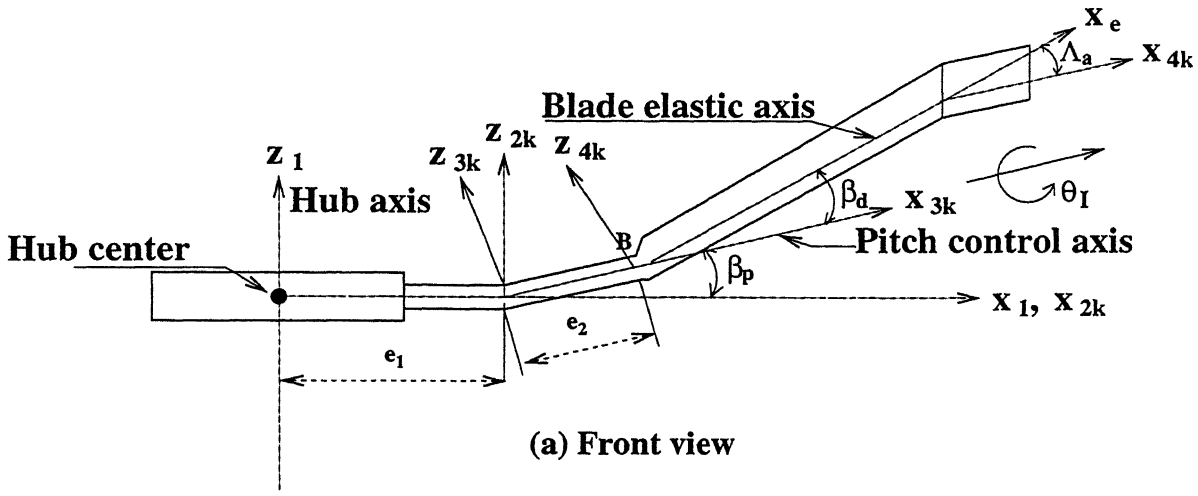

(a) Front view

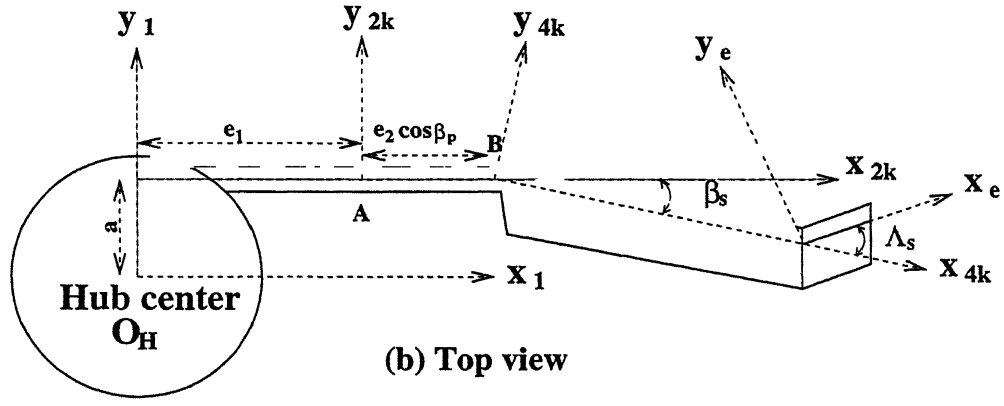

(b) Top view

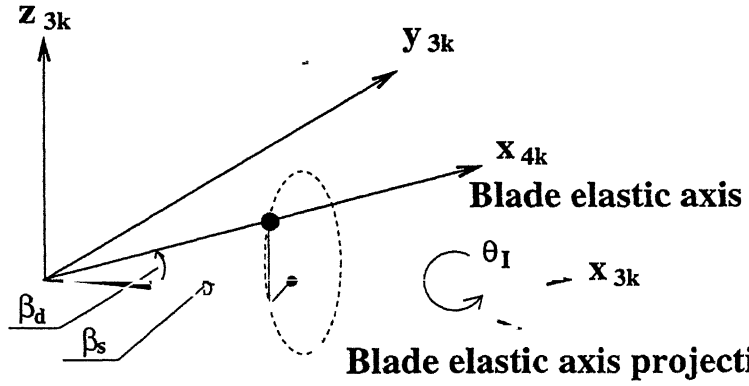

Blade elastic axis projection in x_{3k} - y_{3k} plane

(c) Blade motion due to pitch input

Figure 3 5 Blade coordinate system 3k and 4k

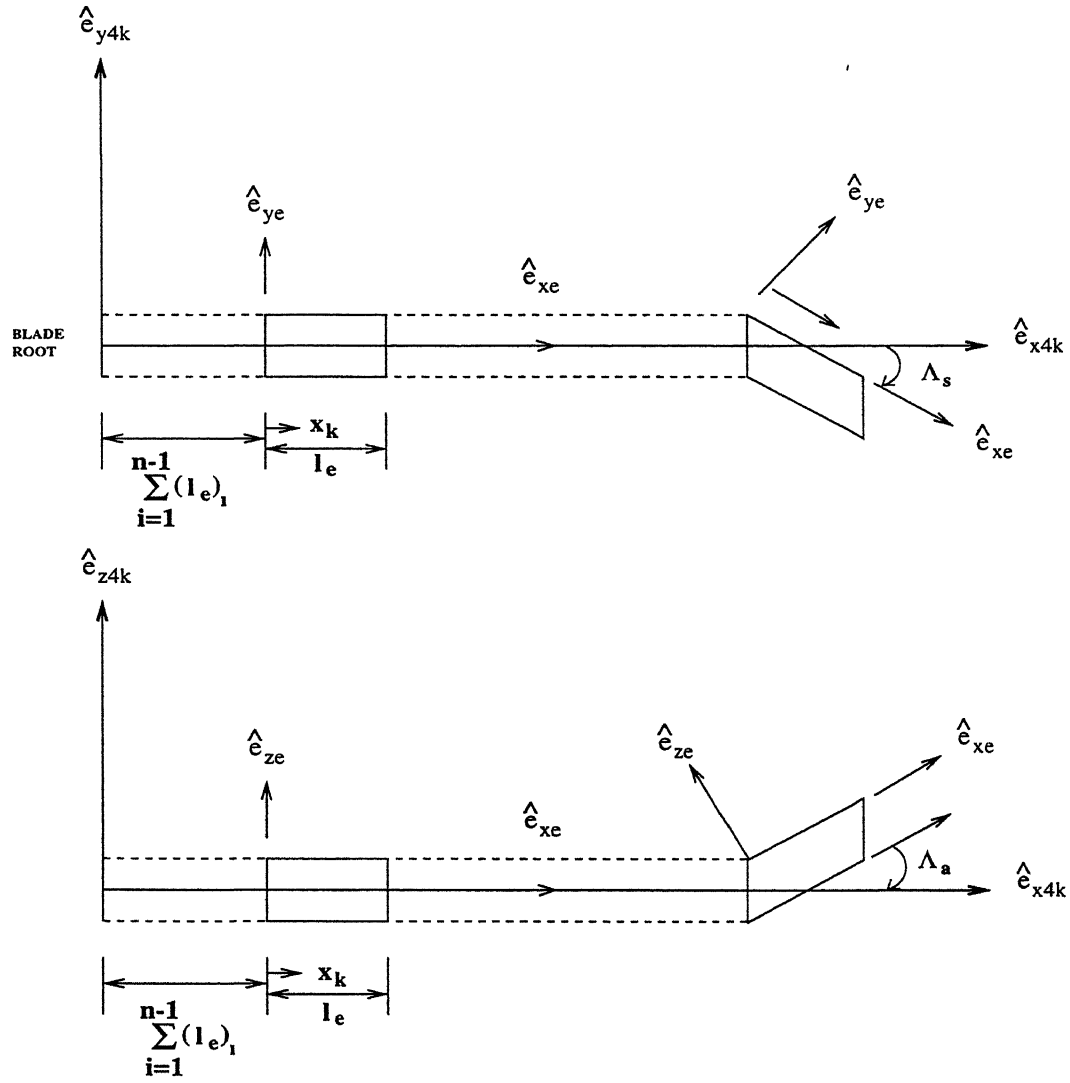

Figure 3 6 Undeformed element coordinate system

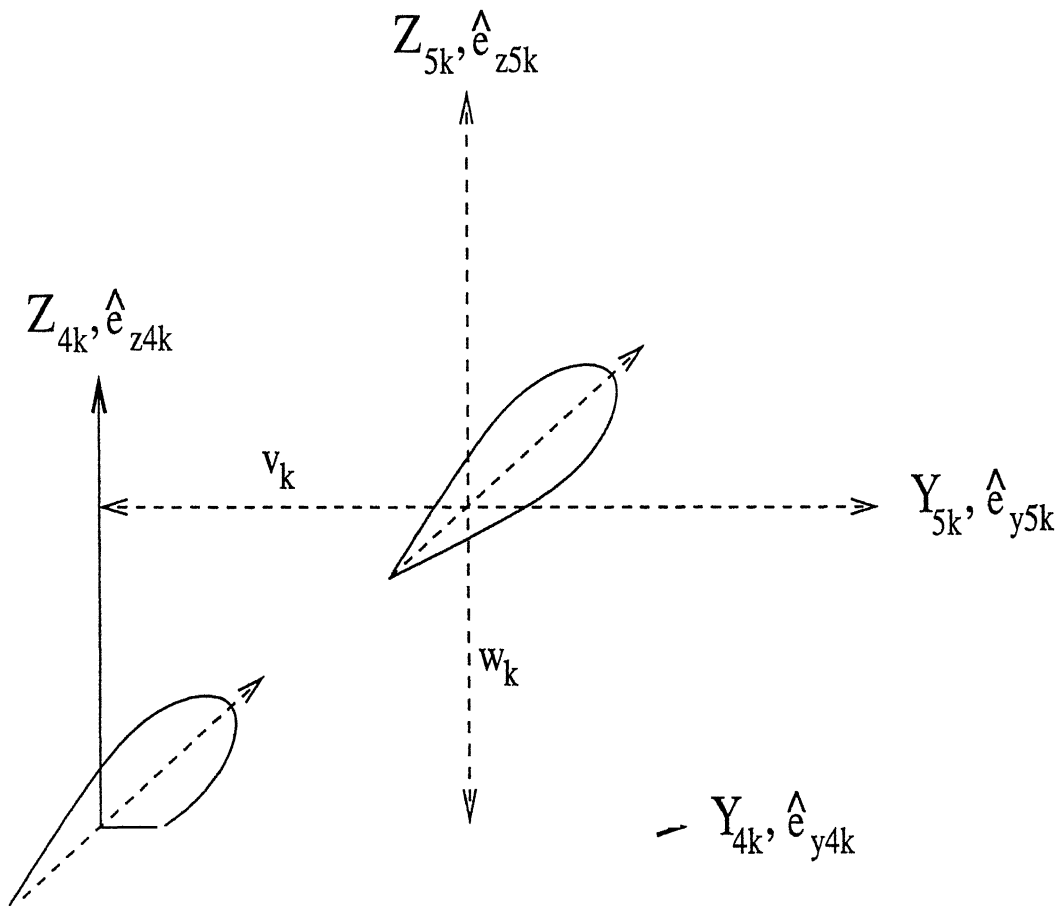

Figure 3 7 Rotating blade fixed system - 5k

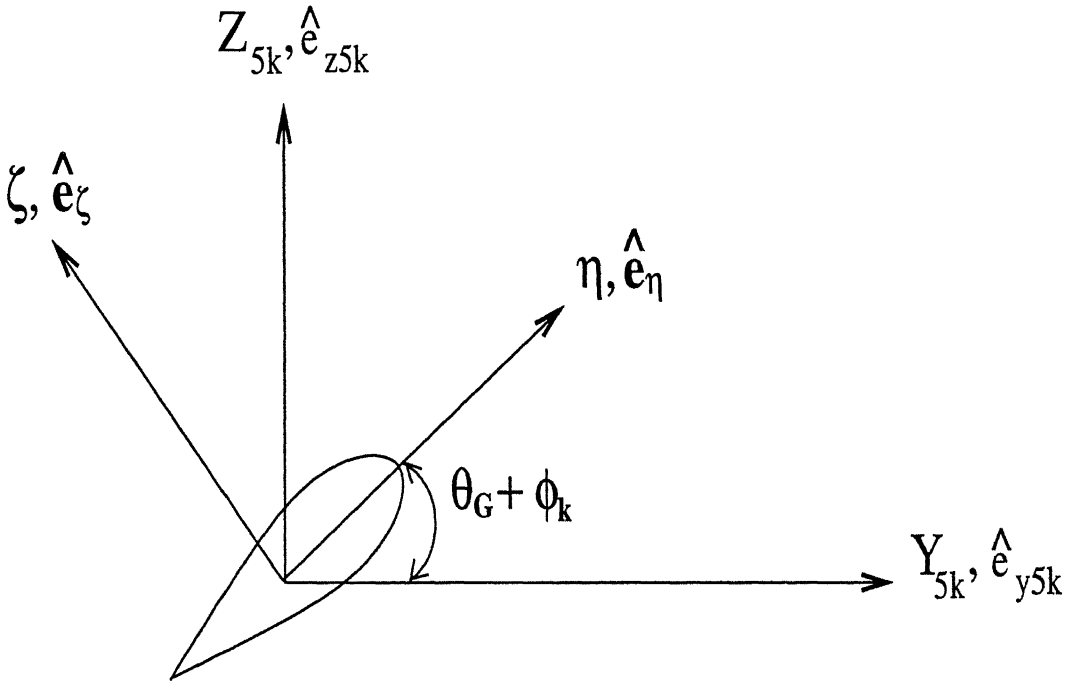

Figure 3 8 Cross-sectional principle coordinate system

Chapter 4

KINEMATICS

During operation, the rotor blade undergoes in-plane bending (lag), out-of-plane bending (flap), torsion and axial modes In addition, the hub centre has both translational (R_x, R_y, R_z) and rotational $(\theta_x, \theta_y, \theta_z)$ perturbational motion The formulation of inertia operator and aerodynamic operator requires a proper description of kinematics of the blade motion In this section, an expression for the absolute velocity vector at any arbitrary point 'p' on the blade is derived

4.1 POSITION VECTOR OF A POINT

The position vector of any arbitrary point 'p' in the n^{th} finite element of the deformed blade with respect to the hub centre O_H, is given by

$$\vec{r_p} = a\hat{e}_{y_1} + e_1\hat{e}_{x_{2k}} + e_2\hat{e}_{x_{3k}} + \sum_{i=1}^{n-1}(l_e)_i\hat{e}_{x_{4k}} + (x_k + u_k)\hat{e}_{x_e} + v_k\hat{e}_{y_e} + w_k\hat{e}_{z_e} + \eta\hat{e}_\eta + \zeta\hat{e}_\zeta \quad (4.1)$$

Transforming all the unit vectors to the 4K-system and neglecting the higher order terms, the position vector can be written as

$$
\begin{aligned}
\vec{r}_p = \quad & \hat{e}_{x_{4k}} l[-a(\beta_s \cos\theta_I + \beta_d \sin\theta_I) + e_1 + e_2 + \sum_{i=1}^{n-1}(l_e)_i \\
& + \cos\Lambda_s \cos\Lambda_a (x_k + u_k) + v_k i \sin\Lambda_s \cos\Lambda_a - w_k \sin\Lambda_a \\
& + \eta\{-v'_k \cos\Lambda_s \cos\Lambda_a \cos(\theta_G + \phi_k) - w'_k \cos\Lambda_s \cos\Lambda_a \sin(\theta_G + \phi_k) \\
& - \sin\Lambda_s \cos(\theta_G + \phi_k) + \cos\Lambda_s \sin\Lambda_a \sin(\theta_G + \phi_k)\} \\
& + \zeta\{v'_k \cos\Lambda_s \cos\Lambda_a \sin(\theta_G + \phi_k) - w'_k \cos\Lambda_s \cos\Lambda_a \cos(\theta_G + \phi_k) \\
& + \sin\Lambda_s \sin(\theta_G + \phi_k) + \cos\Lambda_s \sin\Lambda_a \cos(\theta_G + \phi_k)\}] \\
& + \hat{e}_{y_{4k}} l[a\cos\theta_I + e_1(\beta_s \cos\theta_I + \beta_d \sin\theta_I - \beta_p \sin\theta_I) + e_2(\beta_s \cos\theta_I \\
& + \beta_d \sin\theta_I) \sin\Lambda_s (x_k + u_k) + v_k \cos\Lambda_s + \eta\{-v'_k \sin\Lambda_s \cos\Lambda_a \cos(\theta_G + \phi_k) \\
& - w'_k \sin\Lambda_s \cos\Lambda_a \sin(\theta_G + \phi_k) + \cos\Lambda_s \cos(\theta_G + \phi_k) \\
& + \sin\Lambda_s \sin\Lambda_a \sin(\theta_G + \phi_k)\} + \zeta\{v'_k \sin\Lambda_s \cos\Lambda_a \sin(\theta_G + \phi_k) - w'_k \sin\Lambda_s \\
& \cos\Lambda_a \sin(\theta_G + \phi_k) - \cos\Lambda_s \sin(\theta_G + \phi_k) + \sin\Lambda_s \sin\Lambda_a \cos(\theta_G + \phi_k)\}] \\
& + \hat{e}_{z_{4k}} l[-a\sin\theta_I + e_1(-\beta_d \cos\theta_I + \beta_s \sin\theta_I - \beta_p \cos\theta_I) + e_2(-\beta_d \cos\theta_I \\
& + \beta_s \sin\theta_I) + \cos\Lambda_s \sin\Lambda_a (x_k + u_k) + v_k \sin\Lambda_s \sin\Lambda_a + w_k \cos\Lambda_a \\
& + \eta\{v'_k \sin\Lambda_a \cos(\theta_G + \phi_k) + w'_k \sin\Lambda_a \sin(\theta_G + \phi_k) + \cos\Lambda_a \sin(\theta_G + \phi_k)\} \\
& + \zeta\{w'_k \sin\Lambda_a \cos(\theta_G + \phi_k) - v'_k \sin\Lambda_a \sin(\theta_G + \phi_k) + \cos\Lambda_a \cos(\theta_G + \phi_k)\}]
\end{aligned}
\tag{4 2}
$$

In Eq 4 2 all the length quantities are non-dimensionalised with respect to the length of the blade l For the sake of convenience, the non-dimensional length quantities are referred without an overbar(¯) The expression given in Eq 4 2 is general, in the sense that for position vector of any point in the straight portion of blade Λ_a and Λ_s are set equal to zero Eq 4 2 can also be written in symbolic form as

$$
\vec{r_p} = l[r_x \hat{e}_{x_{4k}} + r_y \hat{e}_{y_{4k}} + r_z \hat{e}_{z_{4k}}]
$$

4.2 ANGULAR VELOCITY VECTOR

The angular velocity vector $\vec{\omega}$ of k^{th} blade consists of three components They are

- The constant rotational speed (Ω) of the rotor,
- the rigid body angular velocity($\vec{\omega}_{rigid}$) of the hub due to perturbational rotation in roll-pitch-yaw ($\theta_x, \theta_y, \theta_z$)
- the angular velocity contribution due to the rate of change of control pitch input $\Omega\theta_I$ to the blade

$$\vec{\omega} = \Omega\hat{e}_{zH} + \vec{\omega}_{rigid} + \Omega\theta_I\hat{e}_{x_{3k}} \tag{4 3}$$

where

$$\vec{\omega}_{rigid} = \Omega\theta_x\hat{e}_{x_{1k}} + \Omega\theta_y\hat{e}_{y_{1k}} + \Omega\theta_z\hat{e}_{z_{1k}} \tag{4 4}$$

where ( ) indicates differentiation with respect to the non-dimensional time ψ,

$$\psi = \Omega t$$

Note that

$$\frac{d}{dt}(\,) = \Omega\frac{d}{d\Omega t}(\,) = \Omega\frac{d}{d\psi}(\,) = \Omega(\,)$$

Transforming all the unit vectors of Eq 4 3 to the 4K-system and neglecting the higher order terms, the angular velocity of k^{th} blade can be written in symbolic form as

$$\vec{\omega} = \Omega[\omega_x\hat{e}_{x_{4k}} + \omega_y\hat{e}_{y_{4k}} + \omega_z\hat{e}_{z_{4k}}] \tag{4 5}$$

Where

$$\omega_x = [\theta_x\cos\psi_k + \theta_y\sin\psi_k + \theta_I(\beta_p + \beta_d\cos\theta_I - \beta_s\sin\theta_I)] \tag{4 6}$$

$$\omega_y = [-\theta_x\cos\theta_I\sin\psi_k + \theta_y\cos\theta_I\cos\psi_k + \theta_z\sin\theta_I + \theta_I(\beta_s\cos\theta_I + \beta_d\sin\theta_I)] \tag{4 7}$$

$$\omega_z = [\theta_x \sin\theta_I \sin\psi_k - \theta_y \sin\theta_I \cos\psi_k + \theta_z \cos\theta_I + \cos\theta_I + \theta_I(-\beta_d \cos\theta_I + \beta_s \sin\theta_I)] \tag{4 8}$$

4.3 VELOCITY AT A POINT

The absolute velocity vector $\vec{V}$ at a point 'p' on the deformed beam can be written as

$$\vec{V} = \vec{V}_H + \vec{r_p} + (\vec{\omega} \times \vec{r_p}) \tag{4 9}$$

where $\vec{V}_H$ is the rigid body perturbational translation of the hub center O_H which is given as

$$\vec{V}_H = \Omega l[R_x \hat{e}_{xR} + R_y \hat{e}_{yR} + R_z \hat{e}_{zR}] \tag{4 10}$$

Transforming all the unit vectors to 4K-system

$$\vec{V}_H = (V_H)_x \hat{e}_{x_{4k}} + (V_H)_y \hat{e}_{y_{4k}} + (V_H)_z \hat{e}_{z_{4k}} \tag{4 11}$$

where

$$\begin{aligned}(V_H)_x = \quad & \Omega l R_x\{\cos\psi_k + \sin\psi_k(\beta_s \cos\theta_I + \beta_d \sin\theta_I)\} \\ & + \Omega l R_y\{\cos\psi_k(\beta_s \cos\theta_I + \beta_d \sin\theta_I) + \sin\psi_k\} \\ & + \Omega l R_z\{(\beta_p + \beta_d \cos\theta_I - \beta_s \sin\theta_I)\}\end{aligned} \tag{4 12}$$

$$\begin{aligned}(V_H)_y = \quad & \Omega l R_x\{\cos\psi_k(\beta_s \cos\theta_I + \beta_d \sin\theta_I - \beta_p \sin\theta_I) - \sin\psi_k \cos\theta_I\} \\ & + \Omega l R_y\{\cos\psi_k \cos\theta_I + \sin\psi_k(\beta_s \cos\theta_I + \beta_d \sin\theta_I - \beta_p \sin\theta_I)\} \\ & + \Omega l R_z\{\sin\theta_I\}\end{aligned} \tag{4 13}$$

$$(V_H)_z = \Omega l R_x\{\cos\psi_k(-\beta_d\cos\theta_I + \beta_s\sin\theta_I - \beta_p\cos\theta_I) + \sin\psi_k\sin\theta_I\}$$

$$+ \Omega l R_x\{\cos\psi_k(-\sin\theta_I) + \sin\psi_k(-\beta_d\cos\theta_I + \beta_s\sin\theta_I - \beta_p\cos\theta_I)\}$$

$$+ \Omega l R_z\{\cos\theta_I\} \qquad (4\ 14)$$

$$\vec{r_p} = \hat{e}_{x_{4k}} l\Omega[-a\theta_I(-\beta_s\sin\theta_I + \beta_d\cos\theta_I) + \cos\Lambda_s\cos\Lambda_a u_k$$

$$+v_k\sin\Lambda_s\cos\Lambda_a - w_k\sin\Lambda_a + \eta\{-v_k'\cos\Lambda_s\cos\Lambda_a\cos(\theta_G+\phi_k)$$

$$+v_k'\phi_k\cos\Lambda_s\cos\Lambda_a\sin(\theta_G+\phi_k) - w_k'\cos\Lambda_s\cos\Lambda_a\sin(\theta_G+\phi_k)$$

$$-w_k'\cos\Lambda_s\cos\Lambda_a\phi_k\cos(\theta_G+\phi_k) - w_k'\cos\Lambda_s\cos\Lambda_a\sin(\theta_G+\phi_k)$$

$$+\phi_k\cos\Lambda_s\sin\Lambda_a\cos(\theta_G+\phi_k)\}$$

$$+\zeta\{-w_k'\cos\Lambda_s\cos\Lambda_a\cos(\theta_G+\phi_k) + w_k'\cos\Lambda_s\cos\Lambda_a\sin(\theta_G+\phi_k)$$

$$+v_k'\cos\Lambda_s\cos\Lambda_a\sin(\theta_G+\phi_k) + v_k'\cos\Lambda_s\cos\Lambda_a\phi_k\cos(\theta_G+\phi_k)$$

$$+\sin\Lambda_s\phi_k\cos(\theta_G+\phi_k) - \phi_k\cos\Lambda_s\sin\Lambda_a\sin(\theta_G+\phi_k)\}]$$

$$+\hat{e}_{y_{4k}} l\Omega[-a\theta_I\sin\theta_I + e_1\theta_I(-\beta_s\sin\theta_I + \beta_d\cos\theta_I - \beta_p\cos\theta_I)$$

$$+e_2\theta_I(-\beta_s\sin\theta_I + \beta_d\cos\theta_I) - u_k\sin\Lambda_s + v_k\cos\Lambda_s$$

$$+\eta\{-v_k'\sin\Lambda_s\cos\Lambda_a\cos(\theta_G+\phi_k) + v_k'\sin\Lambda_s\cos\Lambda_a\phi_k\sin(\theta_G+\phi_k)$$

$$-w_k'\sin\Lambda_s\cos\Lambda_a\sin(\theta_G+\phi_k) - w_k'\phi_k\sin\Lambda_s\cos\Lambda_a\cos(\theta_G+\phi_k)$$

$$-\phi_k\cos\Lambda_s\sin(\theta_G+\phi_k) + \phi_k\sin\Lambda_s\sin\Lambda_a\cos(\theta_G+\phi_k)\}$$

$$+\zeta\{-w_k'\sin\Lambda_s\cos\Lambda_a\cos(\theta_G+\phi_k) + w_k'\phi_k\sin\Lambda_s\cos\Lambda_a\sin(\theta_G+\phi_k)$$

$$+v_k'\sin\Lambda_s\cos\Lambda_a\sin(\theta_G+\phi_k) + v_k'\sin\Lambda_s\cos\Lambda_a\phi_k\cos(\theta_G+\phi_k)$$

$$-\phi_k\cos\Lambda_s\sin(\theta_G+\phi_k) - \phi_k\sin\Lambda_s\sin\Lambda_a\sin(\theta_G+\phi_k)\}]$$

$$+\hat{e}_{z_{4k}} l\Omega[-a\theta_I\cos\theta_I + e_1\theta_I(\beta_d\sin\theta_I + \beta_s\cos\theta_I + \beta_p\sin\theta_I)$$

$$+e_2\theta_I(\beta_d\sin\theta_I + \beta_s\cos\theta_I) + u_k'\cos\Lambda_s\sin\Lambda_a$$

$$+v_k \sin\Lambda_s \sin\Lambda_a + w_k \cos\Lambda_a$$

$$+\eta\{v'_k \sin\Lambda_a \cos(\theta_G+\phi_k) - v'_k\phi_k \sin(\theta_G+\phi_k) + w'_k \sin\Lambda_a$$

$$+\sin(\theta_G+\phi_k) + w'_k\phi_k \sin\Lambda_a \cos(\theta_G+\phi_k) + \phi_k \cos\Lambda_a \cos(\theta_G+\phi_k)\}$$

$$+\zeta\{w'_k \sin\Lambda_a \cos(\theta_G+\phi_k) - w'_k \sin\Lambda_a\phi_k \sin(\theta_G+\phi_k) - v'_k \sin\Lambda_a$$

$$+\sin(\theta_G+\phi_k) - v'_k \sin\Lambda_a\phi_k \cos(\theta_G+\phi_k) - \phi_k \cos\Lambda_a \sin(\theta_G+\phi_k)\}]$$

(4 15)

and

$$(\vec{\omega}\times\vec{r}) = \begin{vmatrix} \hat{e}_{x_{4k}} & \hat{e}_{y_{4k}} & \hat{e}_{z_{4k}} \\ \omega_x & \omega_y & \omega_z \\ r_x & r_y & r_z \end{vmatrix} \qquad (4\ 16)$$

where r_x, r_y, r_z and $\omega_x, \omega_y, \omega_z$ are the x,y and z components of $\vec{r_p}$ and $\vec{\omega}$ respectively Substituting various quantities in Eq 4 9 from Eqs 4 2, 4 6-4 8 and 4 11-4 16, the velocity at point p is obtained This can be written in symbolic form as

$$\vec{V} = \Omega l[V_x\hat{e}_{x_{4k}} + V_y\hat{e}_{y_{4k}} + V_z\hat{e}_{z_{4k}}] \qquad (4\ 17)$$

The detailed expression of the components of the velocity vector can be found in Ref [3]

Chapter 5

EQUATIONS OF MOTION FOR ROTOR BLADE

The coupled equations of motion of the rotor blade can be derived using Hamilton's principle The mathematical form of Hamilton's principle is stated as follows

$$\int_{t_1}^{t_2} (\delta U - \delta T - \delta W_e) dt = 0 \tag{5 1}$$

Where U is the strain energy, T is kinetic energy, W_e is the work done by the nonconservative external loads

In this chapter, the expressions for the variation of kinetic energy and strain energy of the rotor blade are derived

5.1 KINETIC ENERGY OF THE BLADE

The total kinetic energy of the beam, T, is defined as

$$\begin{aligned} T &= \frac{1}{2} \sum_i \int \int \int_V \rho \vec{V} \ \vec{V} dVol \\ &= \frac{1}{2} \sum_i \int_0^{(l_e)_i} \int \int_A \rho \vec{V} \ \vec{V} d\eta \ d\zeta \ dx \end{aligned} \tag{5 2}$$

Where $\vec{V}$ is the absolute velocity of an arbitrary point 'p' on the blade cross section with respect to a reference frame The variation of kinetic energy, δT can be written as

$$\delta T = \sum_i \int_0^{(l_e)_i} \int\int_A \rho \vec{V}\, \delta\vec{V} d\eta\, d\zeta\, dx \qquad (5\ 3)$$

Substituting for the velocity $\vec{V}$ from Eq 4 17 and integrating δT by parts with respect to time yields

$$\delta T = \sum_i \int_0^{(l_e)_i} \int\int_A \rho[Z_u\delta u + Z_v\delta v + Z_w\delta w + Z_v'\delta v' + Z_w'\delta w' + Z_\phi\delta\phi]d\eta\, d\zeta\, dx \quad (5\ 4)$$

Where the terms $Z_u, Z_v, Z_w, Z_v', Z_w'$ and Z_ϕ are the coefficients of $\delta u, \delta v, \delta w, \delta v', \delta w'$ and $\delta\phi$ in the variation of kinetic energy expression

Integration of the expression over cross-section yields

$$\delta T = m\Omega^2 l^3 \sum_i \int_0^{(l_e)_i} [\overline{Z}_u\delta u + \overline{Z}_v\delta v + \overline{Z}_w\delta w + \overline{Z}_v'\delta v' + \overline{Z}_w'\delta w' + \overline{Z}_\phi\delta\phi]d\eta\, d\zeta\, dx \quad (5\ 5)$$

after eliminating the higher order terms, the expressions for $\overline{Z_u}, \overline{Z_v}, \overline{Z_w}, \overline{Z_v'}, \overline{Z_w'}, \overline{Z_\phi}$ are obtained The detailed expressions of these terms can be found in Ref [3]

The cross-section integrals are defined as

$$\begin{aligned}
m &= \int\int_A \rho\, d\eta\, d\zeta \\
m\eta_m &= \int\int_A \rho\eta\, d\eta\, d\zeta \\
m\zeta_m &= \int\int_A \rho\zeta\, d\eta\, d\zeta \\
Im_{\eta\eta} &= \int\int_A \rho\zeta^2\, d\eta\, d\zeta \\
Im_{\zeta\zeta} &= \int\int_A \rho\eta^2\, d\eta\, d\zeta \\
Im_{\eta\zeta} &= \int\int_A \rho\eta\zeta\, d\eta\, d\zeta
\end{aligned}$$

Where m is mass per unit length of the blade, $m\eta_m$ and $m\zeta_m$ are first moments of cross-sectional mass per unit length, $Im_{\eta\eta}, Im_{\zeta\zeta}$ and $Im_{\eta\zeta}$ are the cross-sectional mass moments of inertia per unit length of the beam

5.2 TOTAL STRAIN ENERGY

The formulation of strain energy obtained in this section essentially follows the procedure given in Refs [4] and [5]

5.2.1 STRAIN ENERGY OF THE BEAM ELEMENT (BLADE / FLEXBEAM / TORQUE TUBE)

The strain energy of a beam element is given by

$$U_b = \frac{1}{2} E_o l^3 \int_0^{l_e} \int\int \begin{Bmatrix} \epsilon_{xx} \\ \gamma_{x\eta} \\ \gamma_{x\zeta} \end{Bmatrix}^T \begin{Bmatrix} \sigma_{xx} \\ \sigma_{x\eta} \\ \sigma_{x\zeta} \end{Bmatrix} d\eta \, d\zeta \, dx \tag{5 6}$$

5.2.1.1 Explicit Strain-Displacement Relations

The expression for non zero strain components written in terms of u,v,w and ϕ are given in Refs [4] and [5] They are

$$\epsilon_{xx} = \underline{u_x + \tfrac{1}{2}v_x^2 + \tfrac{1}{2}w_x^2} + \tfrac{1}{2}(\eta^2 + \zeta^2)\phi_x^2 + \alpha_x\psi$$
$$+\alpha\tau_0(\zeta\psi_\eta - \eta\psi_\zeta) - [\eta\cos(\theta_g + \phi) - \zeta\sin(\theta_g + \phi)]v_{xx}$$
$$-[\eta\sin(\theta_g + \phi) + \zeta\cos(\theta_g + \phi)]w_{xx} + \eta(\overline{\gamma}_{x\eta,x} - \tau_0\overline{\gamma}_{x\zeta}) + \zeta(\overline{\gamma}_{x\zeta,x} + \tau_0\overline{\gamma}_{x\eta})$$

$$\gamma_{x\eta} = \overline{\gamma}_{x\eta} + \alpha\psi_\eta - \zeta(\phi_x + \phi_0)$$

$$\gamma_{x\zeta} = \overline{\gamma}_{x\zeta} + \alpha\psi_\zeta - \eta(\phi_x + \phi_0)$$

where

$$\phi_0 = (v_{xx}\cos\theta_G + w_{xx}\sin\theta_G)(-v_x\sin\theta_G + w_x\cos\theta_G)$$

The underlined term in ϵ_{xx} represents the axial strain at the elastic axis These strain expressions can be simplified using the following assumptions

- the transverse shear at the elastic axis is assumed to be zero

- The warping amplitude α is assumed to be equal to $-\phi_x$

The simplified strain components can be written as

$$\epsilon_{xx} = u_x + \tfrac{1}{2}v_x^2 + \tfrac{1}{2}w_x^2 + \tfrac{1}{2}(\eta^2+\zeta^2)\phi_x^2 - \psi\phi_{xx} - [\tau_0(\zeta\psi_\eta - \eta\psi_\zeta)]\psi_x$$
$$-[\eta\cos(\theta_G+\theta_k) - \zeta\sin(\theta_G+\phi_K)]v_{xx} - [\eta\sin(\theta_G+\phi_K) + \zeta\cos(\theta_G+\phi_k)]w_{xx}$$

$$\gamma_{x\eta} = -(\psi_\eta + \zeta)\phi_x - \zeta\phi_0$$

$$\gamma_{x\zeta} = -(\psi_\zeta + \eta)\phi_x + \eta\phi_0$$

$$\phi_0 = (v_{xx}\cos\theta_G + w_{xx}\sin\theta_G)(-v_x\sin\theta_G + w_x\cos\theta_G)$$

5.1.1.2 Stress-Strain Relations

Assuming that the blade is made of isotropic material, the stress-strain relationship is given by the following equations

$$\begin{Bmatrix} \sigma_{xx} \\ \sigma_{x\eta} \\ \sigma_{x\zeta} \end{Bmatrix} = \begin{bmatrix} E & 0 & 0 \\ 0 & G & 0 \\ 0 & 0 & G \end{bmatrix} \begin{Bmatrix} \epsilon_{xx} \\ \gamma_{x\eta} \\ \gamma_{x\zeta} \end{Bmatrix} \tag{5 7}$$

5.2.2 STRAIN ENERGY OF THE ELASTOMER

The elastomer is placed between flexbeam and torque tube at a distance of L_{el} from the root as shown in Fig 2 1 It is assumed to be placed between i^{th} node on the flexbeam and j^{th} node on the torque tube The elastomer is modelled as a combination of three linear springs, one each in flap, lag and torsion modes respectively

The strain energy of the elastomer U_{el} can be written as

$$U_{el} = \frac{1}{2}K_F(w_i - w_j)^2 + \frac{1}{2}K_L(v_i - v_j)^2 + \frac{1}{2}K_\phi(\phi_i - \phi_j)^2 \tag{5 8}$$

where K_F, K_L and K_ϕ are elastomer stiffnesses in flap, lag and torsion modes

5.2.3 STRAIN ENERGY OF THE CONTROL SPRING

The control spring is located at a distance of L_c from the root with an offset a_c from the reference elastic axis It is attached at m^{th} node on the torque tube The control spring is assumed to be linear having a stiffness K_c

The deformation of the control spring due to deflection at the m^{th} mode of the torque tube can be written as

$$d_c = w_m + a_c\phi_m$$

The strain energy of the control spring U_c is given as

$$U_c = \frac{1}{2}K_c d_c^2 \tag{5 9}$$

The total strain energy of the system can be written as U= $U_b + U_{el} + U_c$

5.3 TOTAL STRAIN ENERGY VARIATION

5.3.1 VARIATION IN STRAIN ENERGY OF THE BEAM ELEMENT (BLADE / FLEXBEAM / TORQUE TUBE)

The variation in strain energy of a beam element is given by

$$\delta U_b = E_o l^3 \int_0^{l_e} \int\int \left\{ \begin{array}{c} \delta\epsilon_{xx} \\ \delta\gamma_{x\eta} \\ \delta\gamma_{x\zeta} \end{array} \right\}^T \left\{ \begin{array}{c} \sigma_{xx} \\ \sigma_{x\eta} \\ \sigma_{x\zeta} \end{array} \right\} d\eta\, d\zeta\, dx \tag{5 10}$$

5.3.2 VARIATION IN STRAIN ENERGY OF THE ELASTOMER

The variation in strain energy of the elastomer δU_{el} is given as

$$\delta U_{el} = K_F(w_i - w_j)(\delta w_i - \delta w_j) + K_L(v_i - v_j)(\delta v_i - \delta v_j) + K_\phi(\phi_i - \phi_j)(\delta\phi_i - \delta\phi_j) \quad (5\ 11)$$

5.3.3 STRAIN ENERGY OF THE CONTROL SPRING

The variation in strain energy of the control spring δU_c is given as

$$\delta U_c = K_c(w_m + a_c\phi_m)(\delta w_m + a_c\delta\phi_m) \quad (5\ 12)$$

Total strain energy variation is $(\delta U) = \delta U_b + \delta U_{el} + \delta U_c$

The detail expressions of strains and their variations are available in Ref [3]

Chapter 6

FORMULATION OF ELEMENT MATRICES ASSOCIATED WITH KINETIC AND STRAIN ENERGY VARIATION

6.1 FINITE ELEMENT DISCRETIZATION

The variational expressions associated with the kinetic and potential energy of the rotor blades are nonlinear The unknowns are the deformation functions u, v, w and ϕ These are dependent on both space and time The spatial dependence is eliminated using Rayleigh-Ritz finite element formulation The blade is divided into subregions (finite elements) as shown in Fig 6 1, and the total dynamic potential is calculated for each subregion By applying Hamilton's principle to each subregion, a discretized form of the equations of motion can be obtained In this development, each subregion is modelled by a straight beam type finite element These beam elements are located along the reference elastic axis (line of shear centres) of the blade

The discretized form of Hamilton's principle is written as

$$\int_{t1}^{t2} \sum_{i=1}^{N} (\delta U_i - \delta T_i - \delta W_{ei}) dt = 0 \qquad (6\ 1)$$

Where

N= Total number of finite elements in the model

δU_i= Variation of the strain energy of the i^{th} element

δT_i= Variation of the kinetic energy of the i^{th} element

δW_{ei}= Virtual work of the external loads on i^{th} element

The bearingless rotor is divided into three structural elements namely, (1) flexbeam, (2) blade and (3) torque tube Each structural element is divided into finite number of beam elements Assume that the four unknown displacement functions of the beam finite element are expressed in the following form

$$\begin{Bmatrix} v \\ w \\ \phi \\ u \end{Bmatrix} = \begin{bmatrix} \{\phi_v\}^T & 0 & 0 & 0 \\ 0 & \{\phi_w\}^T & 0 & 0 \\ 0 & 0 & \{\phi_\phi\}^T & 0 \\ 0 & 0 & 0 & \{\phi_u\}^T \end{bmatrix} \begin{bmatrix} \{V\} \\ \{W\} \\ \{\Phi\} \\ \{U\} \end{bmatrix} \qquad (6\ 2)$$

where $\{\phi_v\}, \{\phi_w\}, \{\phi_\phi\}, \{\phi_u\}$ are space dependent interpolation functions, and {V}, {W}, {Φ}, {U} are time dependent values of v,w, ϕ, u respectively

$$\{V\} = \begin{Bmatrix} v_1 \\ v_1' \\ v_2 \\ v_2' \end{Bmatrix}, \{W\} = \begin{Bmatrix} w_1 \\ w_1' \\ w_2 \\ w_2' \end{Bmatrix}, \{\Phi\} = \begin{Bmatrix} \phi_1 \\ \phi_{12} \\ \phi_2 \end{Bmatrix}, \{U\} = \begin{Bmatrix} u_1 \\ u_{12} \\ u_2 \end{Bmatrix}$$

The nodal coordinates are shown in Fig 6 2

The variation of the displacement function for the beam can be written as

$$\begin{Bmatrix} \delta v \\ \delta w \\ \delta \phi \\ \delta u \end{Bmatrix} = \begin{bmatrix} \{\phi_v\}^T & 0 & 0 & 0 \\ 0 & \{\phi_w\}^T & 0 & 0 \\ 0 & 0 & \{\phi_\phi\}^T & 0 \\ 0 & 0 & 0 & \{\phi_u\}^T \end{bmatrix} \begin{bmatrix} \{\delta V\} \\ \{\delta W\} \\ \{\delta \Phi\} \\ \{\delta U\} \end{bmatrix} \tag{6 3}$$

In this development a cubic Hermite interpolation polynomial, $\{\Phi_c\}$, is used for the bending deflections (v,w) and a quadratic Lagrangian interpolation polynomial,$\{\Phi_q\}$, is used for torsional rotation (ϕ) and axial deflection (u) The mathematical expressions for these polynomials are given as

$$\left\{ \begin{array}{c} \phi_v \end{array} \right\} = \left\{ \begin{array}{c} \phi_w \end{array} \right\} = \begin{bmatrix} 1 - 3\xi^2 + 2\xi^3 \\ l_e(\xi - 2\xi^2 + \xi^3) \\ 3\xi^2 - 2\xi^3 \\ l_e(-\xi^2 + \xi^3) \end{bmatrix} = \left\{ \begin{array}{c} \Phi_c \end{array} \right\} \tag{6 4}$$

$$\left\{ \begin{array}{c} \phi_\phi \end{array} \right\} = \left\{ \begin{array}{c} \phi_u \end{array} \right\} = \begin{bmatrix} 1 - 3\xi + 2\xi^2 \\ 4\xi - 4\xi^2 \\ (-\xi + \xi^2) \end{bmatrix} = \left\{ \begin{array}{c} \Phi_q \end{array} \right\} \tag{6 5}$$

where

$\xi = x_k/l_e$

x_k = spanwise (axial) coordinate of the beam element

l_e = length of beam element

For bending deformations, the nodal parameters are the displacements and slopes at both ends of the element Therefore, the resulting elements will have inter-element continuity for both displacement and slopes In addition, because of the cubic interpolation polynomial, bending strains vary linearly over the element length The quadratic Lagrangian interpolation polynomial is used for torsion(ϕ) and axial deformation(u) This polynomial has the capability of modelling a linear variation of

strains along the element length and therefore provides the same level of accuracy as the beam bending element The nodal parameters for these elements are chosen as the values of the displacements functions at the two end nodes and at the mid-point of the element

The resulting beam element has 14 degree of freedom They are 4 in-plane (lag) bending degrees of freedom, 4 out-plane (flap) degrees of freedom, and 3 degrees of freedom each of torsion (ϕ), and axial deflection (u) The nodal degrees of freedom are shown in Fig 6 2

6.2 ELEMENT MATRICES ASSOCIATED WITH KINETIC ENERGY VARIATION

The beam element matrices associated with the kinetic energy variation are derived by substituting the assumed expressions for the displacements functions (Eq 6 2) in the kinetic energy variation δT (Eq 5 5) and carrying out the integration over the length of the beam element The resulting variation of the kinetic energy can be written in the form

$$\delta T_i = -\{\delta_q\}^T([M]_{14\times14}\{q\} + [M^C]_{14\times14}\{q\} + [K^{cf}]_{14\times14}\{q\} + \{V^L\}_{14\times1}$$
$$+[M^1]_{14\times3}\begin{Bmatrix} R_x \\ R_y \\ R_z \end{Bmatrix} + [M^2]_{14\times3}\begin{Bmatrix} R_x \\ R_y \\ R_z \end{Bmatrix} + [M^3]_{14\times3}\begin{Bmatrix} \theta_x \\ \theta_y \\ \theta_z \end{Bmatrix}$$
$$+[M^4]_{14\times3}\begin{Bmatrix} \dot{\theta}_x \\ \theta_y \\ \theta_z \end{Bmatrix} + \{V^I\}_{14\times1} + \{V^{NL}\}_{14\times1} \qquad (6\ 6)$$

Where $\{q\}$ represents the vector of unknown nodal degrees of freedom

$$\{q\}_{14\times 1} = \begin{bmatrix} \{V\} \\ \{W\} \\ \{\Phi\} \\ \{U\} \end{bmatrix} \tag{6 7}$$

Detailed expressions for the various matrices defined in Eq 6 6 are given in Ref [3]

6.3 ELEMENT MATRICES ASSOCIATED WITH STRAIN ENERGY VARIATION

The elementary matrices associated with the strain energy can be obtained by taking variation of strain energy It can be written as

$$\delta U_i = E_0 l^3 \{\delta q\}^T \{[K^E]\{q\} + \{F^E\} \tag{6 8}$$

Where { q } represents the vector of unknown degree of freedom

$[K^E]$ is the linear stiffness matrix $\{F^E\}$ is the nonlinear stiffness vector

The detailed expressions for the $[K^E]$ and $\{F^E\}$ are found in Ref [3]

6.4 ASSEMBLY OF ALL THE MATRICES

After formulating all the elementary matrices for flexbeam, blade and torque tube the final assembly is performed The block diagram of global matrix is shown in Fig 6 3

The contributions due to elastomer and control spring are added to the global matrix at the appropriate nodes

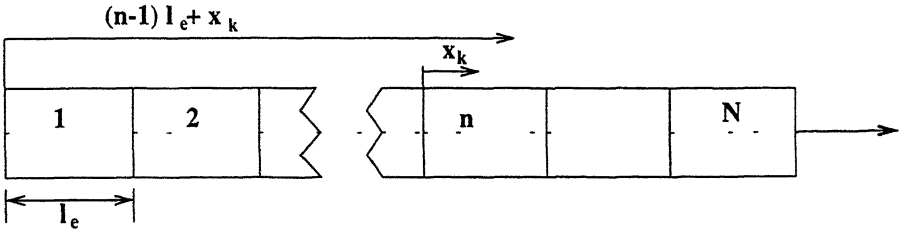

Figure 6 1 Finite element model of a blade

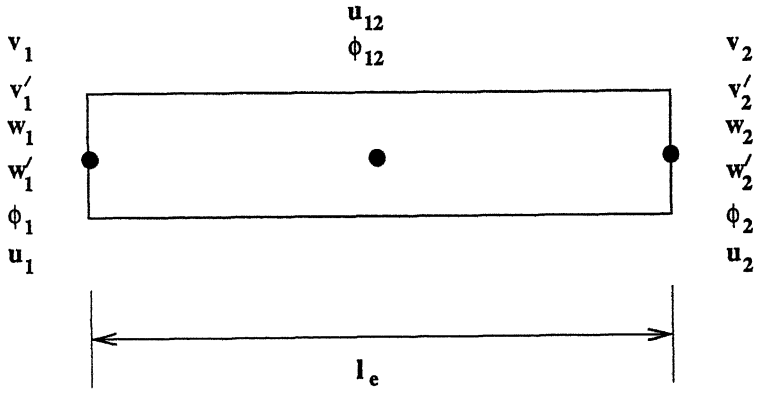

Figure 6 2 Element nodal degrees of freedom

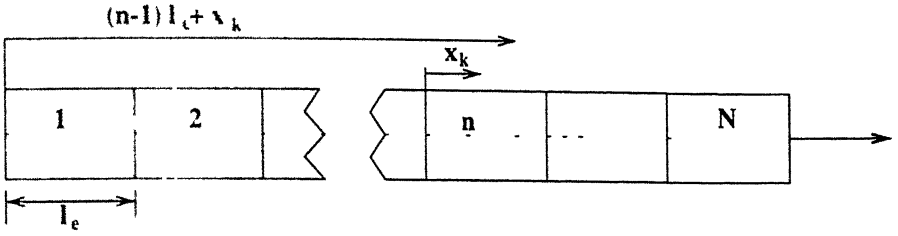

Figure 6 1 Finite element model of a blade

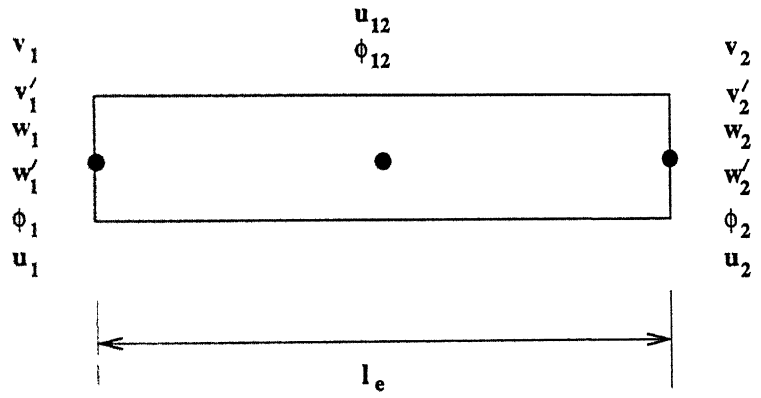

Figure 6 2 Element nodal degrees of freedom

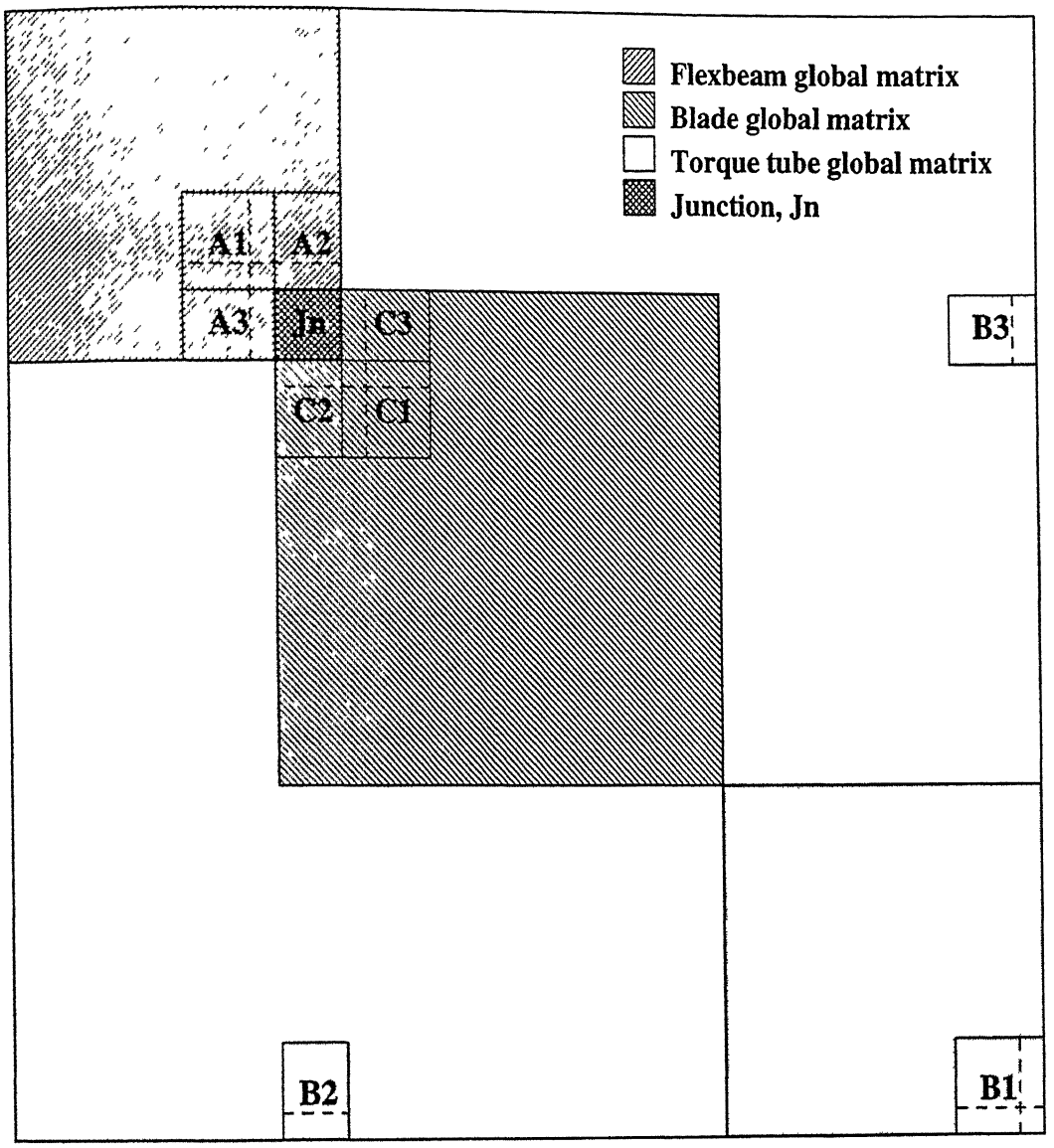

A1, A2, A3 and A4 together will form the junction element for flexbeam.
B1, B2, B3 and B4 together will form the junction element for torque tube.
C1, C2, C3 and C4 together will form the junction element for blade.
A1, B1 and C1 are the independent dof. with junction, of flexbeam, blade and torque rube respectively.
A2 and A3, B2 and B3 and C2 and C3 are the coupling terms of flexbam, blade and torque tube with junction dof.
A4, B4 and C4 are the junction dof. of flexbem, blade and torque tube.

Figure 6 3 Schematic diagram of global matrix

Chapter 7

RESULTS AND DISCUSSION

The first step in any aeroelastic response and stability analysis is the evaluation of natural frequencies and mode shapes of the rotor blade Using the inertial and structural model developed in this study, a structural dynamic analysis was performed It may be noted that the inertial and structural operators given in equation (6 6) and (6 8) respectively, are non-linear Since the structural dynamic analysis requires only linear terms, all the non-linear terms are neglected The corresponding linear equation for ith beam finite element can be written as

$$[M]_i\{q\}_i + [K]_i\{q\}_i = 0 \tag{7 1}$$

Where $[M]_i$ represents the mass matrix of ith element, $[K]_i$ represents the stiffness matrix of the ith element The detailed expressions for $[M]_i$ and $[K]_i$ matrices can be found in Ref [3] The elementary matrices of flexbeam, blade and torque tube are assembled to get the global matrices as shown in Fig 6 3

The contributions due to elastomer and control spring are added to the global matrix at the appropriate nodes Imposing the root boundary conditions, corresponding rows and columns are eliminated from the global matrices Then the resulting final global matrix equation can be written as

$$[M]\{q\} + [K]\{q\} = 0 \tag{7 2}$$

Performing an eigen analysis, the natural frequencies of an undamped rotating blade in vacuum can be evaluated

7.1 VALIDATION

In order to validate the finite element blade model developed in this study, the results of the present analysis are compared (for certain specific cases) with those available in the literature The data shown in Table 7 1, correspond to a uniform, untwisted straight bearingless rotor blade for which uncoupled natural frequencies have been evaluated in Ref [1] In this case the stiffness data for flexbeam and blade are same Torque tube is assumed to be rigid and massless The finite element code developed, in this study is suitably modified to get the natural frequencies for a bearingless rotor blade with rigid and massless torque tube The terminology soft-in-plane blade configuration indicates that the first non-dimensional rotating lag frequency is less than 1

Using the data given in Table 7 1, the coupled natural frequencies of the rotating bearingless rotor blade are calculated The total number of rotor beam elements are 20, of which 6 correspond to flexbeam and the remaining 14 correspond to blade The torque tube is attached to the flexbeam-blade junction at a distance(ξ_1) of 0 3l from the root The free end of the torque tube is at a distance(ξ_2) of 0 1l from the root The elastomer is located at a distance(L_{el}) of 0 1l from the root In this case the control spring(K_c) has zero stiffness The results of the present analysis are shown in Tables 7 2 and 7 3 respectively for flap and lag modes

The natural frequencies were evaluated for two different values of elastomer stiffnesses It may be noted that even though the present formulation can treat coupled modes, for the assumed data the coupling between flap, lag and torsional modes is zero From Tables 7 2 and 7 3, it can be seen that the results of the present study are in excellent agreement with the results obtained in Ref [1]

7.2 EFFECT OF MODELING OF TORQUE TUBE

Influence of modeling the torque tube on the dynamic characteristics of the bearingless rotor blade has been analysed by treating the torque tube as either a rigid, massless beam(Model I) or as a flexible member having very high stiffness in all modes as compared to the stiffness of the flexbeam(Model II)

The data pertaining to Model I is given in Table 7 1 Model II has the same data as Model I for flexbeam and blade But torque tube stiffness values are assumed to be 500 times more than the properties of the blade in flap, lag and torsion In axial direction, torque tube stiffness is 50 times more than that of the blade Results are generated for two sets of different values of elastomer stiffnesses The non-dimensional stiffness values of the elastomer for the two cases are $K_L = 30\ 1, K_F = 10\ 6$ and $K_L = 90\ 3, K_F = 31\ 8$ The natural frequencies of the rotor blade corresponding to the two torque tube models are shown in Table 7 4

The results indicate that the natural frequencies are high for Model II as compared to Model I in flap and lag modes The influence of modelling the torque tube is dominant in fundamental flap and lag modes The reason for this behaviour could be attributed to the strain energy stored in the torque tube for the Model II, whereas in Model I due to the assumption of rigid torque tube, there is no strain energy associated with it

7.3 INFLUENCE OF CONTROL SYSTEM STIFFNESS

For the study presented in Sec 7 1 and 7 2, the control system stiffness K_c has been set equal to zero To simulate a realistic bearingless rotor blade, a control spring has been added to the rotor blade model A study has been performed to analyse the effect of control spring stiffness on the natural frequencies and the magnitude of coupling between flap-lag-torsion in various mode shapes The data

corresponding to this study are given in Table 7 5 The geometric parameters are $\xi_1 = 0\ 3l, \xi_2 = 0\ 01l, L_c = 0\ 02l$ and $L_{el} = 0\ 05l$

The influence of increasing control spring stiffness(K_c) on natural frequencies in first six modes are shown in Figs 7 1 to 7 6 Since control spring does not affect lag modes, natural frequencies in lag modes are not influenced by variation in control spring stiffness as can be seen in Figs 7 1 and 7 4 The other four natural frequencies exhibit an increase and reach asymptotic values with increase in K_c

The effects of control spring on mode shapes are shown in Figs 7 7 to 7 12 Lag mode shapes are not influenced by control spring as can be seen in Figs 7 7 and 7 10 The effect of control spring is to highly couple the flap and torsional deformations, in flap modes as shown in Figs 7 8, 7 9 and 7 12 It is interesting to note that the participation of torsional motion substantially increases with increase in natural frequency in these modes

The influence of control spring on torsion is shown in Fig 7 11 The effect of control spring seems to increase the torsional frequency from $\overline{\omega}_n$= 3 7095(with $K_c = 0$) to $\overline{\omega}_n$= 4 4108(with $K_c = 1000$) with marginal influence on the mode shapes

7.4 EFFECTS OF LOCATION OF ELASTOMER, CONTROL SPRING AND FLEXBEAM-TORQUE TUBE JUNCTION

The effect of varying the elastomer location, control spring location and the location of flexbeam-torque tube junction on the natural frequencies have been analysed for several combination of the geometric parameters The data used for this analysis is given in Table 7 5 the control spring stiffness is taken as $K_c = 1000$ The control spring location(L_c) is varied from 0 01l to 0 03l in steps of 0 01l The elastomer location from the root(L_{el}) is varied from 0 05l to 0 15l in steps of 0 02l The

junction, where flexbeam blade and torque tube meets, is located at a distance(ξ_1) from the root and it is varied from 0 2l to 0 3l in steps of 0 02l The offset of the control spring from the elastic axis is set at a_c = 0 05l The variation of natural frequencies are shown in 3D plots in Figs 7 13 to 7 18

It is evident from all these figures that the general behaviour of the variation of natural frequencies seems to be less influenced by the variation in location of control spring L_c The figures shows that all natural frequencies decrease as the elastomer moves away from the root This may be due to the increase in the length of the flexible element near the root of the rotor blade The first two (1st lag, 1st flap) natural frequencies exhibit a slightly increase and then decrease as the junction moves away from the root as shown in Figs 7 13 to 7 14 However the third and fourth natural frequencies(Figs 7 15 and 7 16) decrease as the location of the junction(ξ_1) moves away from root On the otherhand, the sixth natural frequency(3rd flap) increases as the junction moves away from the root(Fig 7 18) The natural frequency in torsion increases as the junction moves away from the root For all these cases the numerical values are given in Appendix A

7.5 EFFECTS OF TIP SWEEP AND ANHEDRAL ANGLES WITH AND WITHOUT CONTROL STIFFNESS

The influence of tip sweep and anhedral angles on the natural frequencies and bending-torsion couplings of the rotor blade are analysed The bearingless rotor blade data is given in Table 7 5 The flexbeam, blade and torque tube are divided into 3, 7 and 4 elements elements respectively The swept tip portion of the blade is taken as one element having a length 0 1l The geometric parameters for all the cases are set at ξ_1 = 0 3l, ξ_2 = 0 01l, L_{el} = 0 05l and L_c = 0 02l The sweep and anhedral angles are varied from -30 to +30 in steps of 5 degrees The coupled

natural frequencies and mode shapes for two cases of control spring stiffness($K_c = 0$ and $K_c = 1000$), have been evaluated In total there are 169+169 = 338 cases The variation of natural frequencies with sweep angles are shown in 3D plots from Fig 7 19 to 7 24

Figure 7 24 shows the variation of first lag frequency with sweep angles Depending on the value of anhedral angle(Λ_a), the first natural frequency decreases monotonically with sweep angle(for Λ_a = + 30deg) or decreases and increases with increase in sweep angles(for Λ_a = -30deg) The first lag frequency varies from 0 7533(for Λ_s = -30deg, Λ_a = 30deg) to 0 6396(for Λ_s = 30deg, Λ_a = 20deg) The control stiffness does not have any influence on lag frequencies A similar nature is also observed for second lag frequency, as shown in Fig 7 22 The second lag frequency varies from 3 3755(for Λ_s = -30deg, Λ_a = 30deg) to 3 1550(for Λ_s = 30deg, Λ_a = 30deg)

The variation of first flap frequency with sweep angle is shown in Fig 7 19 Depending on the value of the anhedral angle the flap frequency increases monotonically(for Λ_a = +30deg) or decreases monotonically(for Λ_a = -30deg) with increase in sweep angles The influence of sweep angle is more pronounced for large values of anhedral angles The first flap frequency varies from 1 1883(for $\Lambda_s = \Lambda_a$ = -30deg) to 1 1154(for Λ_s = -25deg, Λ_s = 30deg) without control spring When the control stiffness is included the first flap frequency varies from 1 1942(for $\Lambda_s = \Lambda_a$ = 30deg) to 1 1201(for Λ_s = 30deg, Λ_a = -25deg) A similar behavior can also seen in second and third flap frequencies as shown in Figs 7 21 and 7 24

The torsional frequency seems to be less influenced by sweep and anhedral angles as shown in Fig 7 23 But the addition of control spring stiffness increases the torsional frequency

It is found from the results that anhedral angle alone introduces lag-torsion coupling and sweep angle alone introduces flap-torsion coupling

The sweep angles introduce coupling between flap, lag and torsional deformations in various modes To quantify the lag-torsion and flap-torsion couplings in

various modes, the value of torsional deformation at 0 75l($\Phi_{0\,75}$) is taken as reference parameter, since this cross-section is treated as typical section for aerodynamic load calculations in a rotor blade The variation of $\Phi_{0\,75}$ as a function of sweep angles is shown in Figs 7 25 to 7 30

In first lag mode, for the case with $K_c = 0$, the lag-torsion coupling is significantly influenced by anhedral angle compared to sweep angle as shown in Fig 7 25a With the inclusion of control spring($K_c = 1000$), both sweep and anhedral angle influences the lag-torsion coupling A similar observation can be seen in second lag mode shape

It is interesting to note that for the case with $K_c = 0$, the flap-torsion coupling in first flap is in the range -0 0760(for Λ_s = -30deg, Λ_a = 0deg) to 0 0760(for Λ_s = 30deg, Λ_a = 0deg) With the inclusion of control spring($K_c = 1000$), the coupling range is -0 7967(for Λ_s = -30deg, Λ_a = -30deg) to -0 5859(for Λ_s = 30deg, Λ_a = -20deg) In case of second flap with $K_c = 0$, the flap-torsion coupling is in the range -0 0923(for Λ_s = -30deg, Λ_a = -10deg) to 0 0923(for Λ_s = 30deg, Λ_a = 10deg) With the inclusion of control spring($K_c = 1000$), the coupling range is 2 8224(for Λ_s = -30deg, Λ_a = -30deg) to 3 0150(for Λ_s = 30deg, Λ_a = -15deg) In case of third flap with $K_c = 0$, the flap-torsion coupling is in the range -0 0832(for Λ_s = 30deg, Λ_a = -5deg) to 0 0831(for Λ_s = -30deg, Λ_a = 5deg) With the inclusion of control spring($K_c = 1000$), the coupling range is 20 3640(for Λ_s = -30deg, Λ_a = -30deg) to 26 9634(for Λ_s = 30deg, Λ_a = -15deg)

From the results it can be seen that the control spring introduces a large value of pitch-flap coupling as compared to the effect introduced by tip sweep angles the coupling parameter increases significantly with the increase in flap frequency

The numerical values of frequencies and coupling parameters corresponding to $K_c = 0$ and $K_c = 1000$ are given in Appendix B

			Coupled modes	Ref [1], Uncoupled modes	
Spring stiffness	Mode		FE Analysis No of elements = 20	Power - Series Method	Rayleigh-Ritz Method
$K_L = 0$ $K_F = 10\,6$	LAG	1	0 731		
	LAG	2	4 453		
	FLAP	1	1 133	1 133	1 134
	FLAP	2	3 432	3 413	3 416
	FLAP	3	8 072	7 960	8 152
	TORSION	1	3 263		
	AXIAL	1	6 939		
$K_L = 0$ $K_F = 31\,8$	LAG	1	0 731		
	LAG	2	4 453		
	FLAP	1	1 136	1 135	1 138
	FLAP	2	3 434	3 415	3 422
	FLAP	3	8 190	8 075	8 449
	TORSION	1	3 263		
	AXIAL	1	6 939		

$\xi_1 = 0\,3l, \xi_2 = 0\,1l, L_{el} = 0\,1l$ and $K_c = 0$

Table 7 2 Comparison of natural frequencies in flap

			Coupled modes	Ref [1], Uncoupled modes	
Spring stiffness	Mode		FE Analysis No of elements = 20	Power - Series Method	Rayleigh-Ritz Method
$K_L = 30\ 1$ $K_F = 0$	LAG	1	0 780	0 781	0 792
	LAG	2	4 459	4 489	4 493
	FLAP	1	1 125		
	FLAP	2	3 427		
	FLAP	3	7 715		
	TORSION	1	3 263		
	AXIAL	1	6 939		
$K_L = 90\ 3$ $K_F = 0$	LAG	1	0 795	0 796	0 815
	LAG	2	4 460	4 491	4 499
	FLAP	1	1 125		
	FLAP	2	3 427		
	FLAP	3	7 715		
	TORSION	1	3 263		
	AXIAL	1	6 939		

$\xi_1 = 0\ 3l, \xi_2 = 0\ 1l, L_{el} = 0\ 1l$ and $K_c = 0$

Table 7 3 Comparison of natural frequencies in lag

			Coupled modes	
Spring stiffness	Mode		MODEL I $N = 10$	MODEL II $N = 14$
$K_L = 30\ 1$ $K_F = 10\ 6$	LAG	1	0 780	0 905
	LAG	2	4 459	4 620
	FLAP	1	1 133	1 224
	FLAP	2	3 432	3 617
	FLAP	3	8 072	8 107
	TORSION	1	3 263	3 143
	AXIAL	1	6 939	6 939
$K_L = 90\ 3$ $K_F = 31\ 8$	LAG	1	0 795	0 911
	LAG	2	4 460	4 628
	FLAP	1	1 136	1 224
	FLAP	2	3 434	3 634
	FLAP	3	8 190	8 268
	TORSION	1	3 263	3 143
	AXIAL	1	6 939	6 939

MODEL I Torque tube is assumed as rigid and massless

MODEL II Torque tube is treated as a very stiff member

Location of elastomer $L_{el} = 0\ 1l$

$\xi_1 = 0\ 3l, \xi_2 = 0\ 1l, L_{el} = 0\ 01l$ and $K_c = 0$

Table 7 4 Effect of modelling of torque tube on blade natural frequencies

Soft-in-plane blade data			
	Flexbeam $N = 3$	Blade $N = 7$	Torque tube $N = 4$
$Im_{\zeta\zeta}/ml^2$	0 0004	0 0004	0 0004
$Im_{\eta\eta}/ml^2$	0 0	0 0	0 0
θ_G	0 0	0 0	0 0
m	1 0	0 9	7 5
β_s	0 0	0 0	0 0
β_d	0 0	0 0	0 0
β_p	0 0	0 0	0 0
θ_I	0 0	0 0	0 0
$GJ/m\Omega^2l^4$	0 002	0 003	0 825
$EA/m\Omega^2l^2$	30 0	40 0	50 0
e_1	0 0	0.0	0 0
e_2	0 0	0 0	0 0
a	0 0	0 0	0 0
EAC_0/EA	0 00021036	0 00021036	0 00021036
$EI_{\zeta\zeta}/m\Omega^2l^4$	0 00206	0 645	0 505
$EI_{\eta\eta}/m\Omega^2l^4$	0 0001	0 006	1 5

K_F Elastomer stiffness in flap, 217 78

K_L Elastomer stiffness in lag, 21 78

K_ϕ Elastomer stiffness in torsion, 0

K_c Control spring stiffness, 1000

$\xi_1 = 0\ 3l, \xi_2 = 0\ 1l, L_c = 0\ 02l, a_c = 0\ 05l$ and $L_{el} = 0\ 05l$

Table 7 5 Input data for soft-in-plane blade with flexible torque tube

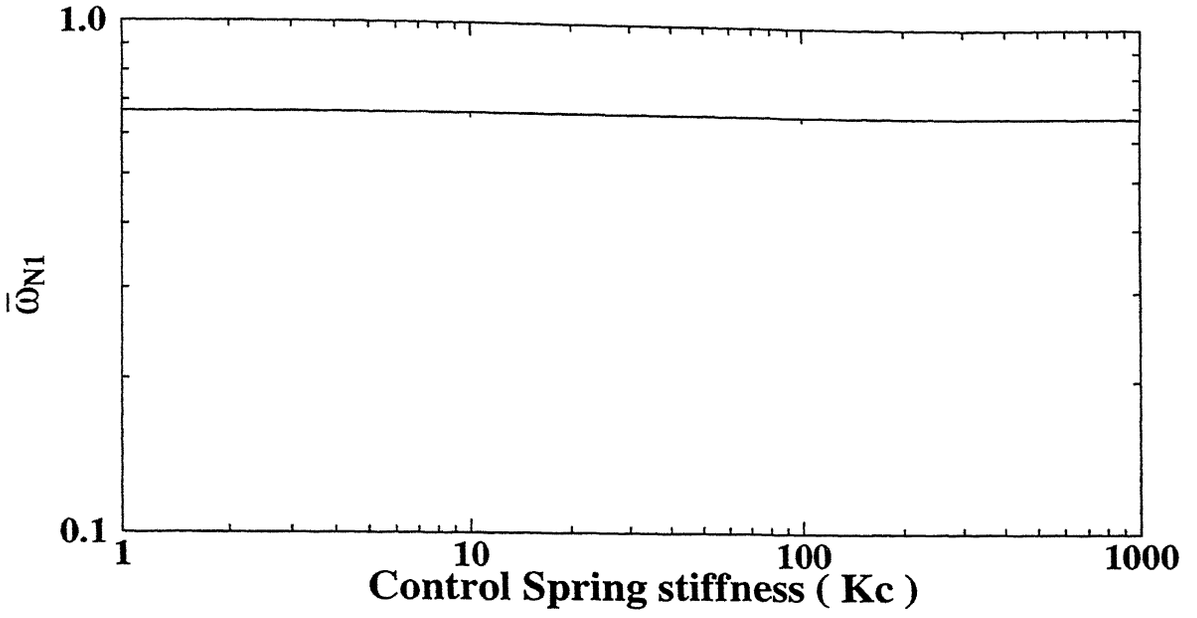

Figure 7 1 Variation of first frequency (1st lag) with control spring stiffness

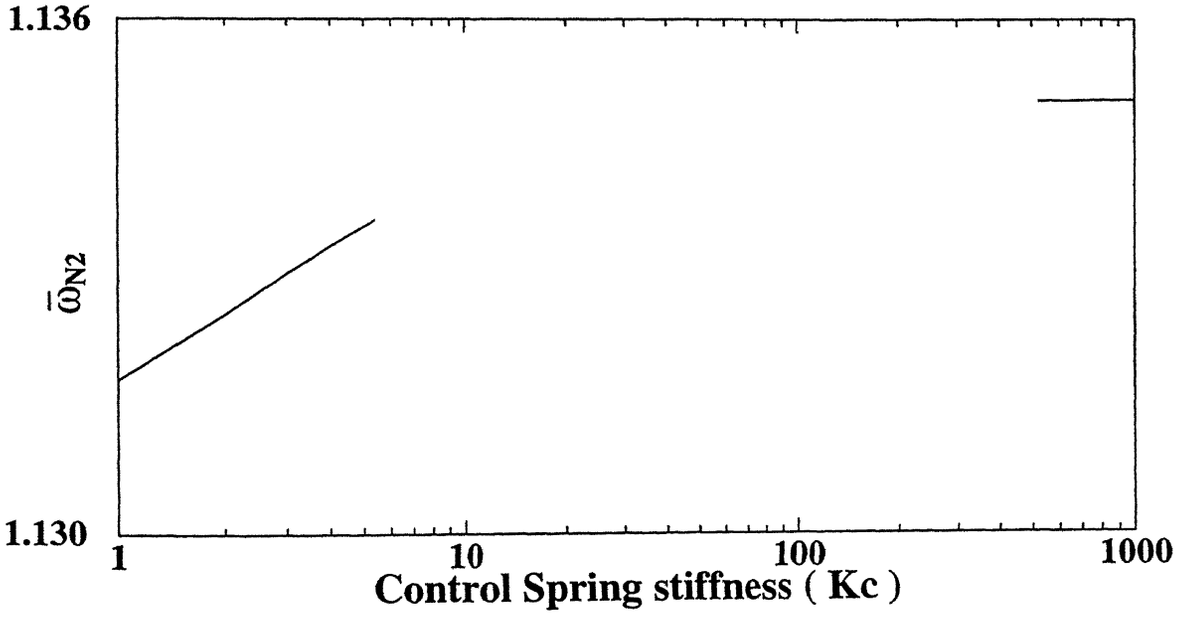

Figure 7 2 Variation of second frequency (1st flap) with control spring stiffness

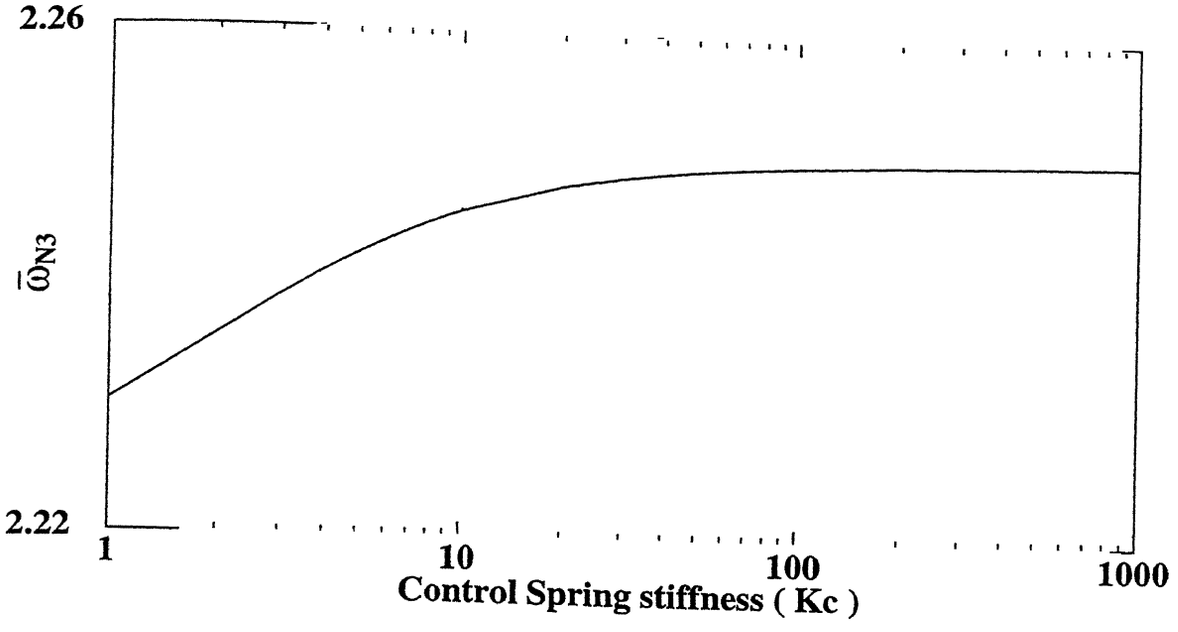

Figure 7 3 Variation of third frequency (2nd flap) with control spring stiffness

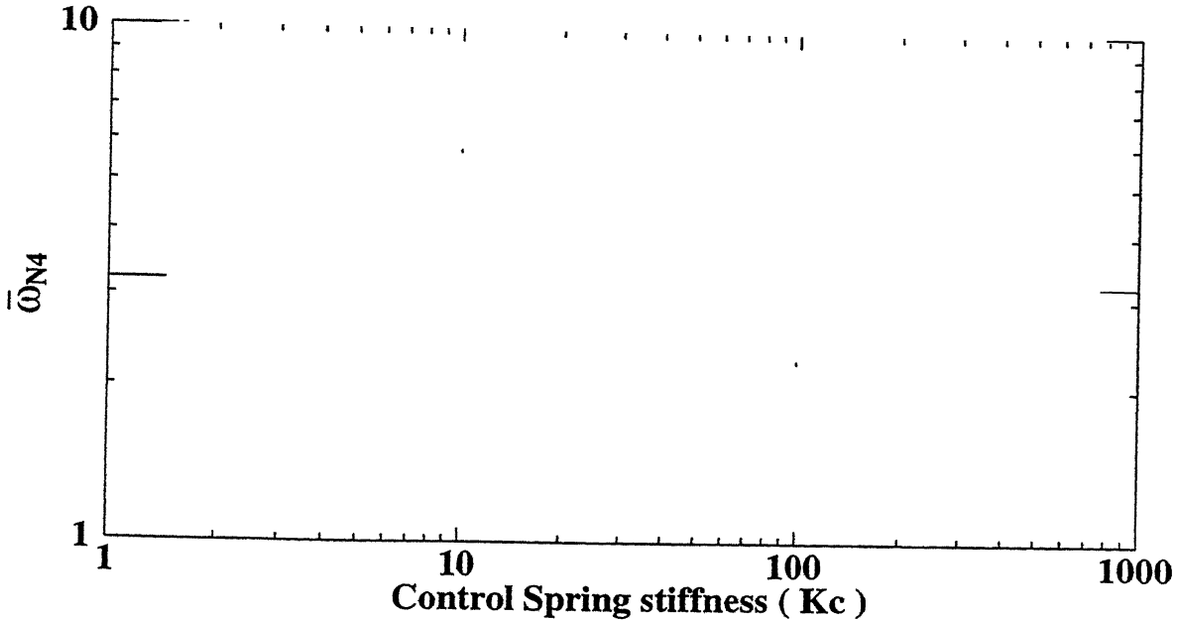

Figure 7 4 Variation of fourth frequency (2nd lag) with control spring stiffness

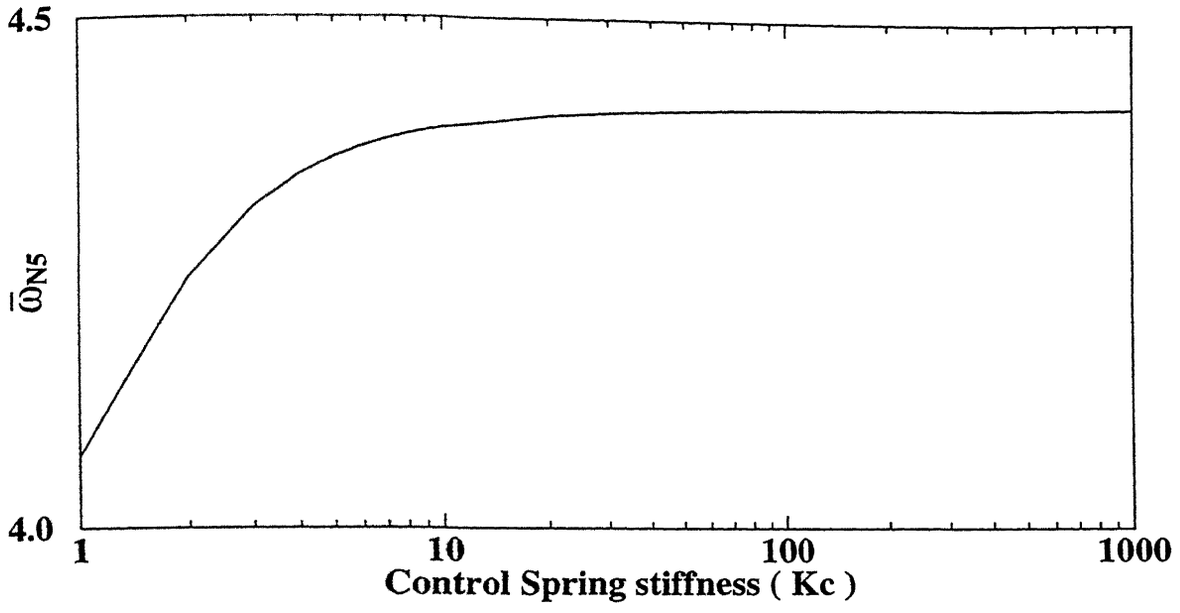

Figure 7 5 Variation of fifth frequency (1st torsion) with control spring stiffness

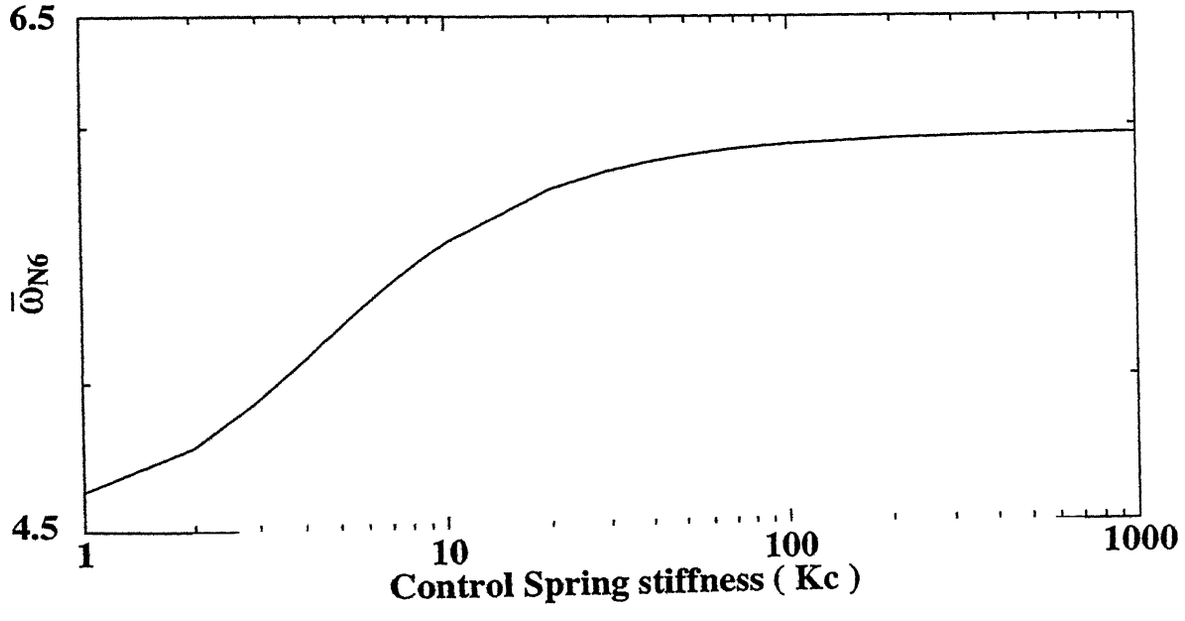

Figure 7 6: Variation of sixth frequency (3rd flap) with control spring stiffness

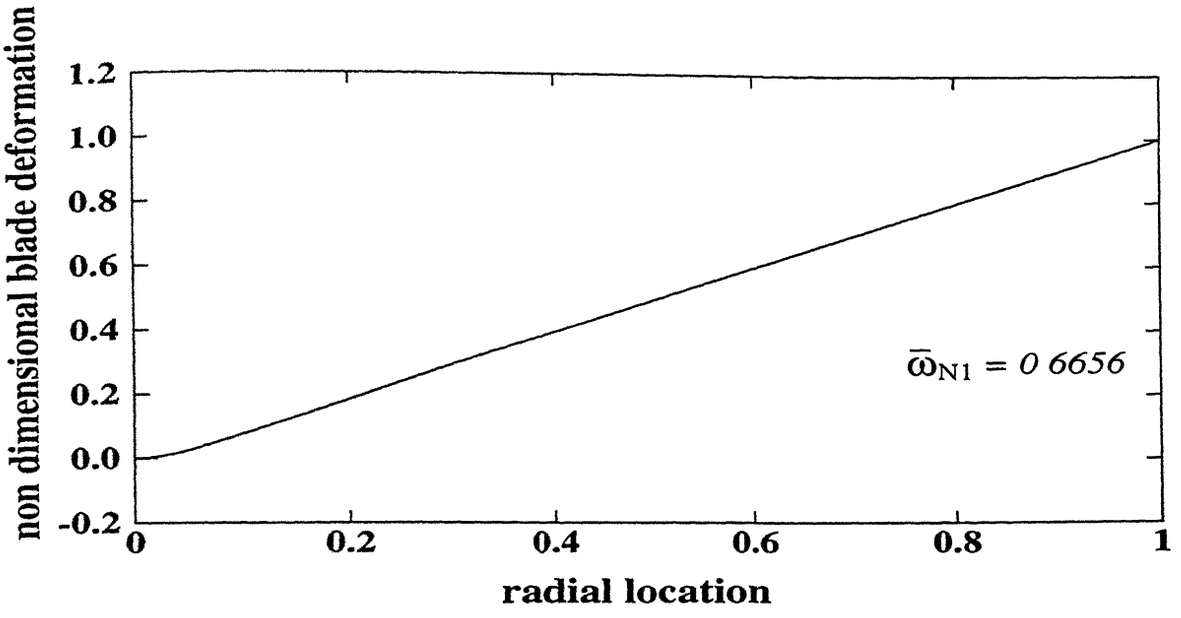

Figure 7.7 (a) First natural frequency (1st lag) mode shape with Kc=0

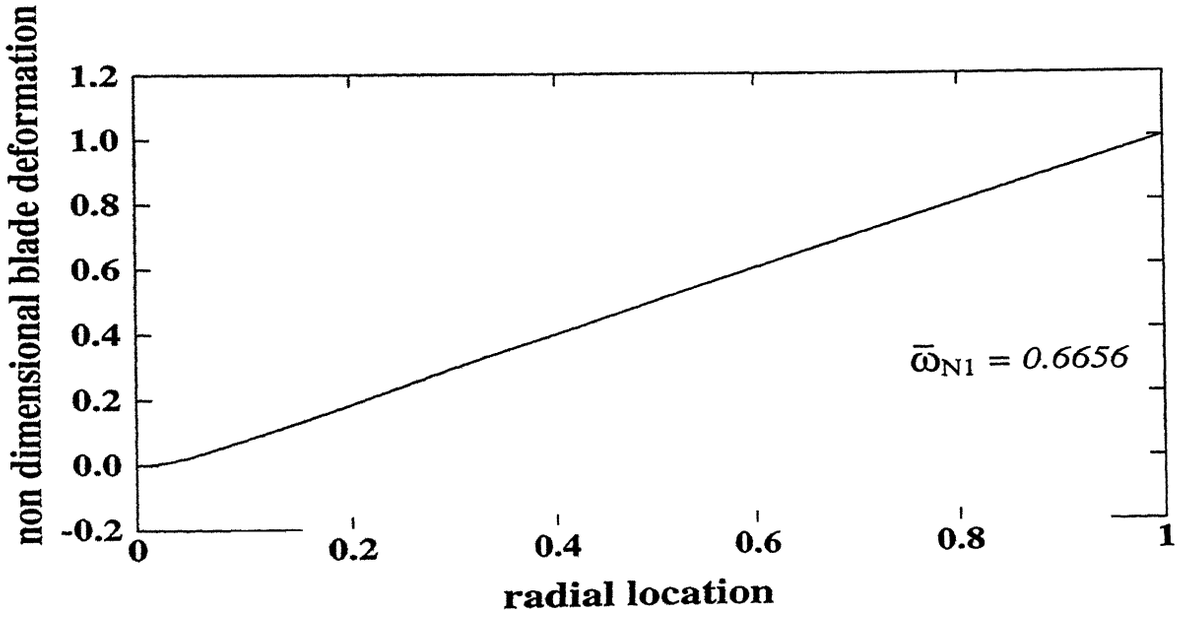

Figure 7 7 (b) First natural frequency (1st lag) mode shape with Kc=1000

Figure 7 7 Effect of control spring on mode shape of first natural frequency

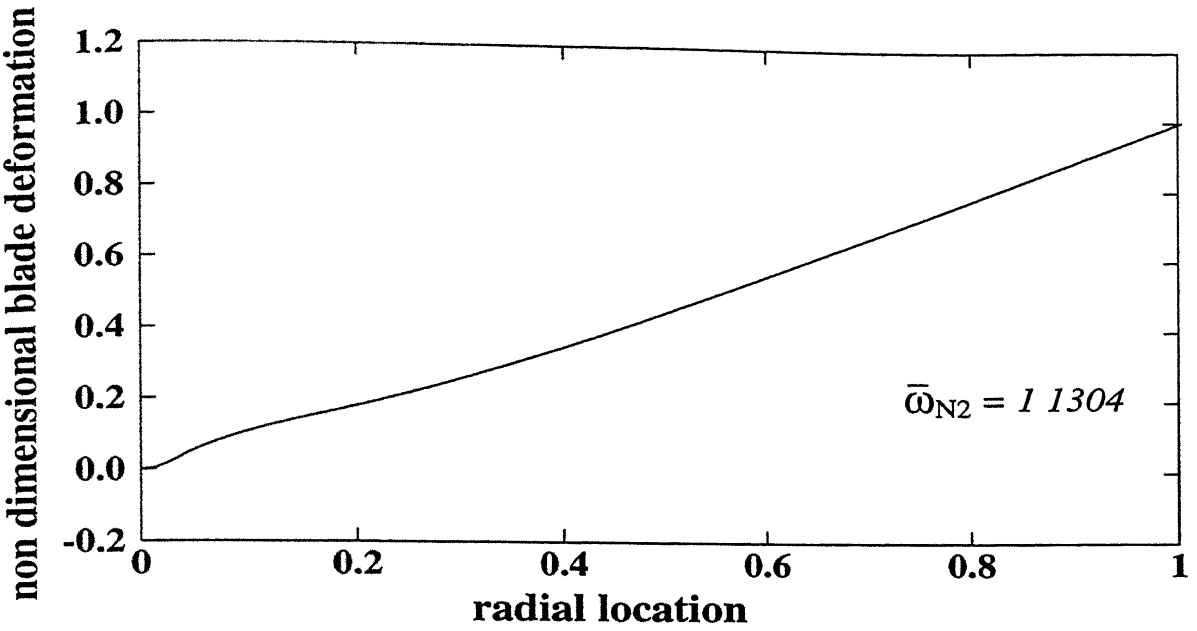

Figure 7 8 (a) Second natural frequency (1st flap) mode shape with Kc=0

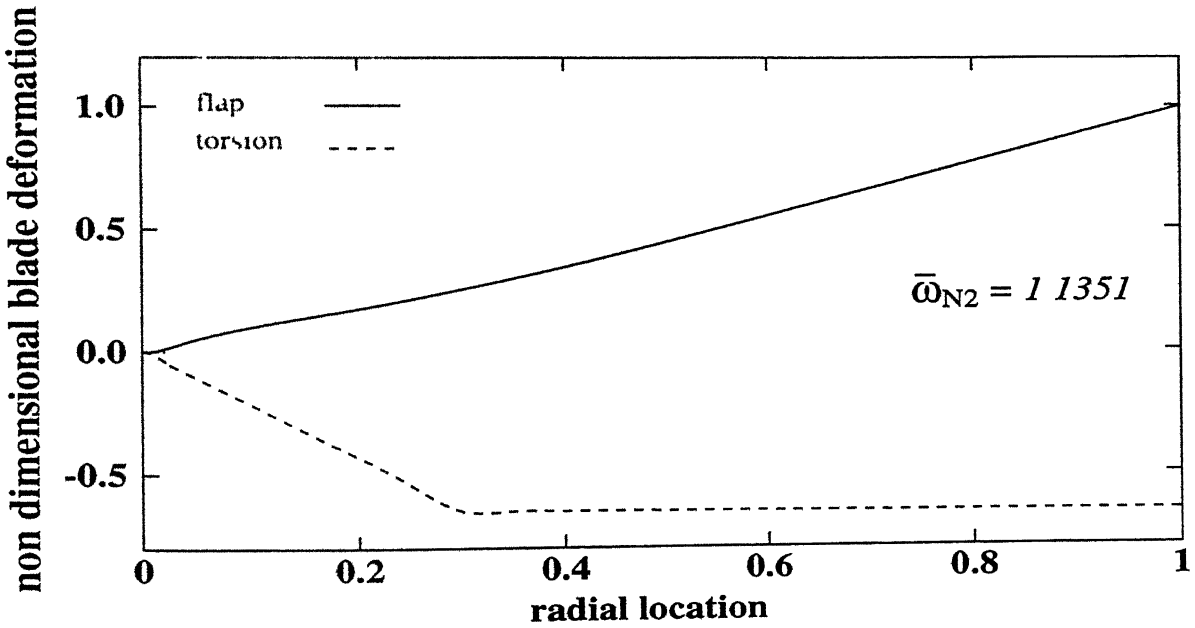

Figure 7 8 (b) Second natural frequency (1st flap) mode shape with Kc=1000

Figure 7 8 Effect of control spring on mode shape of second natural frequency

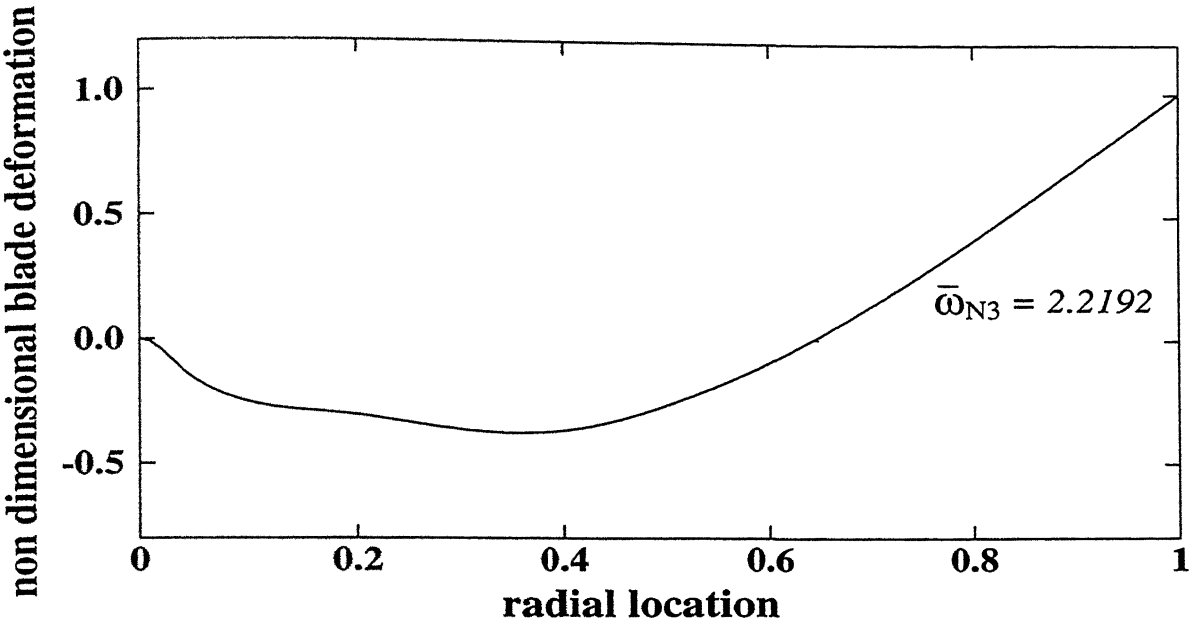

Figure 7 9 (a) Third natural frequency (2nd flap) mode shape with Kc=0

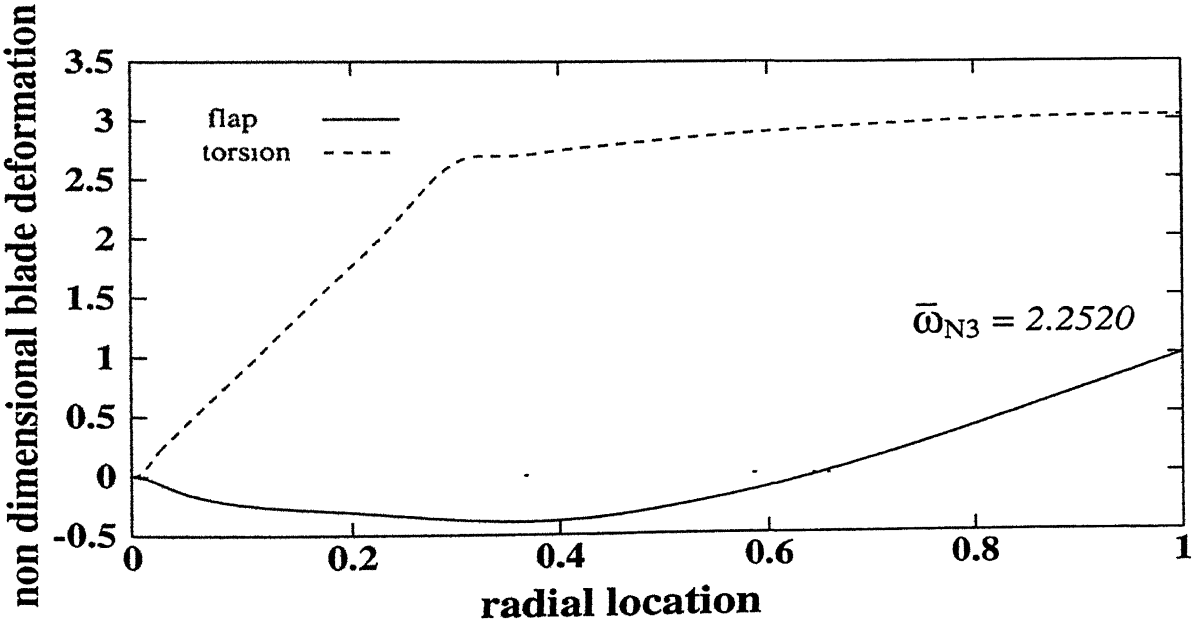

Figure 7 9 (b) Third natural frequency (2nd flap) mode shape with Kc=1000

Figure 7 9 Effect of control spring on mode shape of third natural frequency

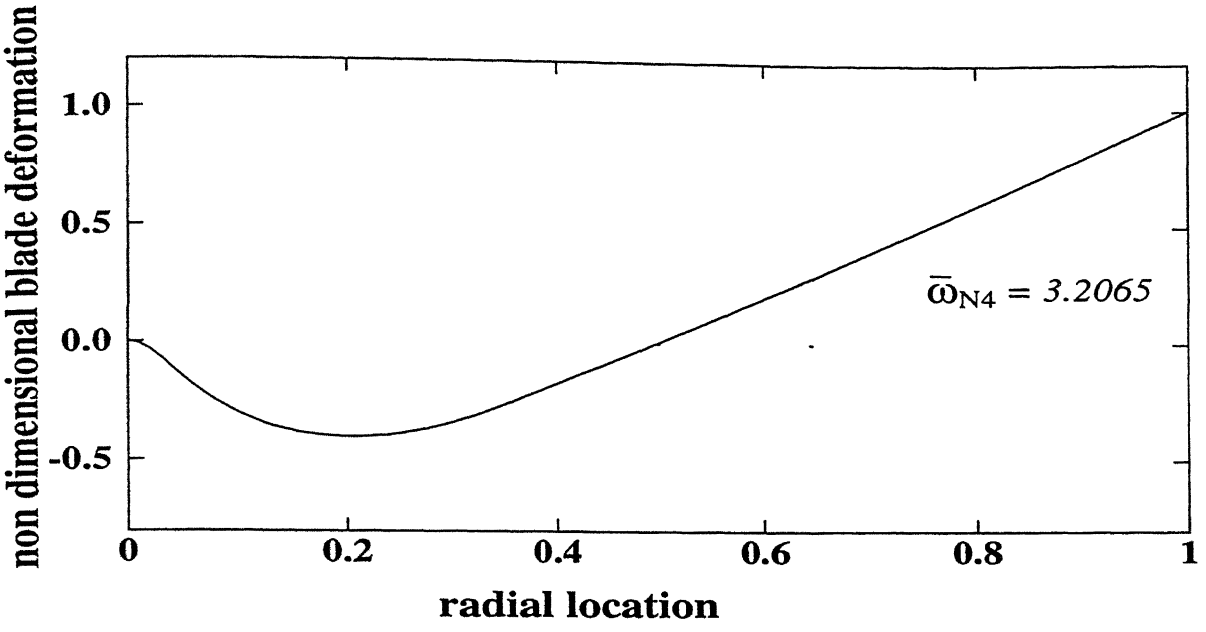

Figure 7 10 (a) Fourth natural frequency (2th lag) mode shape with Kc=0

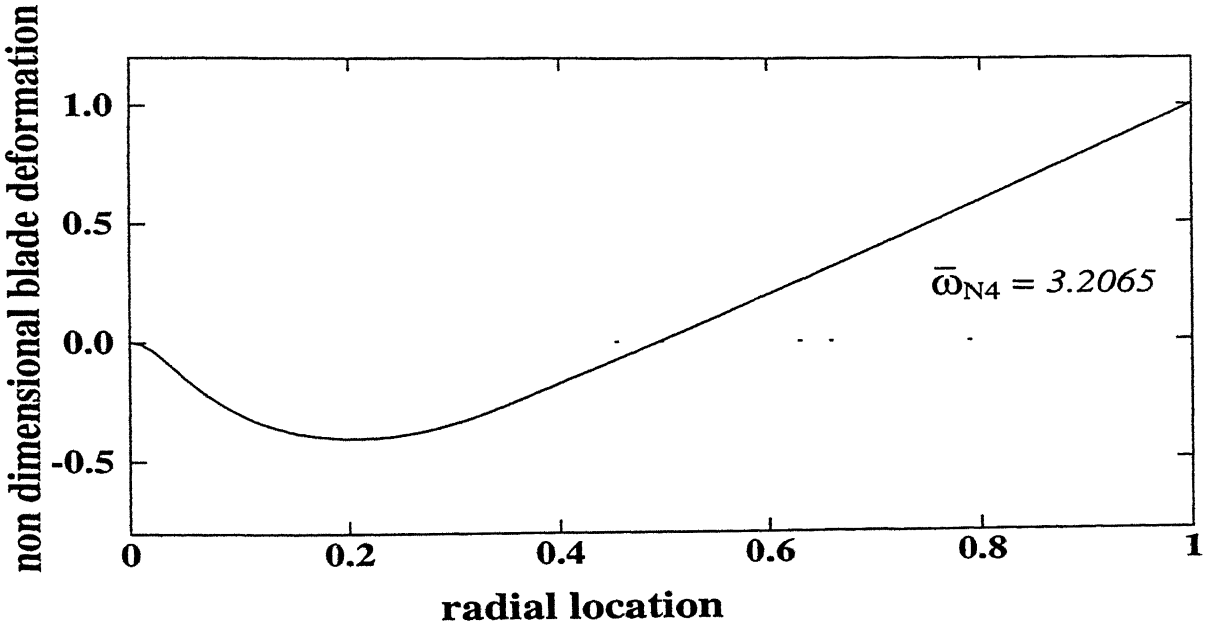

Figure 7 10 (b) Fourth natural frequency (2th lag) mode shape with Kc=1000

Figure 7.10 Effect of control spring on mode shape of fourth natural frequency

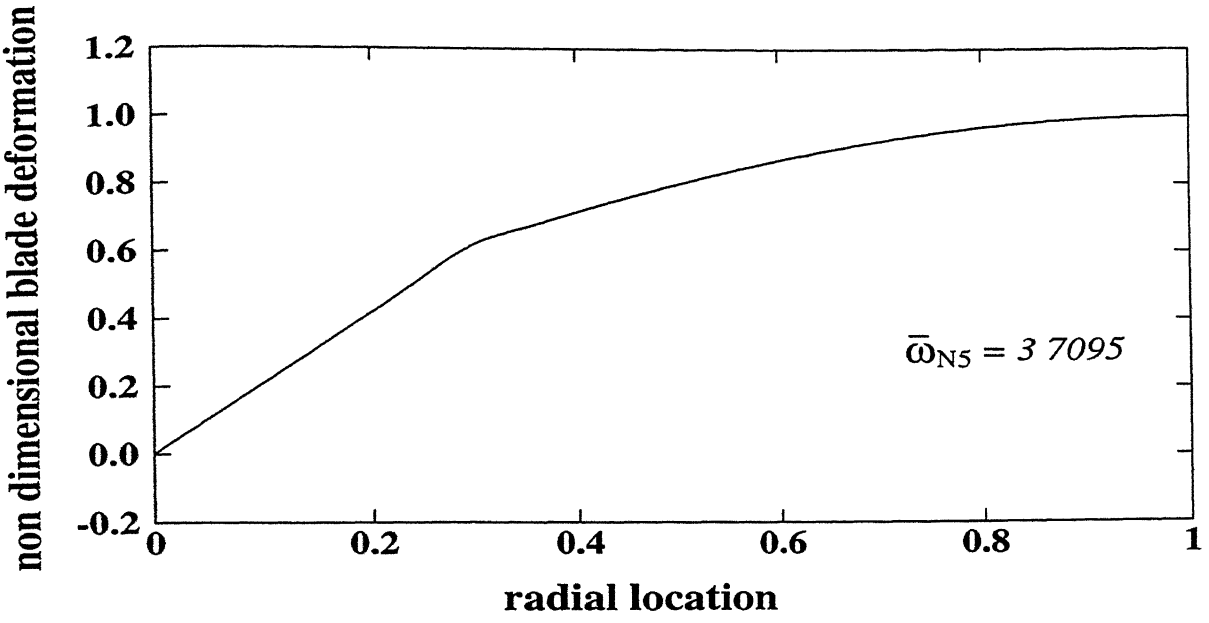

Figure 7 11 (a) Fifth natural frequency (1st torsion) mode shape with Kc=0

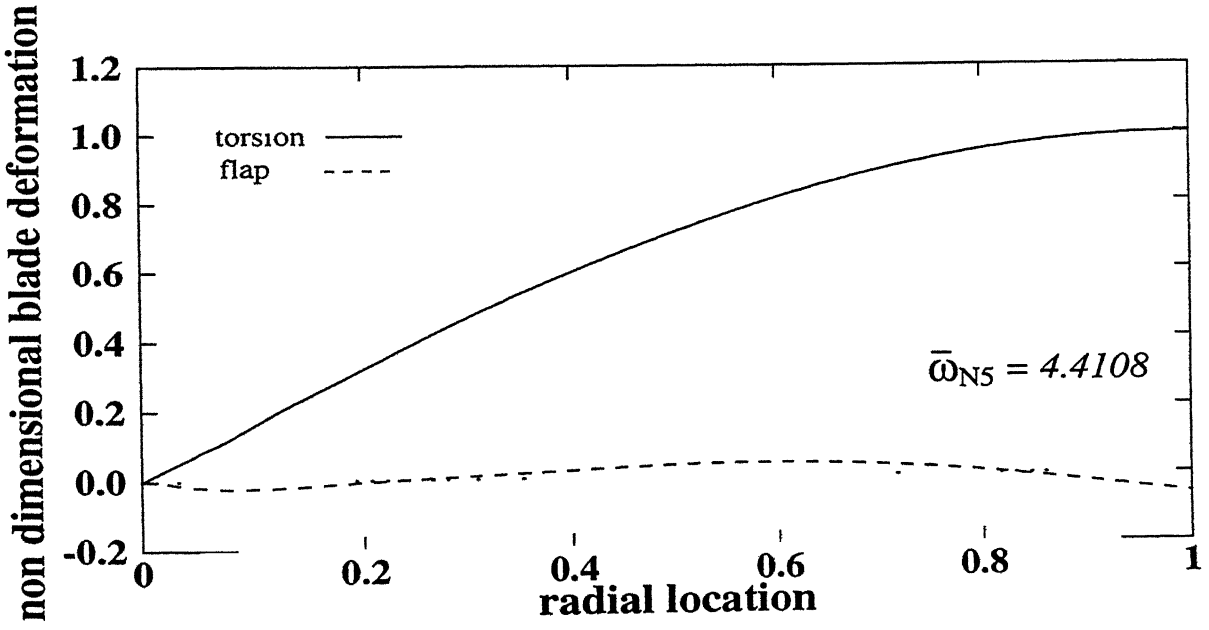

Figure 7 11 (b) Fifth natural frequency (1st torsion) mode shape with Kc=1000

Figure 7 11 Effect of control spring on mode shape of fifth natural frequency

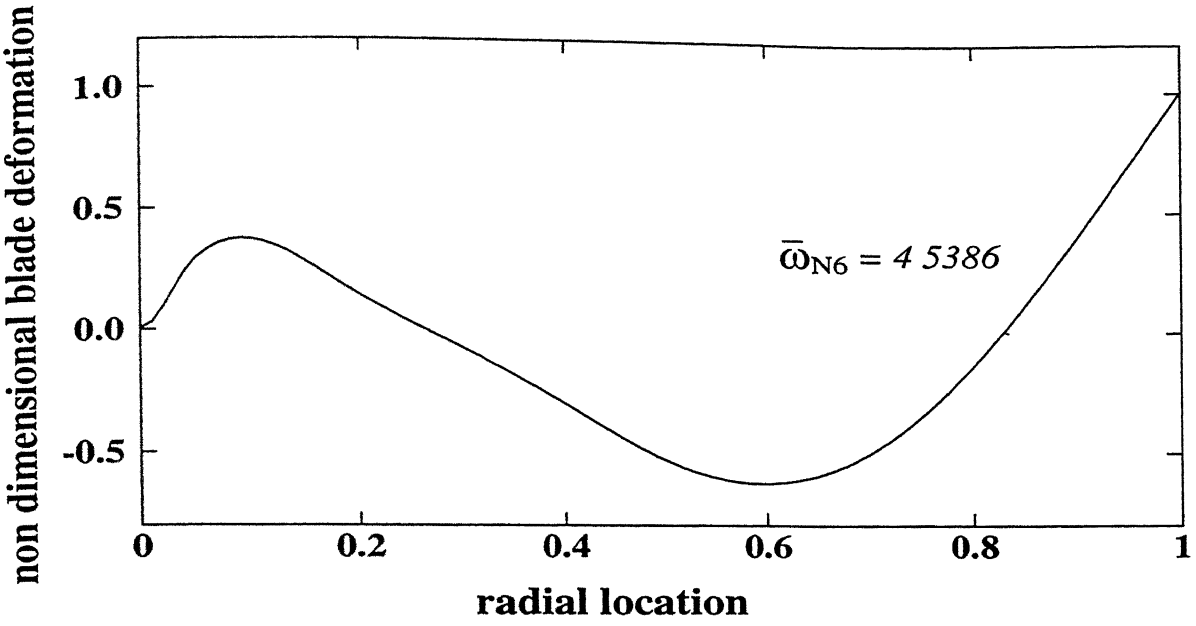

Figure 7 12 (a) Sixth natural frequency (3rd flap) mode shape with Kc=0

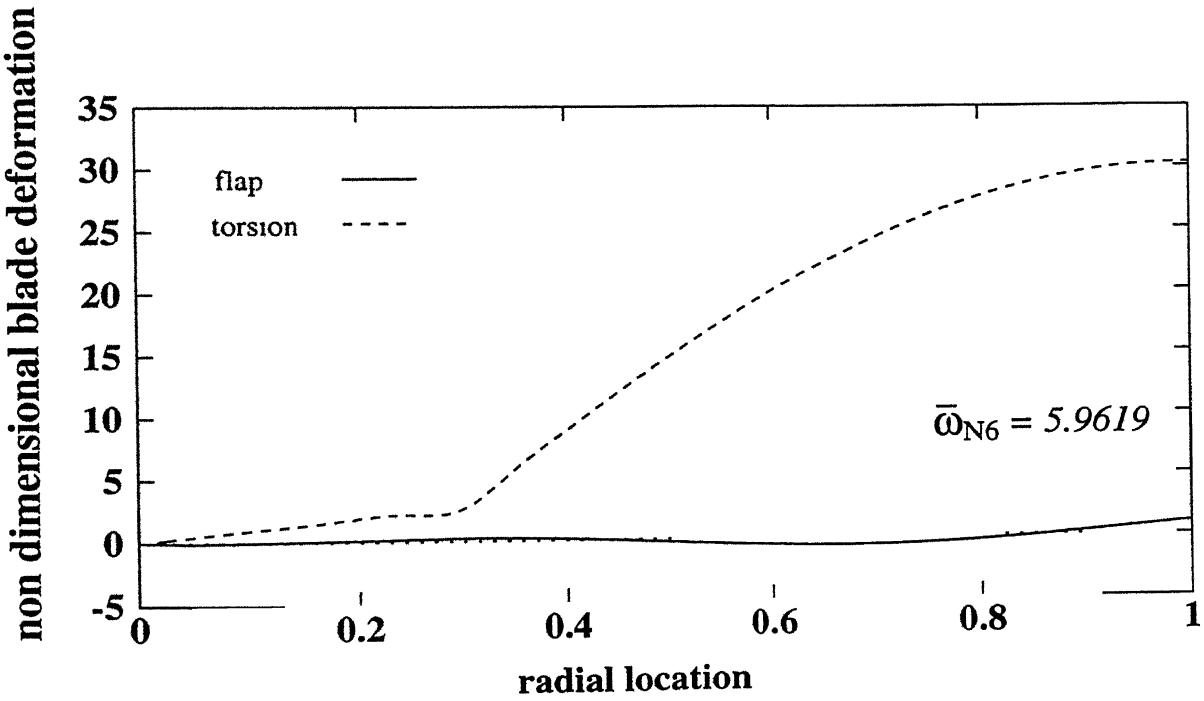

Figure 7 12 (b) Sixth natural frequency (3rd flap) mode shape with Kc=1000

Figure 7 12 Effect of control spring on mode shape of sixth natural frequency

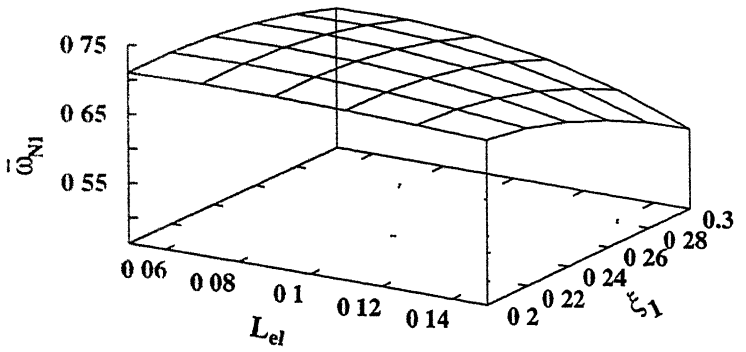

Figure 7 13 (a) Control spring location, L_c=0 01

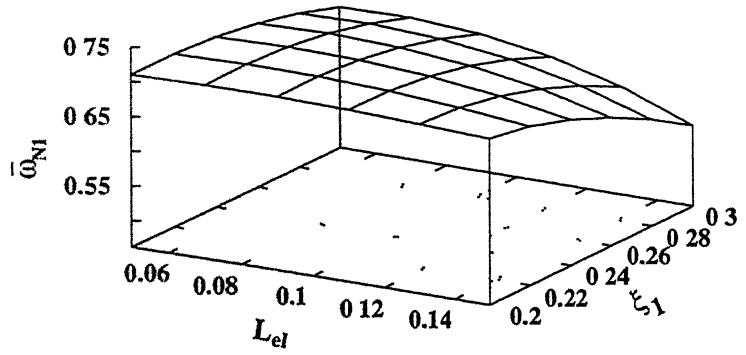

Figure 7 13 (b) Control spring location, L_c=0 02

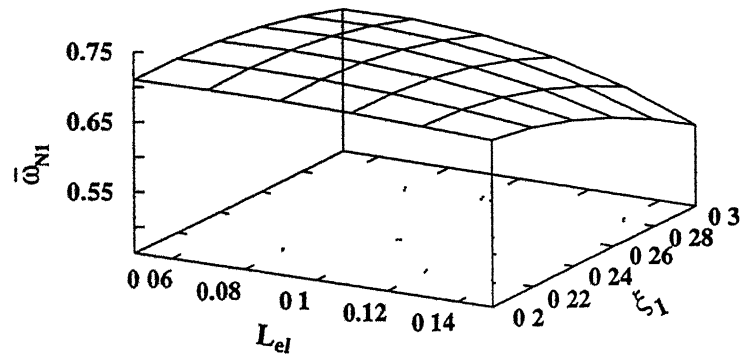

Figure 7 13 (c) Control spring location, L_c=0 03

Figure 7 13 Variation of first natural frequency (1st lag) with location of elastomer and flexbeam-torque tube junction, for various control spring locations

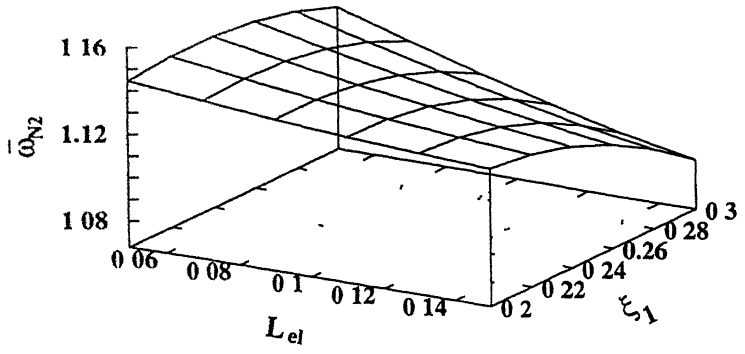

Figure 7 14 (a) Control spring location, L_c=0 01

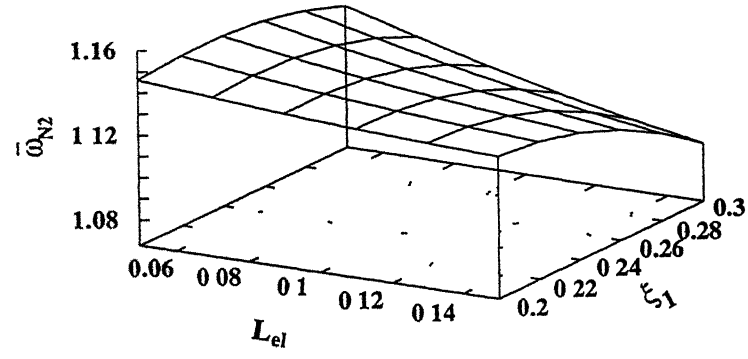

Figure 7 14 (b) Control spring location, L_c=0 02

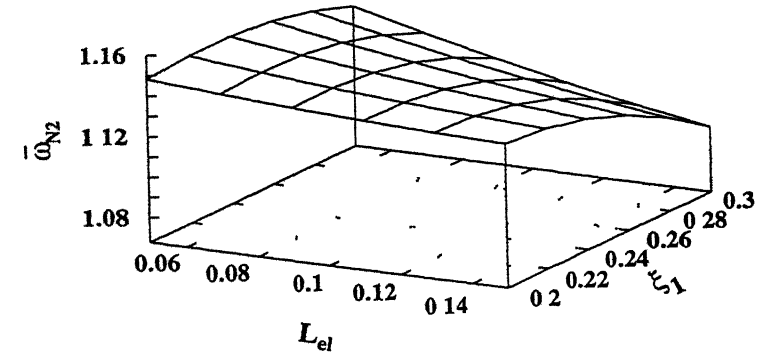

Figure 7 14 (c). Control spring location, L_c=0 03

Figure 7 14 Variation of second natural frequency (1st flap) with location of elastomer and flexbeam-torque tube junction, for various control spring locations

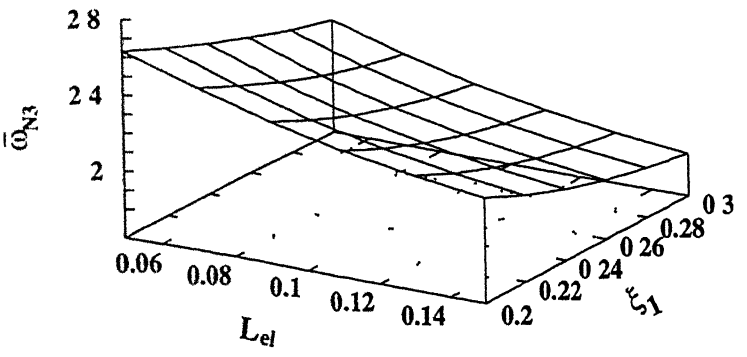

Figure 7 15 (a) Control spring location, L_c=0 01

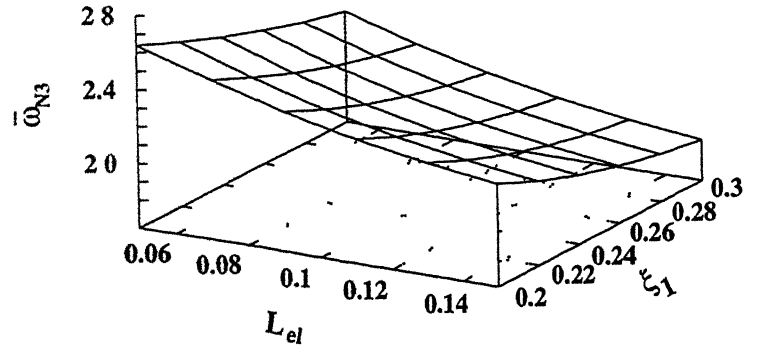

Figure 7 15 (b) Control spring location, L_c=0 02

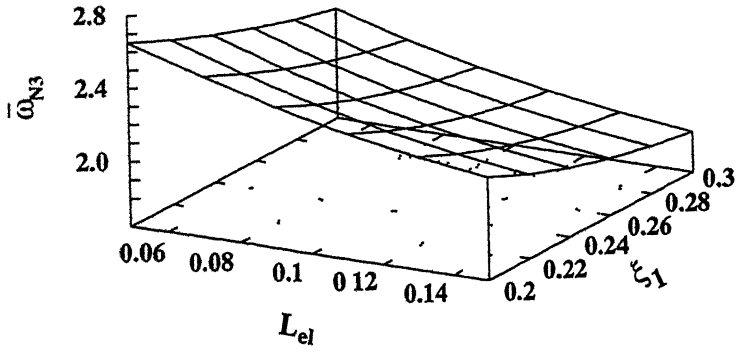

Figure 7 15 (c) Control spring location, L_c=0 03

Figure 7 15· Variation of third natural frequency (2nd flap) with location of elastomer and flexbeam-torque tube junction, for various control spring locations

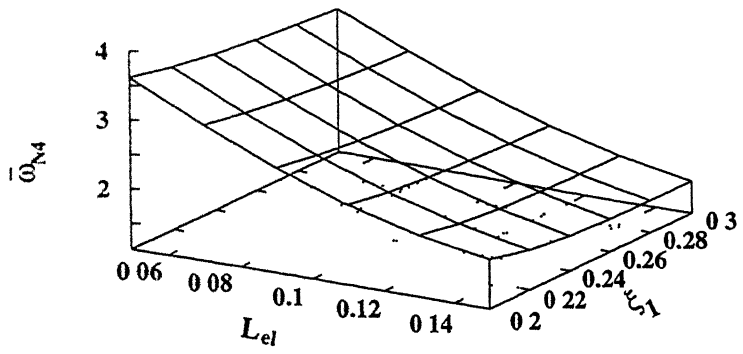

Figure 7 16 (a) Control spring location, L_c=0 01

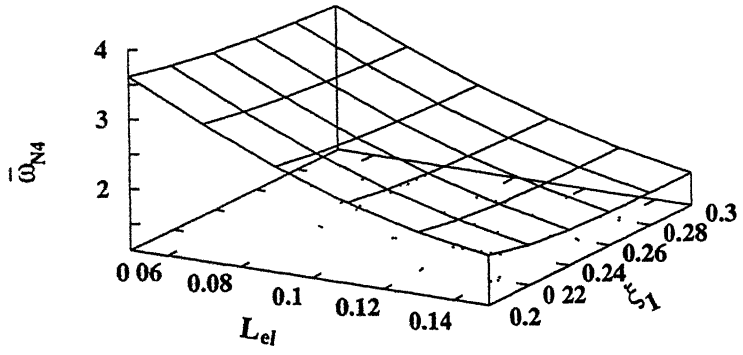

Figure 7 16 (b) Control spring location, L_c=0 02

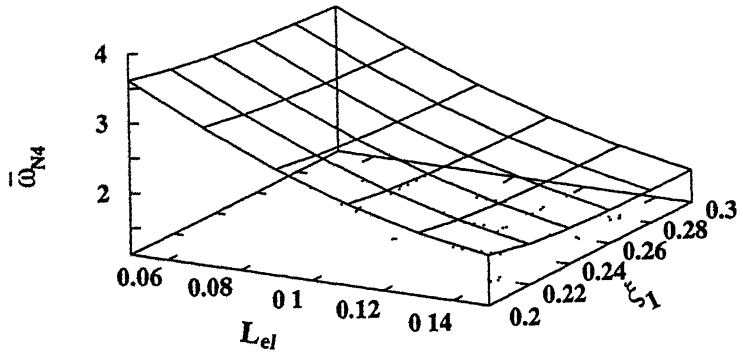

Figure 7 16 (c) Control spring location, L_c=0 03

Figure 7 16 Variation of fourth natural frequency (2nd lag) with location of elastomer and flexbeam-torque tube junction, for various control spring locations

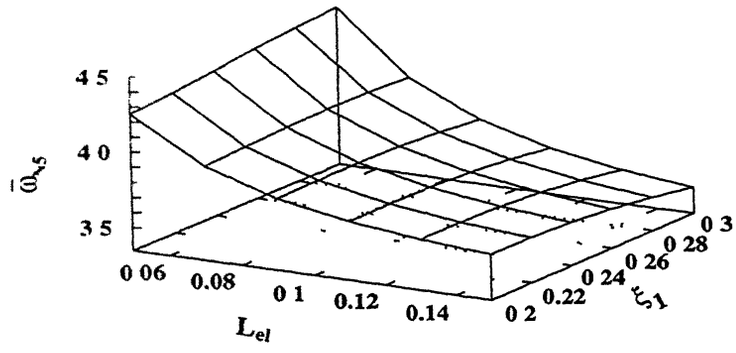

Figure 7 17 (a) Control spring location, L_c=0 01

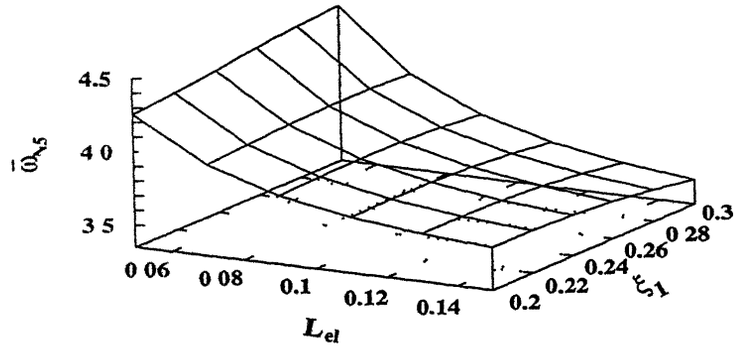

Figure 7 17 (b) Control spring location, L_c=0 02

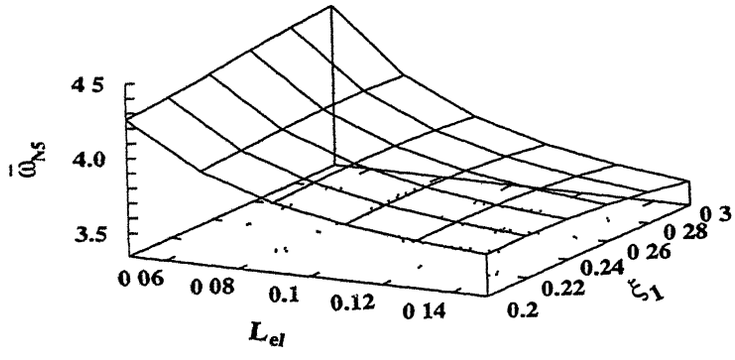

Figure 7 17 (c) Control spring location, L_c=0 03

Figure 7 17 Variation of fifth natural frequency (1st torsion) with location of elastomer and flexbeam-torque tube junction, for various control spring locations

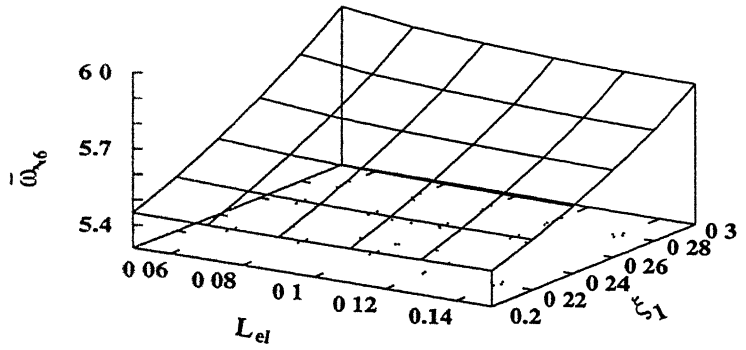

Figure 7 18 (a) Control spring location, L_c=0 01

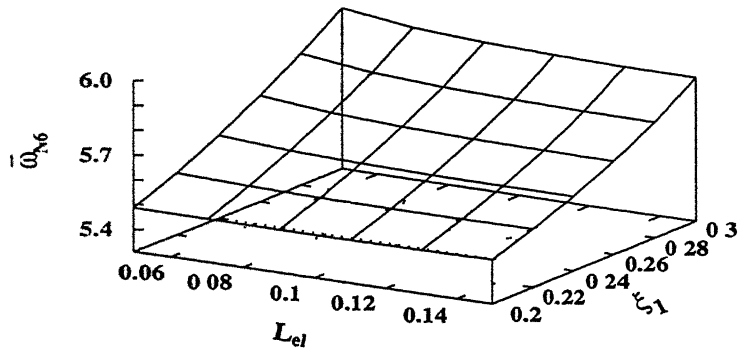

Figure 7 18· (b) Control spring location, L_c=0 02

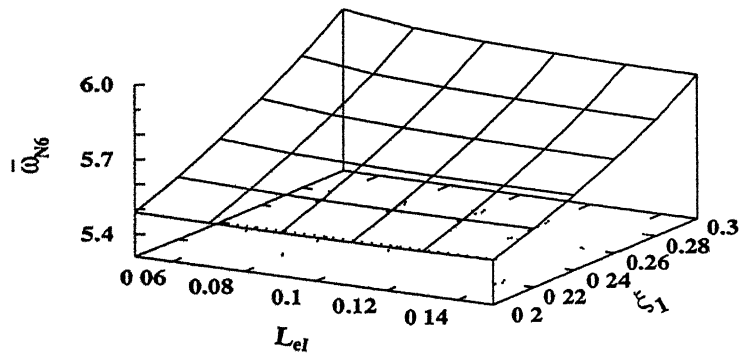

Figure 7 18 (c) Control spring location, L_c=0 03

Figure 7 18 Variation of sixth natural frequency (3rd flap) with location of elastomer and flexbeam-torque tube junction, for various control spring locations

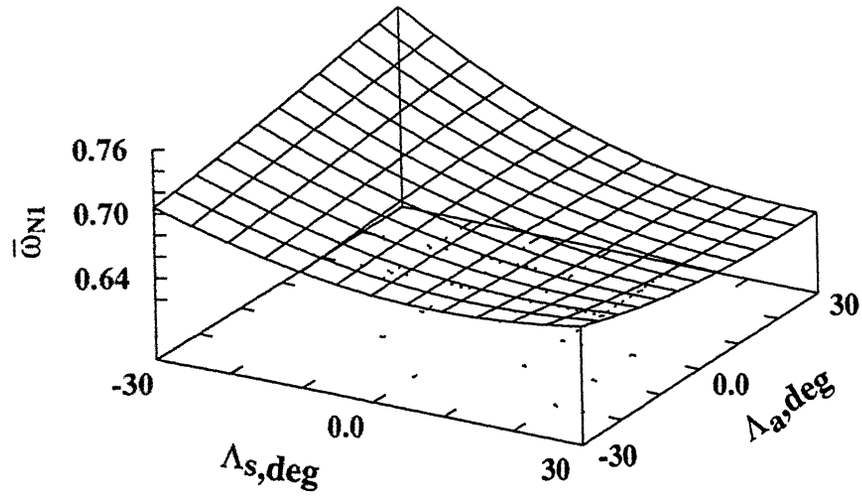

Figure 7 19 (a) for Kc=0

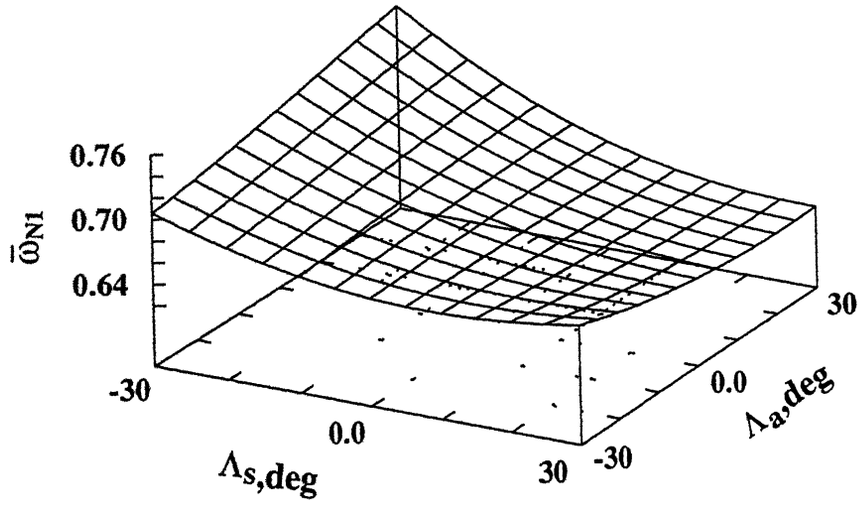

Figure 7 19 (b) for Kc=1000

Figure 7 19 Variation of first natural frequency(1st lag)as a function of tip sweep angle with and without control spring stiffness

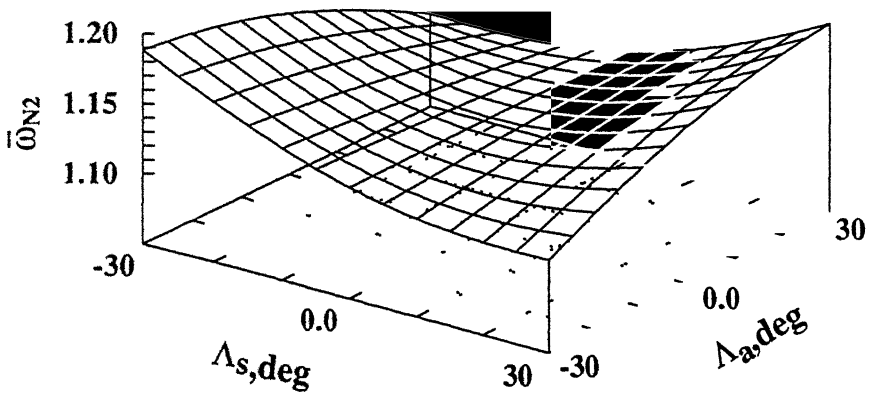

Figure 7 20 (a) for Kc=0

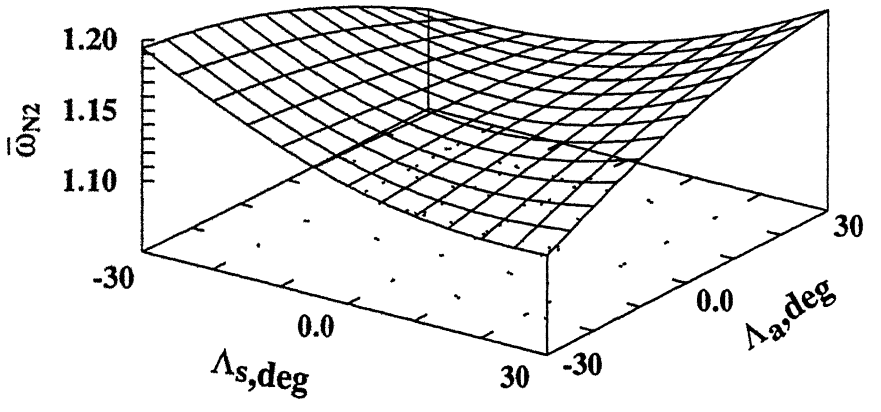

Figure 7 20 (b) for Kc=1000

Figure 7 20 Variation of second natural frequency(1st flap) as a function of tip sweep angle with and without control spring stiffness

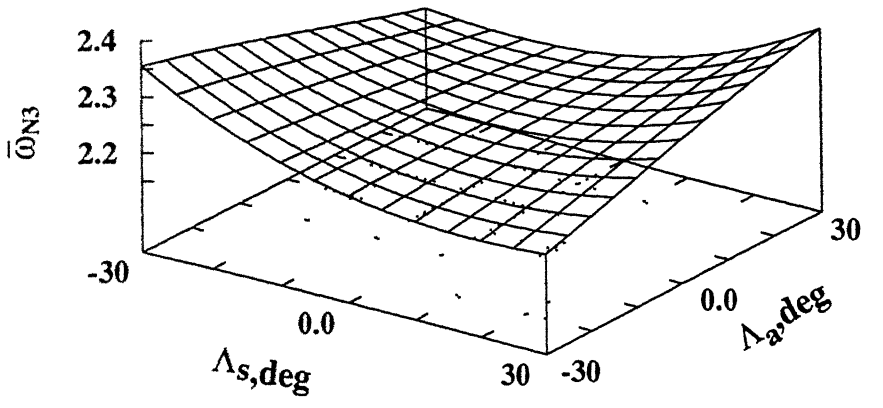

Figure 7 21 (a) for Kc=0

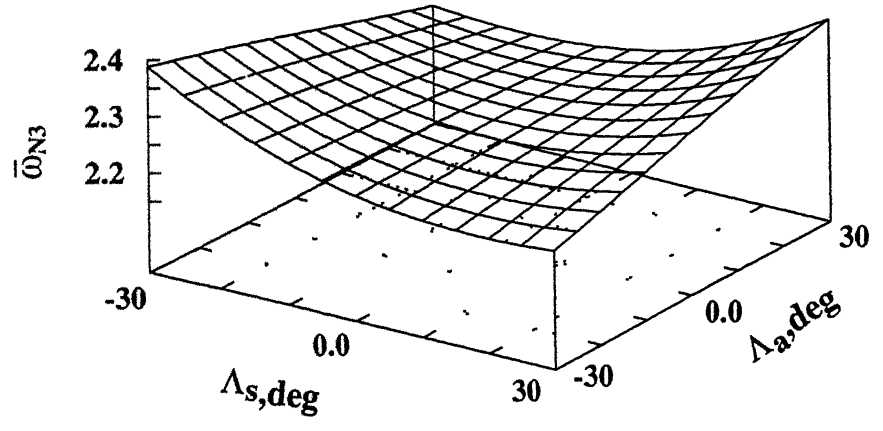

Figure 7 21 (b) for Kc=1000

Figure 7 21 Variation of third natural frequency(2nd flap) as a function of tip sweep angle with and without control spring stiffness

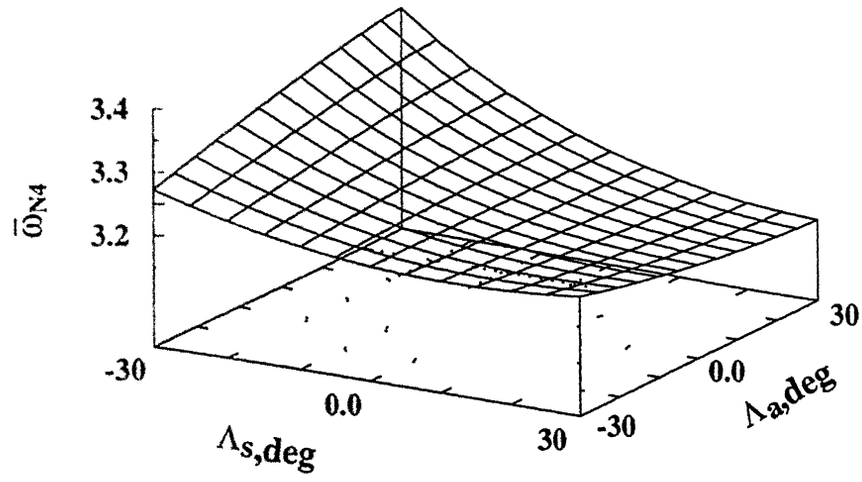

Figure 7 22 (a) for Kc=0

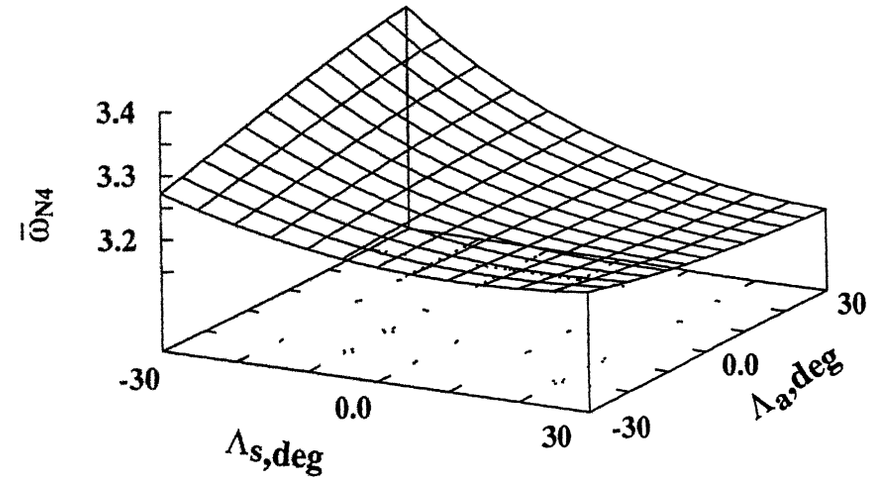

Figure 7 22 (b) for Kc=1000

Figure 7 22 Variation of fourth natural frequency(2nd lag) as a function of tip sweep angle with and without control spring stiffness

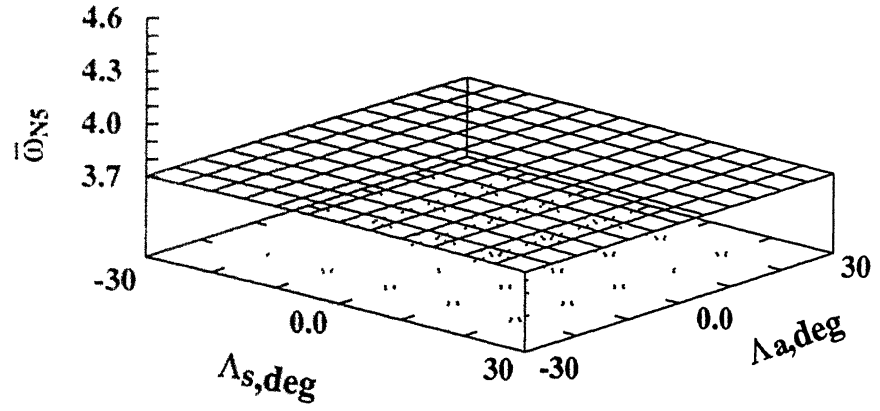

Figure 7 23 (a) for Kc=0

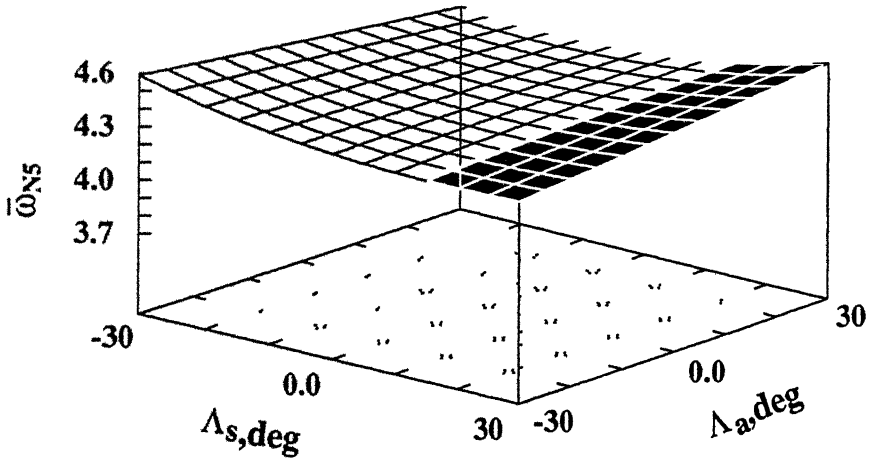

Figure 7 23 (b) for Kc=1000

Figure 7.23 Variation of fifth natural frequency(1st torsion) as a function of tip sweep angle with and without control spring stiffness

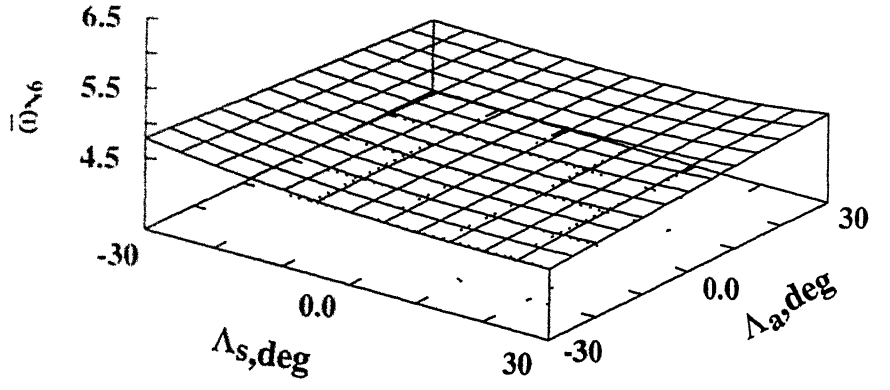

Figure 7 24 (a) for Kc=0

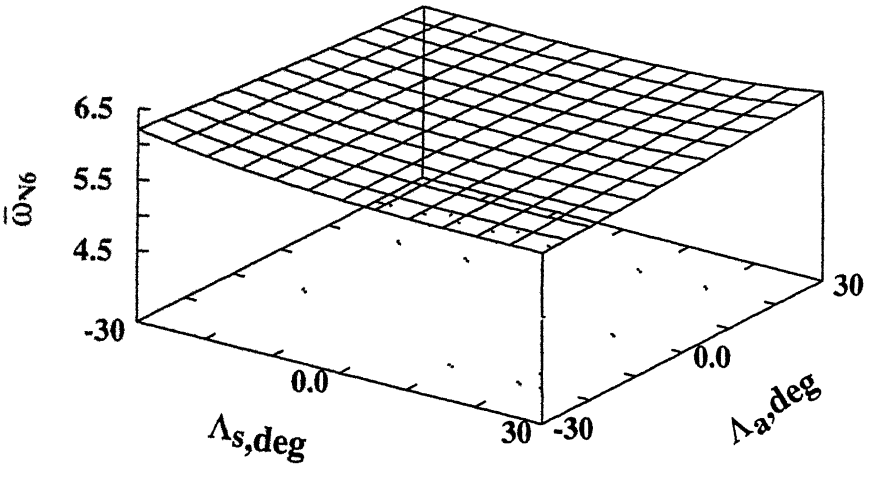

Figure 7 24 (b) for Kc=1000

Figure 7 24 Variation of sixth natural frequency(3rd flap) as a function of tip sweep angle with and without control spring stiffness

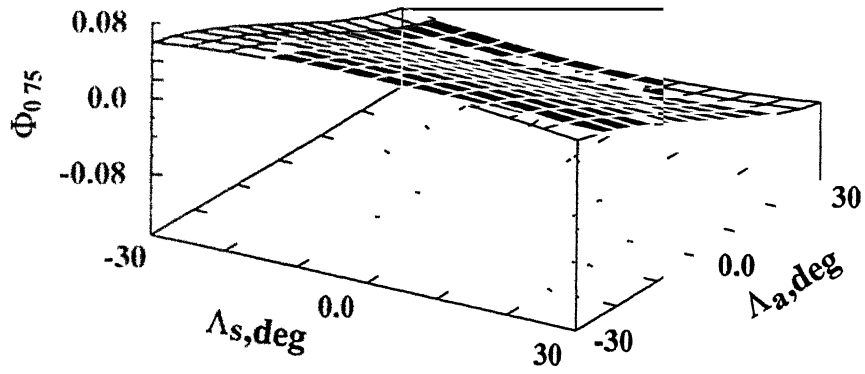

Figure 7 25 (a) for Kc=0

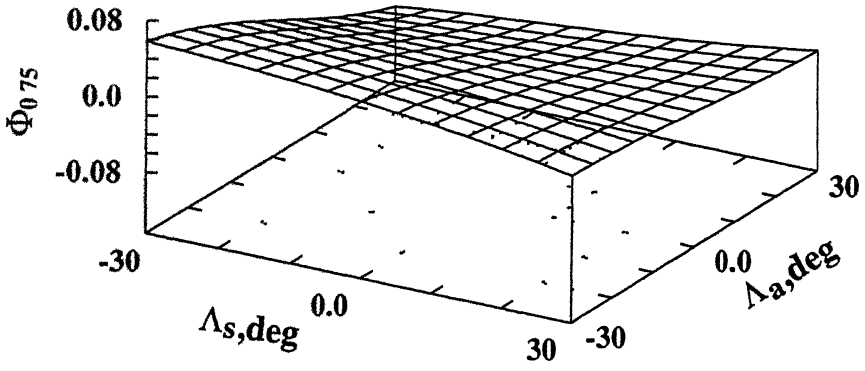

Figure 7 25 (b) for Kc=1000

Figure 7 25 Effect of bending-torsion coupling as a function of tip sweep angle with and without control stiffness in first frequency(1st lag)

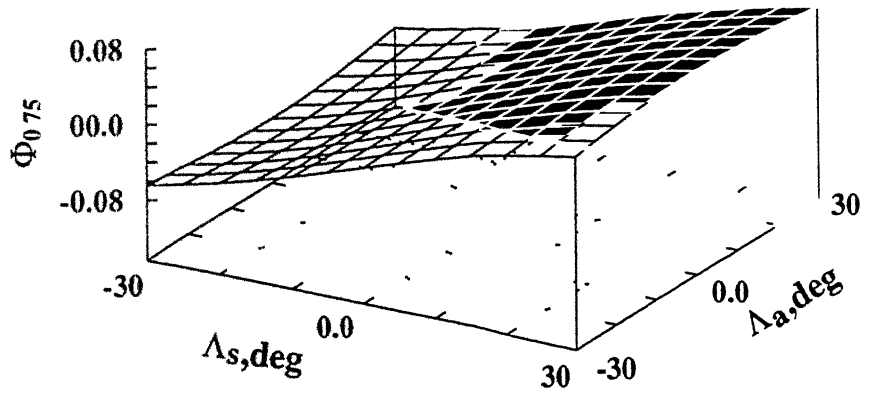

Figure 7 26 (a) for Kc=0

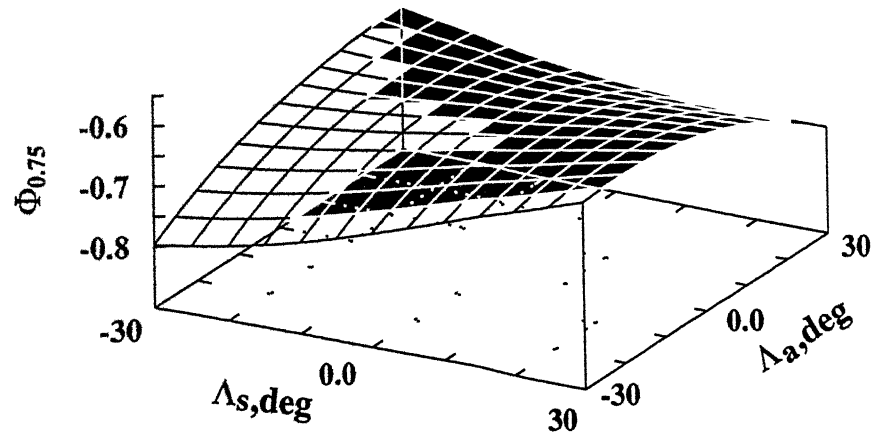

Figure 7.26 (b) for Kc=1000

Figure 7 26 Effect of bending-torsion coupling as a function of tip sweep angle with and without control stiffness second frequency(1st flap)

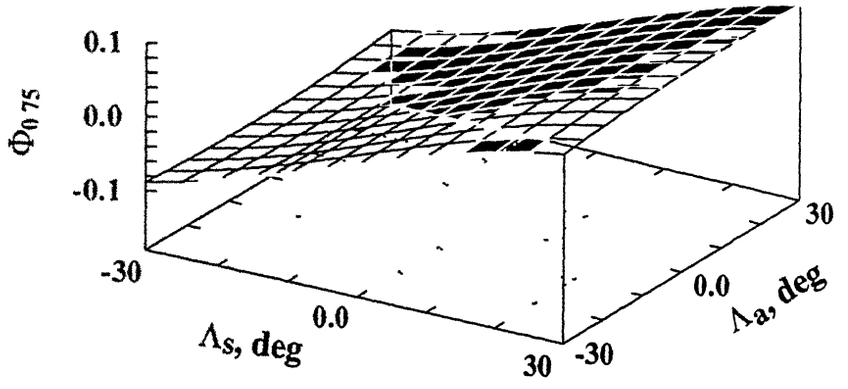

Figure 7 27. (a) for Kc=0

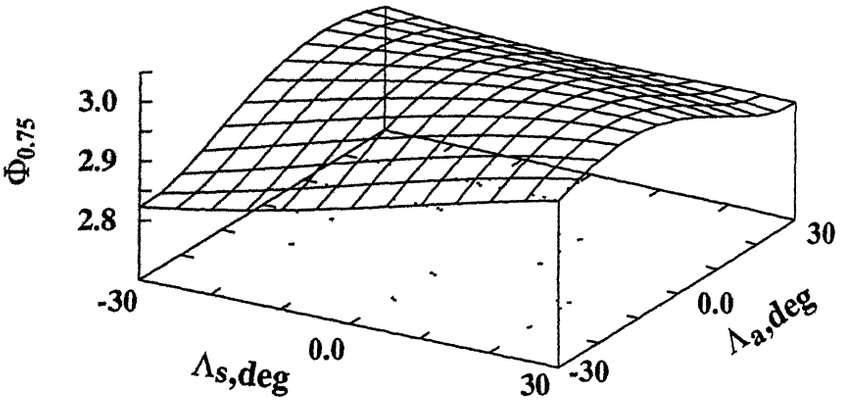

Figure 7 27 (b) for Kc=1000

Figure 7 27 Effect of bending-torsion coupling as a function of tip sweep angle with and without control stiffness third frequency(2nd flap)

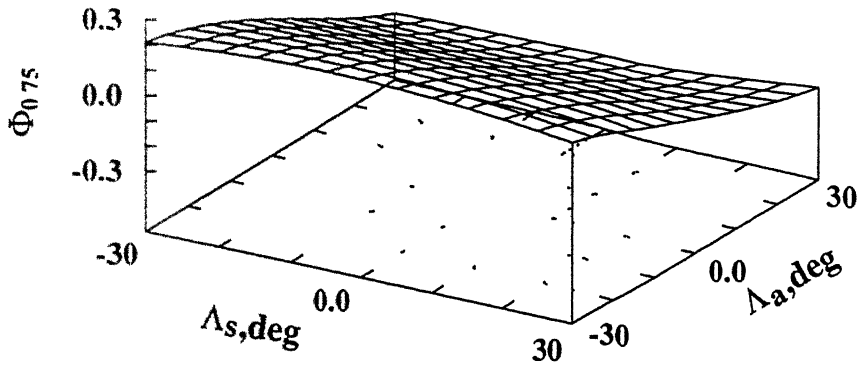

Figure 7 28 (a) for Kc=0

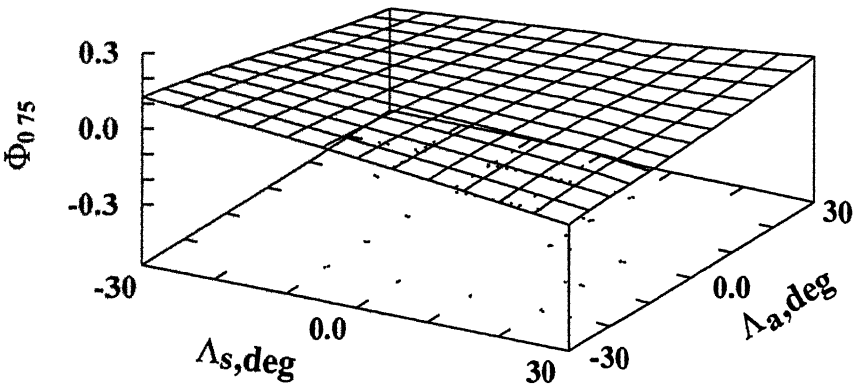

Figure 7 28 (b) for Kc=1000

Figure 7 28 Effect of bending-torsion coupling as a function of tip sweep angle with and without control stiffness fourth frequency(2nd lag)

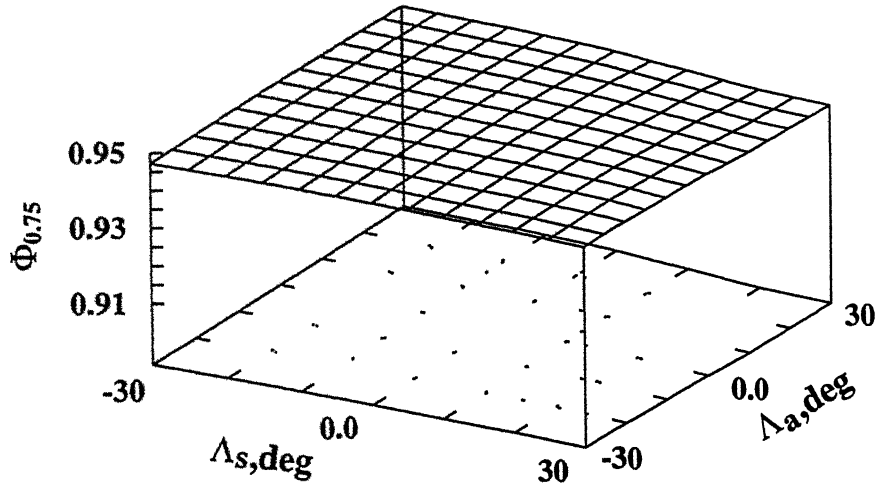

Figure 7.29 (a) for Kc=0

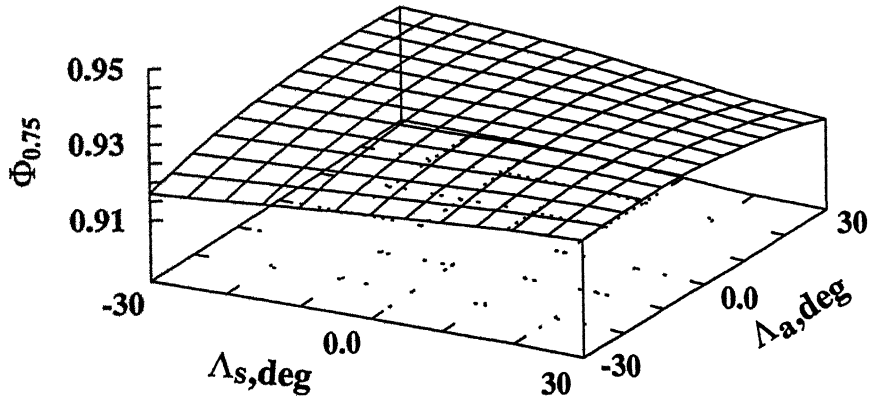

Figure 7 29 (b) for Kc=1000

Figure 7.29 Effect of bending-torsion coupling as a function of tip sweep angle with and without control stiffness fifth frequency(1st torsion)

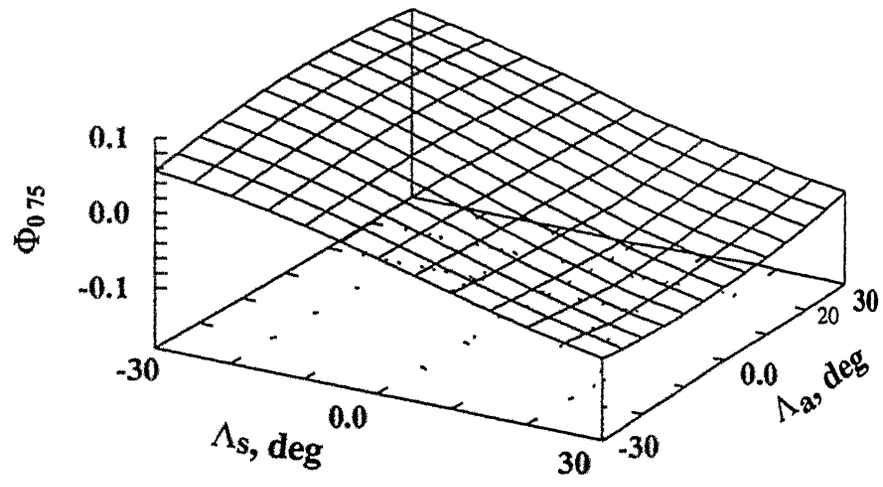

Figure 7.30: (a) for Kc=0

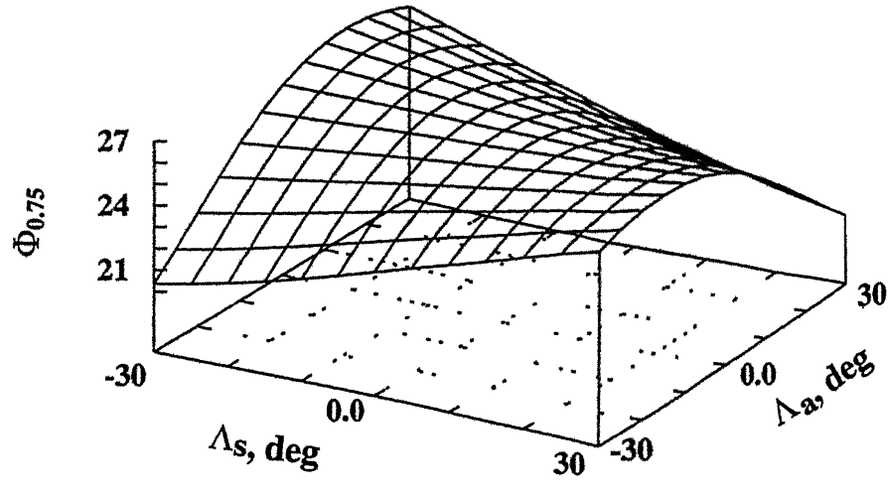

Figure 7.30: (b) for Kc=1000

Figure 7.30. Effect of bending-torsion coupling as a function of tip sweep angle with and without control stiffness sixth frequency(3rd flap)

Chapter 8

CONCLUDING REMARKS

In this thesis, a finite element model has been developed for the dynamic analysis of a bearingless rotor blade having a general configuration This model includes all geometric complelexities of the hub/blade and tip sweep

The equations of motion have been derived using Hamilton's principle The general equations are then specialised for structural dynamic analysis of the rotor blade The formulation was validated by comparing the results of the present analysis for straight bearingless rotor blade, with those available in literature

It is observed that the control spring stiffness introduces bending-torsion coupling The coupling parameter significantly increases with increase in flap natural frequency. Anhedral angle introduces lag-torsion coupling and sweep angle introduces flap-torsion coupling. The results indicate that the control spring stiffness dominate the bending-torsion coupling as compared to the effect due to tip sweep angles

References

[1] Pohit, G . "**Dynamics of a Bearingless Helicopter Rotor Blade with a Non-linear Elastomatic Constraint**", Ph D Thesis, Dept. of Mechanical Engineering. I.I.T Kanpur, Feb. 1999.

[2] Gupta, P K , "**Structural Dynamics of Helicopter Rotor having Precone - Presweep - Predroop - Pretwist and Torque offset including Hub motions**", M.Tech Thesis, Dept. of Aerospace Engineering. I.I.T Kanpur, July 1996

[3] Venu Gopal, M , "**Structural Dynamic Analysis of Rotor Blades with Swept Tips**", M.Tech Thesis, Dept of Aerospace Engineering. I I T Kanpur, May 1999

[4] Yuan, K.A., Friedmann, P.P and Venkatesan, C., "**A New Aeroelastic Model for Composite Rotor Blades with Straight and Swept Tips**", AIAA Paper No. 92-2259, Proc. 33rd AIAA/ASME/ASCE/AHS/ASC Structures, Structural Dynamics and Materials Conf., Dallas, TX, April 1992, pp. 1371-1390.

[5] Yuan, K.A., and Friedmann, P.P "**Aeroelastic and Structural Optimization of Composite Helicopter Rotor Blades with Swept Tips**", NASA Contractor Report 4665, May 1995.

Appendix A

Natural frequencies for variation of location of elastomer, control spring and flexbeam-blade-torque tube junction

Table A 1 Natural frequencies for $L_c = 0.01l$

L_{el} varies from 0 05l to 0 15l in steps of 0 02l

ξ_1 varies from 0.2l to 0 3l in steps of 0 02l

L_{el}	ξ_1	1 lag	1 flap	2 flap	2 lag	torsion	3 flap
0.05	0 20	0.710	1.145	2.631	3 617	4.252	5 448
0 05	0 22	0.711	1 147	2 533	3 483	4.279	5 522
0 05	0 24	0 708	1 147	2.443	3 383	4 312	5 608
0 05	0 26	0 699	1.145	2 366	3 307	4 350	5 703
0 05	0 28	0 685	1 140	2 299	3.249	4 379	5 809
0 05	0 30	0 666	1.133	2.247	3 206	4 401	5.932
0 07	0 20	0.712	1 141	2 505	3 096	3 973	5 444
0.07	0.22	0.714	1.142	2.404	2.986	3.989	5.512
0.07	0.24	0.710	1.141	2.318	2.905	4.006	5.590
0 07	0.26	0.702	1.138	2.244	2.846	4 015	5 678
0 07	0 28	0 687	1.132	2.184	2.803	4.015	5.778
0 07	0 30	0 668	1.123	2.136	2.772	3.999	5.899
0 09	0 20	0 712	1.138	2.402	2 647	3 824	5 443
0 09	0 22	0 713	1 138	2 302	2 549	3 834	5.507
0 09	0 24	0 709	1 136	2 216	2 482	3 838	5 582
0 09	0 26	0 699	1 131	2 146	2 435	3 833	5 666
0.09	0 28	0 683	1 124	2 089	2 402	3 815	5 765
0 09	0 30	0 661	1 114	2.046	2 381	3 785	5 884

0 11	0.20	0 711	1 135	2 323	2 291	3 740	5 444
0 11	0 22	0.710	1.134	2 222	2 194	3 743	5 506
0 11	0 24	0.702	1.131	2.138	2.134	3 740	5 578
0 11	0 26	0 689	1 125	2 070	2 095	3 725	5 661
0 11	0.28	0.670	1.117	2.017	2 071	3 698	5.758
0.11	0 30	0.646	1 105	1 975	2 057	3 658	5 877
0 13	0.20	0 707	1.133	2.260	2 025	3.687	5 447
0 13	0.22	0.702	1 132	2 160	1 915	3 687	5 507
0 13	0 24	0 691	1 128	2 077	1 855	3 677	5 577
0 13	0 26	0 673	1.121	2 011	1 822	3 657	5 658
0.13	0.28	0 649	1 111	1 959	1 805	3 623	5 754
0 13	0 30	0 619	1 098	1 920	1.798	3 577	5 873
0.15	0.20	0.703	1.132	2 211	1.851	3 655	5.450
0.15	0 22	0.693	1.129	2.110	1.708	3 651	5 509
0.15	0.24	0.674	1 124	2.028	1 638	3 637	5 578
0 15	0 26	0 648	1 116	1 963	1.606	3 611	5 658
0 15	0 28	0 617	1 105	1.913	1 595	3 573	5 753
0 15	0 30	0.580	1 091	1 875	1.594	3 523	5 872

Table A 2: Natural frequencies for $L_c = 0.02l$

L_{el} varies from 0 05l to 0 15l in steps of 0 02l

ξ_1 varies from 0 2l to 0.3l in steps of 0 02l

L_{el}	ξ_1	1 lag	1 flap	2 flap	2 lag	torsion	3 flap
0 05	0.20	0.710	1.146	2 639	3 617	4.255	5 487
0.05	0.22	0 711	1 148	2.540	3.483	4 283	5 560
0 05	0 24	0 708	1.148	2 449	3 383	4 317	5 645
0 05	0 26	0 699	1.146	2 371	3 307	4 357	5 738
0.05	0.28	0 685	1 142	2 304	3 249	4 387	5 842
0.05	0.30	0 666	1 135	2 250	3 206	4 411	5 962
0.07	0 20	0 712	1 143	2 515	3 096	3 972	5 484
0 07	0 22	0.714	1.144	2 412	2 986	3 990	5.551
0 07	0 24	0 710	1 143	2 325	2 905	4.008	5 627
0 07	0 26	0.702	1.140	2 249	2.846	4 018	5 713
0 07	0.28	0.687	1.134	2.188	2.803	4.019	5 810
0 07	0.30	0.668	1 126	2.139	2.772	4 005	5 927
0.09	0.20	0.712	1.141	2.411	2.647	3.819	5 483
0 09	0 22	0 713	1 141	2 309	2.549	3 831	5 546
0 09	0 24	0 709	1 139	2 222	2 482	3 836	5 619
0.09	0 26	0 699	1.134	2.151	2 435	3.833	5 701
0.09	0 28	0.683	1 127	2.093	2 402	3 816	5.795
0 09	0 30	0.661	1.117	2 049	2 381	3 786	5 911

Table A 3: Natural frequencies for $L_c = 0\ 03l$

L_{el} varies from $0.05l$ to $0\ 15l$ in steps of $0\ 02l$

ξ_1 varies from $0\ 2l$ to $0\ 3l$ in steps of $0\ 02l$

L_{el}	ξ_1	1 lag	1 flap	2 flap	2 lag	torsion	3 flap
0 05	0 20	0.710	1.148	2 649	3 617	4 258	5 526
0 05	0 22	0 711	1 150	2 548	3 483	4 287	5 598
0 05	0 24	0 708	1 150	2 456	3 383	4 323	5 682
0 05	0 26	0 699	1.149	2 376	3 307	4 364	5 774
0.05	0.28	0.685	1.144	2 308	3 249	4.395	5 876
0 05	0 30	0.666	1 137	2 254	3 206	4 420	5 993
0 07	0 20	0 712	1.146	2.525	3 096	3 971	5 524
0.07	0.22	0 714	1.147	2 421	2 986	3 989	5 589
0 07	0 24	0 710	1.146	2 331	2 905	4 009	5 665
0 07	0 26	0 702	1 143	2 254	2.846	4 021	5 748
0 07	0 28	0.687	1 137	2.193	2 803	4.023	5.842
0.07	0 30	0.668	1.129	2 143	2.772	4 009	5 956
0.09	0.20	0.712	1.144	2.420	2.647	3.813	5.523
0 09	0 22	0 713	1.144	2 316	2.549	3 826	5 585
0 09	0 24	0 709	1.142	2 227	2 482	3 833	5 656
0 09	0 26	0 699	1 138	2 155	2 435	3 831	5 735
0 09	0 28	0 683	1.130	2 096	2 402	3.815	5.826
0.09	0 30	0 661	1.121	2 051	2 381	3 786	5.938

0 11	0 20	0 711	1 142	2 336	2 291	3 723	5 524
0 11	0 22	0.710	1 142	2 232	2 194	3 730	5 584
0 11	0 24	0.702	1.139	2.146	2 134	3 729	5 651
0 11	0 26	0 689	1 133	2.076	2 095	3 717	5 728
0 11	0 28	0 670	1.125	2 020	2 071	3 692	5 817
0 11	0 30	0 646	1.113	1 978	2 057	3 653	5 929
0 13	0 20	0 707	1.141	2 270	2 025	3 667	5 526
0.13	0.22	0.702	1.140	2 166	1.915	3 670	5 584
0 13	0 24	0 691	1 136	2.081	1 855	3 663	5 650
0 13	0 26	0 673	1 129	2 013	1 822	3 645	5 725
0 13	0 28	0 649	1 119	1 959	1 805	3 613	5 813
0 13	0 30	0 619	1 107	1 919	1 798	3 569	5 924
0 15	0 20	0 703	1 140	2 217	1 851	3 631	5 529
0.15	0.22	0.693	1.138	2.113	1.708	3 631	5 586
0.15	0 24	0 674	1.133	2 029	1 638	3 620	5 650
0 15	0 26	0 648	1 125	1 962	1 606	3 597	5 723
0.15	0 28	0 617	1.115	1 911	1.595	3 560	5.810
0.15	0 30	0 580	1.101	1.872	1 594	3 511	5 921

Appendix B

Natural frequencies and coupling measures

Table B 1 Natural frequencies with tip sweep angles variation for $K_c = 0$

Λ_s, deg	Λ_a deg	1 lag	1 flap	2 flap	2 lag	torsion	3 flap
-30 0	-30 0	0 706	1 188	2 355	3 272	3 703	4 791
-25 0	-30 0	0 695	1 186	2 344	3 255	3 704	4 768
-20 0	-30 0	0 686	1 183	2 333	3 241	3 704	4 744
-15 0	-30 0	0 678	1 180	2 321	3 229	3 704	4 719
-10 0	-30 0	0 672	1 175	2 309	3 219	3 704	4 695
-05 0	-30 0	0 667	1 170	2 296	3 211	3 705	4 671
00 0	-30 0	0 664	1 164	2 283	3 206	3 705	4 647
05 0	-30 0	0 663	1 158	2 270	3 203	3 705	4 623
10 0	-30 0	0 663	1 151	2 256	3 202	3 704	4 600
15 0	-30 0	0 664	1 143	2 243	3 202	3 704	4 578
20 0	-30 0	0 667	1 134	2 230	3 205	3 704	4 557
25.0	-30 0	0 671	1 125	2 217	3 210	3 704	4 536
30 0	-30 0	0 676	1 116	2 205	3 216	3 703	4 516
-30 0	-25 0	0 709	1 176	2 319	3 283	3 705	4 720
-25 0	-25 0	0 698	1 174	2 311	3 264	3 705	4 703
-20 0	-25 0	0 689	1 171	2 302	3 247	3 706	4 686
-15 0	-25 0	0 681	1 168	2 293	3 233	3 706	4 668
-10 0	-25 0	0 674	1 164	2 284	3 222	3 706	4 649
-05 0	-25 0	0 669	1 159	2 274	3 213	3 706	4 631
00 0	-25 0	0 665	1 155	2 263	3 206	3 706	4 612
05 0	-25 0	0 662	1 149	2 253	3 202	3 706	4 594
10 0	-25 0	0 661	1 143	2 242	3 199	3 706	4 576
15 0	-25 0	0 661	1 137	2 231	3 199	3 706	4 558
20 0	-25 0	0 663	1 130	2 221	3 200	3 706	4 541
25 0	-25 0	0 666	1 123	2 210	3 203	3 705	4 523
30 0	-25 0	0 669	1 115	2 200	3 207	3 705	4 507

-30 0	-20 0	0 712	1 164	2 289	3 293	3 707	4 662
-25 0	-20 0	0 701	1 162	2 283	3 272	3 707	4 650
-20 0	-20 0	0 691	1 160	2 277	3 253	3 707	4 638
-15 0	-20 0	0 683	1 157	2 270	3 238	3 707	4 626
-10 0	-20 0	0 676	1 154	2 263	3 225	3 707	4 612
-05 0	-20 0	0 670	1 150	2 255	3 214	3 707	4 599
00 0	-20 0	0 665	1 146	2 247	3 206	3 707	4 585
05 0	-20.0	0 662	1 142	2 239	3 200	3 707	4 571
10 0	-20 0	0 660	1 137	2 231	3 197	3 707	4 557
15 0	-20 0	0 659	1 132	2 222	3 195	3 707	4 543
20 0	-20 0	0 660	1.127	2 214	3 195	3 707	4 529
25 0	-20 0	0 661	1 121	2 206	3 197	3 707	4 515
30 0	-20 0	0 663	1 116	2 197	3 200	3 707	4 501

-30 0	-15 0	0 716	1 153	2 264	3 303	3 708	4 615
-25 0	-15 0	0 704	1 152	2 260	3 280	3 708	4 608
-20 0	-15 0	0 694	1 150	2 256	3 259	3 708	4 600
-15 0	-15 0	0 685	1 148	2 251	3 242	3 708	4 592
-10 0	-15 0	0 677	1 145	2 246	3 228	3 708	4 583
-05 0	-15 0	0 671	1 142	2 241	3 216	3 708	4 574
00 0	-15 0	0 665	1 139	2 235	3 206	3 708	4 564
05 0	-15 0	0 661	1 136	2 229	3 199	3 708	4 554
10 0	-15 0	0 659	1 133	2 223	3 194	3 708	4 544
15 0	-15 0	0 657	1 129	2 217	3 191	3 708	4 533
20 0	-15 0	0 656	1 125	2 210	3 190	3 708	4 522
25 0	-15 0	0 657	1 121	2 204	3 191	3 708	4 511
30 0	-15 0	0 658	1 117	2 197	3 193	3 708	4 500

-30 0	-10 0	0 720	1 144	2 243	3 313	3 709	4 578
-25 0	-10 0	0 708	1 143	2 241	3 288	3 709	4 575
-20 0	-10 0	0 697	1 141	2 239	3 265	3 709	4 571
-15 0	-10 0	0 687	1 140	2 236	3 246	3 709	4 567
-10 0	-10 0	0 679	1 138	2 233	3 230	3 709	4 562
-05 0	-10 0	0 671	1 136	2 230	3 217	3 709	4 556
00 0	-10 0	0 665	1 134	2 226	3 206	3 709	4 550
05 0	-10 0	0 661	1 132	2 222	3 198	3 709	4 543
10 0	-10 0	0 657	1 130	2 218	3 192	3 709	4 536
15 0	-10 0	0 655	1 128	2 214	3 188	3 709	4 529
20 0	-10 0	0 654	1 125	2 209	3 186	3 709	4 521
25 0	-10 0	0 653	1 123	2 205	3 185	3 709	4 513
30 0	-10 0	0 654	1 120	2 200	3 186	3 709	4 504

-30 0	-05 0	0 724	1 136	2 227	3 323	3 709	4 549
-25 0	-05 0	0 711	1 135	2 227	3 295	3 709	4 549
-20 0	-05 0	0 699	1 135	2 226	3 271	3 709	4 549
-15 0	-05 0	0 689	1 134	2 225	3 250	3 709	4 548
-10 0	-05 0	0 680	1 133	2 224	3 233	3 709	4 546
-05 0	-05 0	0 672	1 132	2 223	3 218	3 709	4 544
00 0	-05 0	0 666	1 131	2 221	3 206	3 709	4 541
05 0	-05 0	0 660	1 130	2 219	3 197	3 709	4 538
10 0	-05 0	0 656	1 129	2 217	3 190	3 709	4 534
15 0	-05 0	0 653	1 128	2 214	3.185	3 709	4 530
20 0	-05 0	0 651	1 127	2 212	3 182	3 709	4 525
25 0	-05 0	0 650	1 125	2 209	3 180	3 709	4 519
30 0	-05 0	0 650	1 124	2 206	3 180	3 709	4 513

-30 0	00 0	0 728	1 129	2 215	3 333	3 709	4 528
-25 0	00 0	0 715	1 130	2 216	3 303	3 709	4 531
-20 0	00 0	0 702	1 130	2 217	3 277	3 709	4 534
-15 0	00 0	0 691	1 130	2 218	3 254	3 709	4 536
-10 0	00 0	0 681	1 130	2 219	3 235	3 709	4 537
-05 0	00 0	0 673	1 130	2 219	3 219	3 709	4 538
00 0	00 0	0 666	1 130	2 219	3 206	3 709	4 539
05 0	00 0	0 660	1 130	2 219	3 196	3 709	4 538
10 0	00 0	0 655	1 130	2 219	3 188	3 709	4 537
15 0	00 0	0 651	1 130	2 218	3 182	3 709	4 536
20 0	00 0	0 649	1 130	2 217	3 178	3 709	4 534
25 0	00 0	0 647	1 130	2 216	3 176	3 709	4 531
30 0	00 0	0 646	1 129	2 215	3 175	3 709	4 528
-30.0	05 0	0 732	1 124	2 206	3 342	3 709	4 513
-25 0	05 0	0 718	1 125	2 209	3 310	3 709	4 519
-20 0	05 0	0 705	1 127	2 212	3 282	3 709	4 525
-15 0	05 0	0 693	1 128	2 214	3 258	3 709	4 530
-10 0	05 0	0 682	1 129	2 217	3 237	3 709	4 534
-05 0	05 0	0 673	1 130	2 219	3 220	3 709	4 538
00 0	05 0	0 666	1 131	2 221	3 206	3 709	4 541
05 0	05 0	0 659	1 132	2 223	3 195	3 709	4 544
10 0	05 0	0 654	1 133	2 224	3 186	3 709	4 546
15 0	05 0	0 650	1 134	2 225	3 180	3 709	4 548
20 0	05 0	0 647	1 135	2 226	3 175	3 709	4 549
25 0	05 0	0 645	1 135	2 227	3 172	3 709	4 549
30 0	05 0	0 644	1 136	2 227	3 170	3 709	4 549

-30 0	10 0	0 737	1 120	2 200	3 350	3 709	4 504
-25 0	10 0	0 721	1 123	2 205	3 316	3 709	4 513
-20 0	10.0	0 707	1 125	2 209	3 286	3 709	4 521
-15 0	10 0	0 695	1 128	2 214	3 261	3 709	4 529
-10 0	10 0	0 683	1 130	2 218	3 239	3 709	4 536
-05 0	10 0	0 674	1 132	2 222	3 221	3 709	4 543
00 0	10 0	0 665	1 134	2 226	3 206	3 709	4 550
05 0	10 0	0 659	1 136	2 230	3 194	3 709	4 556
10 0	10 0	0 653	1 138	2 233	3 185	3 709	4 562
15 0	10 0	0 649	1 140	2 236	3 177	3 709	4 567
20 0	10 0	0 645	1 141	2 239	3 172	3 709	4 571
25 0	10 0	0 643	1 143	2 241	3 168	3 709	4 575
30.0	10 0	0 642	1 144	2 243	3 166	3 709	4 578
-30 0	15 0	0 741	1 117	2 197	3 358	3 708	4 500
-25 0	15 0	0 725	1 121	2 204	3 322	3 708	4 511
-20 0	15 0	0 710	1 125	2 210	3 290	3 708	4 522
-15 0	15 0	0 696	1 129	2 217	3 264	3 708	4 533
-10 0	15 0	0 684	1 133	2 223	3 241	3 708	4 544
-05 0	15 0	0 674	1 136	2 229	3 222	3 708	4 554
00 0	15 0	0 665	1 139	2 235	3 206	3 708	4 564
05 0	15 0	0 658	1 142	2 241	3 194	3 708	4 574
10 0	15 0	0 652	1 145	2 246	3 183	3 708	4 583
15 0	15 0	0 647	1 148	2 251	3 175	3 708	4 592
20 0	15 0	0 644	1 150	2 256	3 169	3.708	4 600
25 0	15 0	0 642	1 152	2 260	3.165	3 708	4 608
30 0	15 0	0 640	1 153	2 264	3 162	3 708	4 615

-30 0	20 0	0 745	1 116	2 197	3 365	3 707	4 501
-25 0	20 0	0 728	1 122	2 206	3 327	3 707	4 515
-20 0	20 0	0 712	1 127	2 214	3 294	3 707	4 529
-15 0	20 0	0 697	1 132	2 222	3 266	3 707	4 543
-10 0	20 0	0 685	1 137	2 231	3 243	3 707	4 557
-05 0	20 0	0 674	1 142	2 239	3 223	3 707	4 571
00 0	20 0	0 665	1 146	2 247	3 206	3 707	4 585
05 0	20 0	0 657	1 150	2 255	3 193	3 707	4 599
10 0	20 0	0 651	1 154	2 263	3 182	3 707	4 612
15 0	20 0	0 647	1 157	2 270	3 173	3 707	4 626
20 0	20 0	0 643	1 160	2 277	3 167	3 707	4 638
25 0	20 0	0 641	1 162	2 283	3 162	3 707	4 650
30 0	20 0	0 640	1 164	2 289	3 159	3 707	4 662
-30 0	25 0	0 749	1 116	2 200	3 371	3 705	4 507
-25 0	25 0	0 731	1 123	2 210	3 331	3 705	4 523
-20 0	25 0	0 714	1 130	2 221	3 297	3 706	4 541
-15 0	25 0	0 699	1 137	2 231	3 268	3 706	4 558
-10 0	25 0	0 686	1 143	2 242	3 244	3 706	4 576
-05 0	25 0	0 674	1 149	2 253	3 223	3 706	4 594
00 0	25 0	0 665	1 155	2 263	3 206	3 706	4 612
05 0	25 0	0 657	1 159	2 274	3 192	3 706	4 631
10 0	25 0	0 651	1 164	2 284	3 181	3 706	4 649
15 0	25 0	0 646	1 168	2 293	3 172	3 706	4 668
20 0	25 0	0 643	1 171	2 302	3 165	3 706	4 686
25 0	25 0	0 641	1 173	2 311	3.160	3 705	4 703
30 0	25 0	0 640	1 175	2 319	3 157	3 705	4 720

-30 0	30 0	0 753	1 117	2 205	3 376	3 703	4 516
-25 0	30 0	0 734	1 126	2 217	3 335	3 704	4 536
-20 0	30 0	0 716	1 134	2 230	3 300	3 704	4 557
-15 0	30 0	0 700	1 143	2 243	3 270	3 704	4 578
-10 0	30 0	0 686	1 151	2 256	3 245	3 704	4 600
-05 0	30 0	0 674	1 158	2 270	3 224	3 705	4 623
00 0	30 0	0 664	1 164	2 283	3 206	3 705	4 647
05 0	30 0	0 656	1 170	2 296	3 192	3 705	4 671
10 0	30 0	0 650	1 175	2 309	3 180	3 704	4 695
15 0	30 0	0 646	1 180	2 321	3 171	3 704	4 719
20 0	30 0	0 643	1 183	2 333	3 164	3 704	4 744
25 0	30 0	0 641	1 186	2 344	3 159	3 704	4 768
30 0	30 0	0 640	1 188	2 355	3 155	3 703	4 791

Table B 2 Natural frequencies with tip sweep angles variation for $K_c = 1000$

Λ_i deg	Λ_a deg	1 lag	1 flap	2 flap	2 lag	torsion	3 flap
-30 0	-30 0	0 706	1 194	2 388	3 272	4 588	6 213
-25 0	-30 0	0 695	1 192	2 377	3 255	4 572	6 186
-20 0	-30 0	0 686	1 189	2 366	3 241	4 556	6 159
-15 0	-30 0	0 678	1 185	2 353	3 229	4 539	6 133
-10 0	-30 0	0 672	1 181	2 341	3 219	4 523	6 107
-05 0	-30 0	0 667	1 176	2 328	3 211	4 506	6 082
00 0	-30 0	0 664	1 170	2 314	3 206	4 489	6 058
05 0	-30 0	0 663	1 163	2 301	3 203	4 472	6 035
10 0	-30 0	0 663	1 156	2 287	3 202	4 456	6 013
15 0	-30 0	0 664	1 148	2 274	3 202	4 440	5 993
20 0	-30 0	0 667	1 139	2 261	3 205	4 424	5 973
25 0	-30 0	0 671	1 130	2 248	3 210	4 409	5 955
30 0	-30 0	0 676	1 121	2 235	3 216	4 394	5 938
-30 0	-25 0	0 709	1 181	2 352	3 283	4 539	6 136
-25 0	-25 0	0 698	1 179	2 344	3 264	4 528	6 118
-20 0	-25 0	0 689	1 176	2 335	3 247	4 516	6 100
-15 0	-25 0	0 681	1 173	2 325	3 233	4 503	6 081
-10 0	-25 0	0 674	1 169	2 315	3 222	4 491	6 063
-05 0	-25 0	0 669	1 165	2 305	3 213	4 478	6 044
00 0	-25 0	0 665	1 160	2 295	3 206	4 465	6 026
05 0	-25 0	0 662	1 154	2 284	3 202	4 451	6 009
10 0	-25 0	0 661	1 148	2 273	3 199	4 438	5 992
15 0	-25 0	0 661	1 142	2 262	3 199	4 425	5 976
20 0	-25 0	0 663	1 135	2 251	3 200	4 412	5 960
25 0	-25 0	0 666	1 127	2 241	3 203	4 399	5 945
30 0	-25 0	0 669	1 120	2 230	3 207	4 387	5 931

-30 0	-20 0	0 712	1 169	2 322	3 293	4 499	6 077
-25 0	-20 0	0 701	1 167	2 315	3 272	4 491	6 066
-20 0	-20 0	0 691	1 165	2 309	3 253	4 483	6 053
-15 0	-20 0	0 683	1 162	2 302	3 238	4 474	6 041
-10 0	-20 0	0 676	1 159	2 294	3 225	4 464	6 028
-05 0	-20 0	0 670	1 155	2 287	3 214	4 455	6 015
00 0	-20 0	0 665	1 151	2 279	3 206	4 445	6 002
05 0	-20 0	0 662	1 147	2 270	3 200	4 435	5 989
10 0	-20 0	0 660	1 142	2 262	3 197	4 425	5 976
15 0	-20 0	0 659	1 137	2 253	3 195	4 414	5 963
20 0	-20 0	0 660	1 132	2 245	3 195	4 404	5 951
25 0	-20 0	0 661	1 126	2 236	3 197	4 393	5 939
30 0	-20 0	0 663	1 120	2 228	3 200	4 383	5 927

-30 0	-15 0	0 716	1 158	2 296	3 303	4 465	6 032
-25 0	-15 0	0 704	1 157	2 292	3 280	4 461	6 025
-20 0	-15 0	0 694	1 155	2 288	3 259	4 455	6 018
-15 0	-15 0	0 685	1 152	2 283	3 242	4 450	6 010
-10 0	-15 0	0 677	1 150	2 278	3 228	4 443	6 002
-05 0	-15 0	0 671	1 147	2 272	3 216	4 437	5 993
00 0	-15 0	0 665	1 144	2 266	3 206	4 430	5 984
05 0	-15 0	0 661	1 141	2 260	3 199	4 423	5 974
10 0	-15 0	0 659	1 137	2 254	3 194	4 415	5 965
15 0	-15 0	0 657	1 134	2 247	3 191	4 407	5 955
20 0	-15 0	0 656	1 130	2 241	3 190	4 399	5 946
25 0	-15 0	0 657	1 126	2 234	3 191	4 391	5 936
30 0	-15 0	0 658	1 122	2 228	3 193	4 383	5 927

-30 0	-10 0	0 720	1 149	2 275	3 313	4 439	5 998
-25 0	-10 0	0 708	1 148	2 273	3 288	4 437	5 995
-20 0	-10 0	0 697	1 146	2 271	3 265	4 434	5 991
-15 0	-10 0	0 687	1 145	2 268	3 246	4 431	5 987
-10 0	-10 0	0 679	1 143	2 265	3 230	4 427	5 982
-05 0	-10 0	0 671	1 141	2 261	3 217	4 424	5 977
00 0	-10 0	0 665	1 139	2 257	3 206	4 419	5 971
05 0	-10 0	0 661	1 137	2 253	3 198	4 414	5 965
10 0	-10 0	0 657	1 135	2 249	3 192	4 409	5 959
15 0	-10 0	0 655	1 132	2 245	3 188	4 404	5 952
20 0	-10 0	0 654	1 130	2 240	3 186	4 398	5 945
25 0	-10 0	0 653	1 127	2 235	3 185	4 392	5 938
30 0	-10 0	0 654	1 125	2 230	3 186	4 386	5 931

-30 0	-05 0	0 724	1 141	2 259	3 323	4 418	5 972
-25 0	-05 0	0 711	1 140	2 258	3 295	4 418	5 973
-20 0	-05 0	0 699	1 139	2 258	3 271	4 418	5 972
-15 0	-05 0	0 689	1 139	2 257	3 250	4 417	5 971
-10 0	-05 0	0 680	1 138	2 255	3 233	4 416	5 969
-05 0	-05 0	0 672	1 137	2 254	3 218	4 415	5 967
00 0	-05 0	0 666	1 136	2 252	3 206	4 413	5 964
05 0	-05 0	0 660	1 135	2 250	3 197	4 411	5 961
10 0	-05 0	0 656	1 134	2 248	3 190	4 408	5 957
15 0	-05 0	0 653	1 133	2 245	3 185	4 405	5 953
20 0	-05 0	0 651	1 131	2 242	3 182	4 401	5 949
25 0	-05 0	0 650	1 130	2 239	3 180	4 397	5 944
30 0	-05 0	0 650	1 129	2 236	3 180	4 393	5 939

-30 0	00 0	0 728	1 134	2 246	3 333	4 402	5 954
-25 0	00 0	0 715	1 134	2 248	3 303	4 404	5 957
-20 0	00 0	0 702	1 134	2 249	3 277	4 406	5 959
-15 0	00 0	0 691	1 135	2 249	3 254	4 408	5 960
-10 0	00 0	0 681	1 135	2 250	3 235	4 409	5 961
-05 0	00 0	0 673	1 135	2 250	3 219	4 410	5 962
00 0	00 0	0 666	1 135	2 250	3 206	4 411	5 962
05 0	00 0	0 660	1 135	2 250	3 196	4 411	5 961
10 0	00 0	0 655	1 135	2 250	3 188	4 410	5 960
15 0	00 0	0 651	1 135	2 249	3 182	4 409	5 959
20 0	00 0	0 649	1 135	2 248	3 178	4 408	5 957
25 0	00 0	0 647	1 134	2 247	3 176	4 406	5 954
30 0	00 0	0 646	1 134	2 245	3 175	4 404	5 951
-30 0	05 0	0 732	1 128	2 237	3 342	4 391	5 941
-25 0	05 0	0 718	1 130	2 240	3 310	4 395	5 946
-20 0	05 0	0 705	1 131	2 243	3 282	4 399	5 951
-15 0	05 0	0 693	1 132	2 246	3 258	4 403	5 955
-10 0	05 0	0 682	1 134	2 248	3 237	4 407	5 958
-05 0	05 0	0 673	1 135	2 250	3 220	4 410	5 962
00 0	05 0	0 666	1 136	2 252	3 206	4 413	5 964
05 0	05 0	0 659	1 137	2 254	3 195	4 415	5 966
10 0	05 0	0 654	1 138	2 255	3 186	4 417	5 968
15 0	05 0	0 650	1 139	2 256	3 180	4 419	5 969
20 0	05 0	0 647	1 140	2 257	3 175	4 419	5 970
25 0	05 0	0 645	1 140	2 257	3 172	4.420	5 970
30 0	05 0	0 644	1 141	2 258	3 170	4 420	5 970

-30 0	10 0	0 737	1 124	2 231	3 350	4 384	5 933
-25 0	10 0	0 721	1 127	2 236	3 316	4 390	5 940
-20 0	10 0	0 707	1 130	2 241	3 286	4 397	5 947
-15 0	10 0	0 695	1 132	2 245	3 261	4 403	5 954
-10 0	10 0	0 683	1 135	2 249	3 239	4 409	5 960
-05 0	10 0	0 674	1 137	2 253	3 221	4 414	5 966
00 0	10 0	0 665	1 139	2 257	3 206	4 419	5 971
05 0	10 0	0 659	1 141	2 261	3 194	4 424	5 977
10 0	10 0	0 653	1 143	2 264	3 185	4 428	5 981
15 0	10 0	0 649	1 145	2 267	3 177	4 432	5 986
20 0	10 0	0 645	1 147	2 270	3 172	4 436	5 989
25 0	10 0	0.643	1 148	2 272	3 168	4 439	5 992
30 0	10 0	0 642	1 149	2 274	3 166	4 441	5 995
-30 0	15 0	0 741	1 122	2 229	3 358	4 381	5 929
-25 0	15 0	0 725	1 126	2 235	3 322	4 389	5 939
-20 0	15 0	0 710	1 130	2 241	3 290	4 398	5 948
-15 0	15 0	0 696	1 134	2 248	3 264	4 406	5 957
-10 0	15 0	0 684	1 137	2 254	3 241	4 414	5 966
-05 0	15 0	0 674	1 141	2 260	3 222	4 422	5 975
00 0	15 0	0 665	1 144	2 266	3 206	4 430	5 984
05 0	15 0	0 658	1 147	2 272	3 194	4 437	5 992
10 0	15 0	0 652	1 150	2 277	3 183	4 444	6 001
15 0	15 0	0 647	1 153	2 282	3 175	4 451	6 008
20 0	15 0	0 644	1 155	2 287	3 169	4 457	6 016
25 0	15 0	0 642	1 157	2 291	3 165	4 463	6 023
30 0	15 0	0 640	1 159	2 295	3 162	4 468	6 029

-30 0	20 0	0 745	1 120	2 229	3 365	4 381	5 930
-25 0	20 0	0 728	1 126	2 237	3 327	4 392	5 941
-20 0	20 0	0 712	1 131	2 245	3 294	4 402	5 953
-15 0	20 0	0 697	1 137	2 254	3 266	4 413	5 965
-10 0	20 0	0 685	1 142	2 262	3 243	4 424	5 977
-05 0	20 0	0 674	1 147	2 270	3 223	4 434	5 989
00 0	20 0	0 665	1 151	2 279	3 206	4 445	6 002
05 0	20 0	0 657	1 155	2 286	3 193	4 455	6 014
10 0	20 0	0 651	1 159	2 294	3 182	4 465	6 027
15.0	20 0	0 647	1 162	2 301	3 173	4 475	6 039
20 0	20 0	0 643	1 165	2 308	3 167	4 484	6 051
25 0	20 0	0 641	1 167	2 315	3 162	4 493	6 063
30 0	20 0	0 640	1 169	2 320	3 159	4 501	6 074
-30 0	25 0	0 749	1 120	2 231	3 371	4 385	5 933
-25 0	25 0	0 731	1 127	2 241	3 331	4 398	5 947
-20 0	25 0	0 714	1 135	2 252	3 297	4 411	5 962
-15 0	25 0	0 699	1 141	2 263	3 268	4 424	5 977
-10 0	25 0	0 686	1 148	2 273	3 244	4 437	5 993
-05 0	25 0	0 674	1 154	2 284	3 223	4 451	6 009
00 0	25 0	0 665	1 160	2 295	3 206	4 465	6 026
05 0	25 0	0 657	1 165	2 305	3 192	4 478	6 044
10 0	25 0	0 651	1 169	2 315	3 181	4 492	6 061
15 0	25 0	0 646	1 173	2 325	3 172	4 505	6 079
20 0	25 0	0 643	1 177	2 334	3 165	4 518	6 097
25 0	25 0	0 641	1 179	2 343	3 160	4 530	6 115
30 0	25 0	0 640	1 181	2 351	3 157	4 542	6 133

-30 0	30 0	0 753	1 121	2 236	3 376	4 392	5 941
-25 0	30 0	0 734	1 130	2 249	3 335	4 407	5 957
-20 0	30 0	0 716	1 139	2 261	3 300	4 423	5 975
-15 0	30 0	0 700	1 147	2 275	3 270	4 439	5 994
-10 0	30 0	0 686	1 156	2 288	3 245	4 455	6 015
-05 0	30 0	0 674	1 163	2 301	3 224	4 472	6 036
00 0	30 0	0 664	1 170	2 314	3 206	4 489	6 058
05 0	30 0	0 656	1 176	2 328	3 192	4 506	6 082
10 0	30 0	0 650	1 181	2 340	3 180	4 524	6 106
15 0	30 0	0 646	1 186	2 353	3 171	4 541	6 131
20 0	30 0	0 643	1 189	2 365	3 164	4 558	6 157
25 0	30 0	0 641	1 192	2 376	3 159	4 574	6 183
30 0	30 0	0 640	1 194	2 387	3 155	4 590	6 209

Table B 3 Bending-torsion coupling with tip sweep angles variation for $K_c = 0$

Λ_s, deg	Λ_a, deg	1 lag	1 flap	2 flap	2 lag	torsion	3 flap
-30 0	-30 0	0 059	-0 064	-0 088	0 210	0 947	0 056
-25 0	-30 0	0 063	-0 057	-0 078	0 223	0 947	0 051
-20 0	-30 0	0 066	-0 047	-0 065	0 233	0 947	0 043
-15 0	-30 0	0 069	-0 037	-0 050	0 240	0 947	0 035
-10 0	-30 0	0 071	-0 025	-0 034	0 245	0 947	0 024
-05 0	-30 0	0 072	-0 013	-0 017	0 247	0 947	0 013
00 0	-30 0	0 072	0 000	0 000	0 247	0 947	0 000
05 0	-30 0	0 072	0 013	0 017	0 243	0 947	-0 013
10 0	-30 0	0 071	0 025	0 032	0 237	0 947	-0 026
15 0	-30 0	0 069	0 036	0 047	0 228	0 947	-0 039
20 0	-30 0	0 066	0 047	0 060	0 216	0 947	-0 051
25 0	-30 0	0 063	0 055	0 070	0 202	0 947	-0 062
30 0	-30 0	0 059	0 062	0 079	0 186	0 947	-0 072
-30 0	-25 0	0 053	-0 067	-0 090	0 190	0 947	0 063
-25 0	-25 0	0 056	-0 060	-0 079	0 200	0 947	0 056
-20 0	-25 0	0 059	-0 050	-0 066	0 208	0 947	0 048
-15 0	-25 0	0 061	-0 039	-0 051	0 214	0 947	0 038
-10 0	-25 0	0 063	-0 027	-0 035	0 217	0 947	0 026
-05 0	-25 0	0 064	-0 013	-0 017	0 219	0 947	0 014
00 0	-25 0	0 064	0 000	0 000	0 218	0 947	0 000
05 0	-25 0	0 064	0 013	0 017	0 214	0 947	-0 014
10 0	-25 0	0 063	0 026	0 033	0 208	0 947	-0 028
15 0	-25 0	0 061	0 038	0 049	0 199	0 947	-0 042
20 0	-25 0	0 059	0 049	0 062	0 189	0 947	-0 054
25 0	-25 0	0 056	0 059	0 073	0 176	0 947	-0 066
30 0	-25 0	0 053	0 066	0 082	0 161	0 947	-0 076

-30 0	-20 0	0 044	-0 070	-0 091	0 162	0 948	0 068
-25 0	-20 0	0 047	-0 062	-0 080	0 170	0 948	0 061
-20.0	-20 0	0 049	-0 052	-0 067	0 176	0 948	0 052
-15 0	-20 0	0 051	-0 041	-0 052	0 180	0 948	0 041
-10 0	-20 0	0 053	-0 028	-0 035	0 183	0 948	0 028
-05 0	-20 0	0 053	-0 014	-0 018	0 184	0 948	0 014
00 0	-20 0	0 054	0 000	0 000	0 182	0 948	0 000
05 0	-20 0	0 053	0 014	0 018	0 179	0 948	-0 015
10 0	-20 0	0 052	0 028	0 034	0 173	0 948	-0 030
15 0	-20 0	0 051	0 040	0 050	0 166	0 948	-0 044
20 0	-20 0	0 049	0 052	0 064	0 156	0 948	-0 057
25 0	-20 0	0 047	0 061	0 076	0 145	0 948	-0 069
30 0	-20 0	0 044	0 069	0 085	0 133	0 948	-0 079

-30 0	-15 0	0 035	-0 073	-0 092	0 129	0 948	0 073
-25 0	-15 0	0 037	-0 064	-0 081	0 134	0 948	0 065
-20 0	-15 0	0 038	-0 054	-0 068	0 138	0 948	0 055
-15 0	-15 0	0 040	-0 042	-0 053	0 141	0 948	0 043
-10 0	-15 0	0 041	-0 029	-0 036	0 143	0 948	0 030
-05 0	-15 0	0 041	-0 015	-0 018	0 143	0 948	0 015
00 0	-15 0	0 042	0 000	0 000	0 141	0 948	0 000
05 0	-15 0	0 041	0 015	0 018	0 138	0 948	-0 016
10 0	-15 0	0 041	0 029	0 035	0 134	0 948	-0 031
15 0	-15 0	0 040	0 042	0 051	0 128	0 948	-0 046
20 0	-15 0	0 038	0 054	0 065	0 120	0 948	-0 059
25 0	-15 0	0 036	0 064	0 078	0 112	0 948	-0 071
30 0	-15 0	0 034	0 072	0 087	0 102	0 948	-0 081

-30 0	-10 0	0 024	-0 075	-0 092	0 090	0 948	0 077
-25 0	-10 0	0 025	-0 066	-0 082	0 093	0 948	0 069
-20 0	-10 0	0 026	-0 055	-0 068	0 096	0 948	0 058
-15 0	-10 0	0 027	-0 043	-0 053	0 097	0 948	0 045
-10 0	-10 0	0 028	-0 029	-0 036	0 098	0 948	0 031
-05 0	-10 0	0 028	-0 015	-0 018	0 098	0 948	0 016
00 0	-10 0	0 028	0 000	0 000	0 097	0 948	0 000
05 0	-10 0	0 028	0 015	0 018	0 094	0 948	-0 016
10 0	-10 0	0 028	0 029	0 036	0 091	0 948	-0 032
15 0	-10 0	0 027	0 043	0 052	0 087	0 948	-0 047
20 0	-10 0	0 026	0 055	0 067	0 081	0 948	-0 060
25 0	-10 0	0 025	0 066	0 079	0 075	0 948	-0 073
30 0	-10 0	0 023	0 074	0 089	0 069	0 948	-0 083

-30 0	-05 0	0 012	-0 076	-0 092	0 047	0 948	0 080
-25 0	-05 0	0 013	-0 067	-0 082	0 048	0 948	0 071
-20 0	-05 0	0 013	-0 056	-0 068	0 049	0 948	0 060
-15 0	-05 0	0 014	-0 044	-0 053	0 050	0 948	0 046
-10 0	-05 0	0 014	-0 030	-0 036	0 050	0 948	0 032
-05 0	-05 0	0 014	-0 015	-0 018	0 050	0 948	0 016
00 0	-05 0	0 014	0 000	0 000	0 049	0 948	0 000
05 0	-05 0	0 014	0 015	0 018	0 048	0 948	-0 016
10 0	-05 0	0 014	0 030	0 036	0 046	0 948	-0 032
15 0	-05 0	0 014	0 044	0 053	0 044	0 948	-0 047
20 0	-05 0	0 013	0 056	0 068	0 041	0 948	-0 061
25 0	-05 0	0 013	0 067	0 080	0 038	0 948	-0 073
30 0	-05 0	0 012	0 075	0 091	0 034	0 948	-0 083

-30 0	00 0	0 000	-0 076	-0 092	0 000	0 948	0 082
-25 0	00 0	0 000	-0 067	-0 081	0 000	0 948	0 073
-20 0	00 0	0 000	-0 056	-0 068	0 000	0 948	0 061
-15 0	00 0	0 000	-0 044	-0 053	0 000	0 948	0 047
-10 0	00 0	0 000	-0 030	-0 036	0 000	0 948	0 032
-05 0	00 0	0 000	-0 015	-0 018	0 000	0 948	0 016
00 0	00 0	0 000	0 000	0 000	0 000	0 948	0 000
05 0	00 0	0 000	0 015	0 018	0 000	0 948	-0 016
10 0	00 0	0 000	0 030	0 036	0 000	0 948	-0 032
15 0	00 0	0 000	0 044	0 053	0 000	0 948	-0 047
20 0	00 0	0 000	0 056	0 068	0 000	0 948	-0 061
25 0	00 0	0 000	0 067	0 081	-0 000	0 948	-0 073
30 0	00 0	0 000	0 076	0 092	-0 000	0 948	-0 082

-30 0	05 0	-0 012	-0 075	-0 091	-0 049	0 948	0 083
-25 0	05 0	-0 013	-0 067	-0 080	-0 050	0 948	0 073
-20 0	05 0	-0 013	-0 056	-0 068	-0 050	0 948	0 061
-15 0	05 0	-0 014	-0 044	-0 053	-0 051	0 948	0 047
-10 0	05 0	-0 014	-0 030	-0 036	-0 050	0 948	0 032
-05 0	05 0	-0 014	-0 015	-0 018	-0 050	0 948	0 016
00 0	05 0	-0 014	0 000	0 000	-0 049	0 948	0 000
05 0	05 0	-0 014	0 015	0 018	-0 048	0 948	-0 016
10 0	05 0	-0 014	0 030	0 036	-0 046	0 948	-0 032
15 0	05 0	-0 014	0 044	0 053	-0 043	0 948	-0 046
20 0	05 0	-0 013	0 056	0 068	-0 040	0 948	-0 060
25 0	05 0	-0 013	0 067	0 082	-0 037	0 948	-0 071
30 0	05 0	-0 012	0 076	0 092	-0 034	0 948	-0 080

-30 0	10 0	-0 024	-0 074	-0 089	-0 099	0 948	0 083
-25 0	10 0	-0 025	-0 065	-0 079	-0 100	0 948	0 073
-20 0	10 0	-0 026	-0 055	-0 067	-0 100	0 948	0 060
-15 0	10 0	-0 027	-0 043	-0 052	-0 100	0 948	0 047
-10 0	10 0	-0 028	-0 029	-0 036	-0 100	0 948	0 032
-05 0	10 0	-0 028	-0 015	-0 018	-0 099	0 948	0 016
00 0	10 0	-0 028	0 000	0 000	-0 097	0 948	0 000
05 0	10 0	-0 028	0 015	0 018	-0 094	0 948	-0 016
10 0	10 0	-0 028	0 029	0 036	-0 090	0 948	-0 031
15 0	10 0	-0 027	0 043	0 053	-0 085	0 948	-0 045
20 0	10 0	-0 026	0 055	0 068	-0 079	0 948	-0 058
25 0	10 0	-0 025	0 066	0 082	-0 073	0 948	-0 069
30 0	10 0	-0 023	0 075	0 092	-0 066	0 948	-0 077
-30 0	15 0	-0 035	-0 072	-0 087	-0 149	0 948	0 081
-25 0	15 0	-0 037	-0 064	-0 078	-0 148	0 948	0 071
-20 0	15 0	-0 039	-0 053	-0 065	-0 148	0 948	0 059
-15 0	15 0	-0 040	-0 042	-0 051	-0 148	0 948	0 046
-10 0	15 0	-0 041	-0 029	-0 035	-0 147	0 948	0 031
-05 0	15 0	-0 041	-0 015	-0 018	-0 145	0 948	0 016
00 0	15 0	-0 042	0 000	0 000	-0 141	0 948	0 000
05 0	15 0	-0 041	0 015	0 018	-0 137	0 948	-0 015
10 0	15 0	-0 041	0 029	0 036	-0 131	0 948	-0 030
15 0	15 0	-0 040	0 042	0 053	-0 124	0 948	-0 043
20 0	15 0	-0 038	0 054	0 068	-0 116	0 948	-0 055
25 0	15 0	-0 036	0 065	0 081	-0 106	0 948	-0 065
30 0	15 0	-0 034	0 073	0 092	-0 096	0 948	-0 073

-30 0	20 0	-0 045	-0 069	-0 085	-0 195	0 948	0 079
-25 0	20 0	-0 048	-0 061	-0 076	-0 194	0 948	0 069
-20 0	20 0	-0 050	-0 051	-0 064	-0 193	0 948	0 057
-15 0	20 0	-0 051	-0 040	-0 050	-0 192	0 948	0 044
-10 0	20 0	-0 053	-0 027	-0 034	-0 190	0 948	0 030
-05 0	20 0	-0 053	-0 014	-0 018	-0 187	0 948	0 015
00 0	20 0	-0 054	0 000	0 000	-0 182	0 948	0 000
05 0	20 0	-0 053	0 014	0 018	-0 176	0 948	-0 014
10 0	20 0	-0 052	0 028	0 035	-0 168	0 948	-0 028
15 0	20 0	-0 051	0 041	0 052	-0 159	0 948	-0 041
20 0	20 0	-0 049	0 052	0 067	-0 148	0 948	-0 052
25 0	20 0	-0 047	0 063	0 080	-0 136	0 948	-0 061
30 0	20 0	-0 044	0 071	0 091	-0 123	0 948	-0 068

-30 0	25 0	-0 054	-0 065	-0 082	-0 238	0 947	0 076
-25 0	25 0	-0 057	-0 058	-0 073	-0 235	0 947	0 066
-20 0	25 0	-0 059	-0 049	-0 062	-0 232	0 947	0 054
-15 0	25 0	-0 061	-0 038	-0 049	-0 230	0 947	0 042
-10 0	25 0	-0 063	-0 026	-0 033	-0 227	0 947	0 028
-05 0	25 0	-0 064	-0 013	-0 017	-0 223	0 947	0 014
00 0	25 0	-0 064	0 000	0 000	-0 218	0 947	0 000
05 0	25 0	-0 064	0 013	0 017	-0 210	0 947	-0 014
10 0	25 0	-0 062	0 027	0 035	-0 201	0 947	-0 026
15 0	25 0	-0 061	0 039	0 051	-0 190	0 947	-0 038
20 0	25 0	-0 058	0 050	0 066	-0 177	0 947	-0 048
25 0	25 0	-0 055	0 060	0 079	-0 162	0 947	-0 056
30 0	25 0	-0 052	0 068	0 090	-0 146	0 947	-0 063

-30 0	30 0	-0 061	-0 061	-0 079	-0 274	0 947	0 071
-25 0	30 0	-0 064	-0 054	-0 070	-0 269	0 947	0 062
-20 0	30 0	-0 067	-0 046	-0 059	-0 265	0 947	0 051
-15 0	30 0	-0 069	-0 036	-0 047	-0 262	0 947	0 039
-10 0	30 0	-0 071	-0 025	-0 032	-0 258	0 947	0 026
-05 0	30 0	-0 072	-0 013	-0 017	-0 253	0 947	0 013
00 0	30 0	-0 072	0 000	0 000	-0 247	0 947	0 000
05 0	30 0	-0 072	0 013	0 017	-0 238	0 947	-0 013
10 0	30 0	-0 071	0 025	0 034	-0 227	0 947	-0 024
15 0	30 0	-0 069	0 037	0 050	-0 215	0 947	-0 035
20 0	30 0	-0 066	0 048	0 065	-0 200	0 947	-0 044
25 0	30.0	-0 063	0 057	0 078	-0 183	0 947	-0 051
30 0	30 0	-0 059	0 065	0 089	-0 166	0 947	-0 056

Table B 4 Bending-torsion coupling with tip sweep angles variation for $K_c = 1000$

Λ_t, deg	Λ_a, deg	1 lag	1 flap	2 flap	2 lag	torsion	3 flap
-30 0	-30 0	0 058	-0 797	2 822	0 126	0 917	20 364
-25 0	-30 0	0 056	-0 788	2 832	0 116	0 918	20 699
-20 0	-30 0	0 054	-0 778	2 842	0 105	0 918	21 077
-15 0	-30 0	0 052	-0 765	2 854	0 094	0 919	21 495
-10 0	-30 0	0 050	-0 749	2 867	0 083	0 920	21 950
-05 0	-30 0	0 047	-0 732	2 880	0 070	0 921	22 435
00 0	-30 0	0 043	-0 713	2 895	0 057	0 921	22 946
05 0	-30 0	0 039	-0 693	2 910	0 043	0 922	23 477
10 0	-30 0	0 035	-0 672	2 925	0 029	0 923	24 019
15 0	-30 0	0 030	-0 651	2 940	0 013	0 924	24 568
20 0	-30 0	0 025	-0 630	2 955	-0 003	0 924	25 116
25 0	-30 0	0 019	-0 609	2 969	-0 019	0 925	25 657
30 0	-30 0	0 013	-0 590	2 982	-0 035	0 925	26 185
-30 0	-25 0	0 052	-0 773	2 824	0 108	0 919	21 354
-25 0	-25 0	0 050	-0 765	2 838	0 100	0 920	21 712
-20 0	-25 0	0 048	-0 754	2 852	0 091	0 920	22 095
-15 0	-25 0	0 046	-0 742	2 867	0 082	0 921	22 501
-10 0	-25 0	0 044	-0 728	2 883	0 072	0 921	22 927
-05 0	-25 0	0 041	-0 712	2 899	0 062	0 922	23 370
00 0	-25 0	0 038	-0 695	2 915	0 051	0 922	23 827
05 0	-25 0	0 035	-0 677	2 931	0 039	0 923	24 292
10 0	-25 0	0 031	-0 659	2 946	0 027	0 924	24 762
15 0	-25 0	0 027	-0 640	2 961	0 013	0 924	25 233
20 0	-25 0	0 022	-0 622	2 975	-0 000	0 925	25 699
25 0	-25 0	0 017	-0 604	2 987	-0 014	0 925	26 157
30 0	-25 0	0 012	-0 587	2 998	-0 028	0 926	26 603

-30 0	-20 0	0 044	-0 752	2 836	0 088	0 921	22 464
-25 0	-20 0	0 042	-0 744	2 852	0 082	0 921	22 790
-20 0	-20 0	0 041	-0 734	2 869	0 075	0 921	23 131
-15 0	-20 0	0 039	-0 723	2 885	0 068	0 922	23 485
-10 0	-20 0	0 037	-0 710	2 902	0 060	0 922	23 851
-05 0	-20 0	0 035	-0 696	2 919	0 052	0 923	24 226
00 0	-20 0	0 032	-0 680	2 935	0 043	0 923	24 608
05 0	-20 0	0 029	-0 664	2 951	0 033	0 924	24 993
10 0	-20 0	0 026	-0 648	2 965	0 023	0 924	25 379
15 0	-20 0	0 023	-0 632	2 979	0 012	0 925	25 762
20 0	-20 0	0 019	-0 616	2 991	0 001	0 925	26 140
25 0	-20 0	0 015	-0 600	3 001	-0 010	0 926	26 510
30 0	-20 0	0 010	-0 586	3 009	-0 022	0 926	26 868
-30 0	-15 0	0 034	-0 733	2 854	0 067	0 922	23 561
-25 0	-15 0	0 033	-0 726	2 871	0 063	0 922	23 824
-20 0	-15 0	0 032	-0 717	2 888	0 057	0 923	24 097
-15 0	-15 0	0 030	-0 707	2 905	0 052	0 923	24 378
-10 0	-15 0	0 029	-0 695	2 921	0 046	0 923	24 665
-05 0	-15 0	0 027	-0 682	2 937	0 040	0 924	24.957
00 0	-15 0	0 025	-0 669	2 953	0 033	0 924	25 251
05 0	-15 0	0 023	-0 655	2 968	0 026	0 924	25 546
10 0	-15 0	0 020	-0 640	2 981	0 019	0 925	25.840
15 0	-15 0	0 018	-0 626	2 992	0 010	0 925	26 131
20 0	-15 0	0 015	-0 612	3 002	0 002	0 926	26 416
25 0	-15 0	0 012	-0 599	3 010	-0 007	0 926	26 694
30 0	-15 0	0 008	-0 587	3 015	-0 016	0 926	26 963

-30 0	-10 0	0 024	-0 718	2 874	0 046	0 923	24 560
-25 0	-10 0	0 023	-0 711	2 891	0 042	0 923	24 745
-20 0	-10 0	0 022	-0 704	2 907	0 039	0 923	24 935
-15 0	-10 0	0 021	-0 694	2 923	0 035	0 924	25 130
-10 0	-10 0	0 020	-0 684	2 938	0 031	0 924	25 328
-05 0	-10 0	0 018	-0 673	2 953	0 027	0 924	25 528
00 0	-10 0	0 017	-0 661	2 967	0 023	0 924	25 728
05 0	-10 0	0 016	-0 648	2 980	0 018	0 925	25 928
10 0	-10 0	0 014	-0 636	2 991	0 013	0 925	26 126
15 0	-10 0	0 012	-0 623	3 000	0 007	0 925	26 320
20 0	-10 0	0 010	-0 611	3 007	0 002	0 926	26 511
25 0	-10 0	0 008	-0 600	3 012	-0 004	0 926	26 695
30 0	-10 0	0 006	-0 590	3 015	-0 011	0 926	26 873

-30 0	-05 0	0 012	-0 704	2 894	0 023	0 924	25 411
-25 0	-05 0	0 012	-0 699	2 909	0 021	0 924	25 509
-20 0	-05 0	0 011	-0 693	2 923	0 020	0 924	25 610
-15 0	-05 0	0 011	-0 685	2 938	0 018	0 924	25 713
-10 0	-05 0	0 010	-0 676	2 952	0 016	0 924	25 816
-05 0	-05 0	0 009	-0 666	2 965	0 014	0 925	25 919
00 0	-05 0	0 009	-0 656	2 976	0 012	0 925	26 022
05 0	-05 0	0 008	-0 645	2 987	0 009	0 925	26 123
10 0	-05 0	0 007	-0 634	2 995	0 007	0 925	26 222
15 0	-05 0	0 006	-0 624	3 002	0 004	0 925	26 319
20 0	-05 0	0 005	-0 614	3 007	0 001	0 926	26 413
25 0	-05 0	0 004	-0 604	3 009	-0 002	0 926	26 503
30 0	-05 0	0 003	-0 596	3 008	-0 005	0 926	26 590

-30 0	00 0	-0 000	-0 693	2 911	-0 000	0 924	26 084
-25 0	00 0	0 000	-0 690	2 924	-0 000	0 924	26 092
-20 0	00 0	0 000	-0 685	2 936	-0 000	0 925	26 100
-15 0	00 0	0 000	-0 678	2 948	-0 000	0 925	26 107
-10 0	00 0	0 000	-0 671	2 960	-0 000	0 925	26 113
-05 0	00 0	0 000	-0 663	2 970	0 000	0 925	26 117
00 0	00 0	0 000	-0 654	2 979	0 000	0 925	26 120
05 0	00 0	0 000	-0 645	2 987	0 000	0 925	26 122
10 0	00 0	0 000	-0 636	2 993	-0 000	0 925	26 122
15 0	00 0	0 000	-0 627	2 998	-0 000	0 925	26 121
20 0	00 0	0 000	-0 619	3 000	-0 000	0 925	26 118
25 0	00 0	0 000	-0 611	2 999	-0 000	0 926	26 114
30 0	00 0	0 000	-0 605	2 996	-0 000	0 926	26 109
-30 0	05 0	-0 012	-0 684	2 924	-0 024	0 925	26 565
-25 0	05 0	-0 012	-0 682	2 934	-0 022	0 925	26 482
-20 0	05 0	-0 011	-0 679	2 944	-0 020	0 925	26 395
-15 0	05 0	-0 011	-0 674	2 953	-0 018	0 925	26 305
-10 0	05 0	-0 010	-0 669	2 962	-0 016	0 925	26 213
-05 0	05 0	-0 009	-0 662	2 970	-0 014	0 925	26 118
00 0	05 0	-0 009	-0 656	2 976	-0 012	0 925	26 022
05 0	05 0	-0 008	-0 648	2 982	-0 009	0 925	25 924
10 0	05 0	-0 007	-0 641	2 985	-0 007	0 925	25 825
15 0	05 0	-0 006	-0 634	2 987	-0 004	0 925	25 726
20 0	05 0	-0 005	-0 627	2 987	-0 001	0 925	25 628
25 0	05 0	-0 004	-0 621	2 984	0 002	0 925	25 531
30 0	05 0	-0 003	-0 616	2 979	0 005	0 925	25 435

-30 0	10 0	-0 025	-0 677	2 931	-0 048	0 925	26 850
-25 0	10 0	-0 024	-0 677	2 938	-0 044	0 925	26 674
-20 0	10 0	-0 022	-0 676	2 945	-0 040	0 925	26 493
-15 0	10 0	-0 021	-0 673	2 952	-0 036	0 925	26 307
-10 0	10 0	-0 020	-0 670	2 958	-0 032	0 925	26 116
-05 0	10 0	-0 018	-0 665	2 963	-0 027	0 925	25 923
00 0	10 0	-0 017	-0 661	2 967	-0 023	0 924	25 728
05 0	10 0	-0 016	-0 655	2 970	-0 018	0 924	25 533
10 0	10 0	-0 014	-0 650	2 972	-0 013	0 924	25 338
15 0	10 0	-0 012	-0 644	2 972	-0 007	0 924	25 144
20 0	10 0	-0 010	-0 639	2 970	-0 002	0 924	24 953
25 0	10 0	-0 008	-0 634	2 966	0 004	0 924	24 766
30 0	10 0	-0 006	-0 631	2 959	0 010	0 924	24 584
-30 0	15 0	-0 037	-0 671	2 933	-0.072	0 925	26 940
-25 0	15 0	-0 035	-0 674	2 937	-0 065	0 925	26 674
-20 0	15 0	-0 033	-0 675	2 941	-0 059	0 925	26 399
-15 0	15 0	-0 031	-0 675	2 945	-0 053	0 924	26 117
-10 0	15 0	-0 029	-0 674	2 948	-0 047	0 924	25 831
-05 0	15 0	-0 027	-0 672	2 951	-0 040	0 924	25 542
00 0	15 0	-0 025	-0 669	2 953	-0 033	0 924	25 251
05 0	15 0	-0 023	-0 665	2 954	-0 026	0 924	24 961
10 0	15 0	-0 020	-0 662	2 954	-0 018	0 924	24 674
15 0	15 0	-0 018	-0 658	2 953	-0 010	0 924	24 391
20 0	15 0	-0 015	-0 654	2 950	-0 001	0 924	24 114
25 0	15 0	-0 012	-0 651	2 945	0 008	0 923	23 845
30 0	15 0	-0 009	-0 648	2 938	0 017	0 923	23 584

-30 0	20 0	-0 048	-0 667	2 930	-0 094	0 925	26 846
-25 0	20 0	-0 045	-0 672	2 931	-0 086	0 925	26 490
-20 0	20 0	-0 042	-0 676	2 932	-0 078	0 924	26 123
-15 0	20 0	-0 040	-0 679	2 933	-0 069	0 924	25 749
-10 0	20 0	-0 037	-0 680	2 934	-0 061	0 924	25 370
-05 0	20 0	-0 035	-0 681	2 934	-0 052	0 924	24 989
00 0	20 0	-0 032	-0 680	2 935	-0 043	0 923	24 608
05 0	20 0	-0 029	-0 679	2 935	-0 033	0 923	24 231
10 0	20 0	-0 026	-0 678	2 934	-0 023	0 923	23 860
15 0	20 0	-0 023	-0 676	2 933	-0 012	0 923	23 498
20 0	20 0	-0 020	-0 673	2 930	-0 000	0 922	23 147
25 0	20 0	-0 016	-0 671	2 925	0 012	0 922	22 810
30 0	20 0	-0 012	-0 669	2 919	0 025	0 922	22 487

-30 0	25 0	-0 057	-0 664	2 922	-0 116	0 925	26 581
-25 0	25 0	-0 054	-0 672	2 919	-0 105	0 924	26 138
-20 0	25 0	-0 050	-0 679	2 918	-0 095	0 924	25 683
-15 0	25 0	-0 047	-0 685	2 916	-0 084	0 924	25 220
-10 0	25 0	-0 044	-0 689	2 915	-0 073	0 923	24 754
-05 0	25 0	-0 041	-0 693	2 915	-0 062	0 923	24 288
00 0	25 0	-0 038	-0 695	2 915	-0 051	0 922	23 827
05 0	25 0	-0 035	-0 697	2 915	-0 039	0 922	23 375
10 0	25 0	-0 031	-0 697	2 914	-0 026	0 922	22 935
15 0	25 0	-0 027	-0 697	2 913	-0 012	0 921	22 513
20 0	25 0	-0 023	-0 696	2 912	0 003	0 921	22 110
25 0	25 0	-0 019	-0 695	2 909	0 018	0 921	21 730
30 0	25 0	-0 014	-0 694	2 905	0 034	0 920	21 375

-30 0	30 0	-0 065	-0 662	2 909	-0 135	0 924	26 165
-25 0	30 0	-0 061	-0 674	2 904	-0 123	0 924	25 639
-20 0	30 0	-0 057	-0 684	2 900	-0 110	0 923	25 101
-15 0	30 0	-0 053	-0 693	2 897	-0 097	0 923	24 556
-10 0	30 0	-0 050	-0 701	2 895	-0 084	0 922	24 011
-05 0	30 0	-0 047	-0 708	2 895	-0 071	0 922	23 473
00 0	30 0	-0 043	-0 713	2 895	-0 057	0 921	22 947
05 0	30 0	-0 040	-0 717	2 896	-0 043	0 921	22 439
10 0	30 0	-0 036	-0 720	2 897	-0 027	0 920	21 957
15 0	30 0	-0 031	-0 722	2 899	-0 011	0 920	21 506
20 0	30 0	-0 026	-0 722	2 900	0 007	0 919	21 091
25 0	30 0	-0 021	-0 722	2 901	0 025	0 919	20 715
30 0	30 0	-0 016	-0 721	2 901	0 044	0 918	20 382